

ADDITION POLYMERIZATION TOWARD THE SYNTHESIS OF PHOTORESISTS  
FOR MICROLITHOGRAPHY WITH CARBON DIOXIDE DEVELOPMENT

Mary Kate Boggiano

A dissertation submitted to the faculty of the University of North Carolina at Chapel Hill in partial fulfillment of the requirements for the degree of Doctorate of Philosophy in the Department of Chemistry.

Chapel Hill  
2006

Approved by

Advisor: Joseph M. DeSimone

Reader: Maurice Brookhart

Reader: Valerie S. Ashby

© 2006  
Mary Kate Boggiano  
ALL RIGHTS RESERVED

## ABSTRACT

Mary Kate Boggiano

Addition polymerization Toward the Synthesis of Photoresists for Microlithography with Carbon Dioxide Development

(Under the direction of Joseph M. DeSimone)

In the drive for smaller image sizes in microelectronic devices, the lithography industry has reached a point where the solvents traditionally used for development are potentially damaging to the images formed. The use of a more gentle solvent, such as supercritical carbon dioxide, has been shown to alleviate this problem. Furthermore, replacement of the solvents in spin-coating and stripping with condensed CO<sub>2</sub> could streamline the lithography process as the “wet” solvents would be eliminated. Also, CO<sub>2</sub> is an environmentally benign and easily recyclable alternative to the solvents currently used in microlithography for the solvent-intensive steps of processing a photoresist.

As next generations of lithographic techniques for imaging a photoresist approach, more stringent requirements are placed on the resist. For 193 nm and 193 nm immersion resists, alicyclic backbones have been shown to impart etch resistance and to elevate glass transition temperatures, while fluorination has been shown to decrease absorbance. As an additional advantage for processing in CO<sub>2</sub>, fluorination also increases CO<sub>2</sub> solubility. Various norbornene-based monomers were synthesized to include fluorinated moieties. Resist materials were synthesized by addition polymerization using allylpalladium chloride dimer. Fluorinated copolymers containing a “chemical switch” have been found to have a significant CO<sub>2</sub> solubility difference, as well as a difference in intrinsic viscosities. Dry plasma etching of these polymers has demonstrated moderate etch resistance compared to

Novolac. Imaging with an ASML 193 nm scanner has resolved 1  $\mu\text{m}$  semidense lines, using  $\text{CO}_2$  as the developer.

## DEDICATION

One beautiful Spring day in 1996, I drove home from school crying. I had just finished taking the AP Calculus test, and unlike many of my classmates, this would be my only AP test. I used my calculator when I wasn't supposed to, and I didn't use it when it was allowed. There were essay questions I left entirely blank. I fumbled through the entire exam.

When I arrived, my brother Kevin was already home. I told him how I had wasted so much time and money (these tests aren't cheap!) trying to do well on the AP test. But he was so good to me. He offered me some of his leftover pizza, and said, "I'm so proud of you. You are the only person in our family who has ever taken an AP test. It doesn't matter how well you did. It's a great accomplishment simply to have taken that test."

Kevin, you never understood my interests in science, but you knew that I'm doing what makes me happy...even if I'm not at the top of my field. All that matters is that I'm living my dream. You made it a point to live out your own dreams. You'll always be an inspiration to me, and you will never be forgotten.

To Kevin Anthony Boggiano

August 5, 1976 – June 27, 2005

## ACKNOWLEDGMENTS

First, I'd like to thank God for guidance seen and unseen. Many thanks to my adviser, Joe DeSimone, particularly for setting me straight on the termination methods of free radical polymerizations. Finishing grad school would have been impossible without the encouragement from my family: Mom, Bryan, Kevin, Judy, Sarah and Amanda, Scott and his family, Buttercup and Chester. I'd like to extend my gratitude to former (and present) group members who have enriched my understanding of lithography, including Devin Flowers, Luke Zannoni, Colin Wood, Ruben Carbonell, Amy Zweber, Ke Wang, Erik Hoggan, Dave Vallenga, and Ginger Yu. Many thanks to Sarah Folk and Karen McAllister for introducing me to two contrasting views of grad school. Thanks to Jasons (Rolland and Yarborough), Derek Schorzman, Ji Guo, Jen Kelly, and Ansley Exner for making the lab a fun environment.

I'd like to thank Dr. Stuart Clough for convincing me to go to grad school with the phrase: "that was the most fun I ever had." Thanks to Hiroshi Ito and Rao Varanasi for taking an interest in the DeSimone lab's work, leading to my internship at IBM, Summer 2003. Further thanks to Chas Archie for being so passionate about his work, and sharing that interest. Thanks to Chet Wasik for helpful discussions into understanding management in a business environment. Thanks to Dr. Yusuf Menciloglu for giving me a rare opportunity to study in his lab in Istanbul. Although the IBM internship and the Sabanci research did not directly contribute to this dissertation, they certainly contributed to my life's experiences.

Thanks to Vicki Haithcock, Debbie Marlow, SaRAH! Kocz, and Rhonda Haithcock for maintaining a sense of order upstairs. Thanks to Peaches, particularly for the Daily Tar Heel

in my mailbox. Many thanks to Dexter Rogers, Art Woody and Walt Boger for providing necessary services to the department. Finally, I'd like to thank Paul Telowicki for good conversations about Spider basketball and Buttercup. Although you may be "just doing your job," these are services I could never take for granted.

## TABLE OF CONTENTS

1. Review of photoresists for microlithography.....	2
1.1. Introduction.....	2
1.1.1. The Technology Roadmap.....	2
1.1.2. Microlithography process.....	3
1.2. Photoresist requirements.....	5
1.3. Previous photoresist platforms and technology nodes.....	6
1.3.1. G-line and I-line microlithography.....	6
1.3.2. 248 nm Microlithography.....	7
1.3.3. 193 nm Microlithography.....	10
1.4. Potential future lithographic technologies and related materials.....	13
1.4.1. 193 nm Immersion lithography.....	13
1.4.2. 157 nm (Immersion) lithography.....	15
1.4.3. Imprint lithography.....	19
1.4.4. Electron beam lithography.....	23
1.4.5. EUV lithography / X-Ray lithography.....	25
1.5. Research Objectives.....	27
1.6. Conclusion.....	28
1.7. References.....	29





2.2.2.2. Elemental Analysis.....	48
2.2.2.3. Infrared Spectroscopy (IR).....	49
2.2.2.4. Intrinsic Viscosity.....	49
2.2.2.5. CO <sub>2</sub> solubility .....	49
2.2.2.6. Differential scanning calorimetry (DSC).....	49
2.2.2.7. Thermal Gravimetric analysis (TGA).....	49
2.2.2.8. Optical Density Measurements.....	50
2.2.2.9. Etching.....	50
2.2.2.10. Interferometry.....	50
2.2.2.11. 193 nm Exposure.....	51
2.2.2.12. Optical microscopy.....	51
2.2.2.13. Scanning Electron Microscopy (SEM).....	51
2.3. Results and discussion.....	51
2.3.1. Monomer characterization.....	51
2.3.1.1. NBFOA.....	51
2.3.1.2. FAE.....	54
2.3.1.3. NBFAE.....	55
2.3.1.4. NBHFA-BOC.....	57
2.3.2. Homopolymer characterization.....	60
2.3.2.1. poly(NBFOA).....	60
2.3.2.2. poly(NBFAE).....	62
2.3.4. Homopolymer comparison.....	62
2.3.4.1. Thermal analysis.....	62

2.3.4.2. DUV absorbance.....	64
2.3.4.3. CO <sub>2</sub> solubility.....	65
2.3.4.4. Etch resistance.....	66
2.3.5. Copolymer characterization.....	67
2.3.5.1. poly(NBFOA/NBHFA).....	67
2.3.5.2. poly(NBFOA/NBHFA-tBOC).....	68
2.3.6. Lithographic evaluation.....	73
2.3.6.1. Mercury arc lamp.....	73
2.3.6.2. Imaging at 193 nm.....	74
2.4. Conclusion.....	77
2.5. References.....	78
3. Bilayer resists for development in compressed CO <sub>2</sub> .....	82
3.1. Introduction.....	82
3.1.1. Dry etch resistance of organic materials.....	82
3.1.2. Bilayer photoresists.....	90
3.1.2.1. Motivation and background.....	90
3.1.2.2. Silicon in bilayer photoresists.....	93
3.1.2.2.1. Polysilanes.....	93
3.1.2.2.2. Polysiloxanes.....	97
3.1.2.2.3. Silsesquioxane-based polymers.....	99
3.1.3. Present approach.....	104
3.2. Experimental.....	105
3.2.1. Synthesis.....	105

3.2.1.1. Materials.....	105
3.2.1.2. Equipment.....	105
3.2.1.3. Monomer synthesis.....	106
3.2.1.3.1. (1H,1H-Perfluorooctyloxy)-propene (FAE).....	106
3.2.1.3.2. 5-(1H,1H-Perfluorooctyloxymethyl)-norborn-2-ene (NBFAE).....	106
3.2.1.4. Polymer synthesis.....	106
3.2.1.4.1. Addition polymerization.....	106
3.2.2. Characterization.....	107
3.2.2.1. Nuclear Magnetic Resonance Spectroscopy (NMR).....	107
3.2.2.2. Elemental Analysis.....	108
3.2.2.3. Etching.....	108
3.2.2.4. Interferometry.....	108
3.3. Results and discussion.....	108
3.3.1. Monomer characterization.....	108
3.3.2. Polymer characterization.....	109
3.4. Conclusion.....	112
3.5. References.....	113
4. Recommendations for future work.....	118
4.1. Optimization of lithographic processing.....	118
4.2. Molecular resists based on POSS.....	119
4.3. References.....	122

## LIST OF TABLES

2.1. Comparison of photoresists processed in condensed CO <sub>2</sub> .....	37
2.2. Elemental analysis results for NBFOA.....	54
2.3. Elemental analysis results for NBFAE.....	57
2.4. Elemental analysis results for NBHFA-BOC.....	60
2.5. Elemental analysis results for poly(NBFOA).....	61
2.6. Elemental analysis results for poly(NBFAE).....	62
2.7. Elemental analysis results for poly(NBFOA/NBHFA).....	68
2.8. Elemental analysis results for poly(NBFOA/NBHFA-BOC).....	70
2.9. Optical and SEM micrographs of dense lines in poly(NBFOA/NBHFA) on Si.....	75
2.10. Optical and SEM micrographs of semidense lines in poly(NBFOA/NBHFA) on Si..	75
3.1. Fractional composition of a typical glow discharge RIE plasma.....	82
3.2. Elemental analysis results for poly(NBFAE/NBPOSS).....	110

## LIST OF FIGURES

1.1.	The rapid increase of transistors on a microchip is reflected by Moore's Law.....	2
1.2.	Photolithography: the transfer of an image onto a silicon wafer.....	3
1.3.	The basic steps of the lithography process.....	4
1.4.	A photoresist with low absorbance or high absorbance at the exposure wavelength...6	
1.5.	Acid-catalyzed synthesis of novolac.....	7
1.6.	Wolff rearrangement of a diazonaphthoquinone.....	7
1.7.	Chemical amplification polymer platforms for 248 nm lithography.....	8
1.8.	Mechanism of acid-catalyzed deprotection of PHOST-tBOC.....	9
1.9.	Mechanism of acid-catalyzed deprotection of poly( <i>tert</i> -butyl acrylate).....	9
1.10.	Lithographic images exhibiting T-topping.....	10
1.11.	Examples of polymer platforms for 193 nm lithography.....	11
1.12.	DOF advantages in immersion lithography.....	14
1.13.	Several of the leading photoresist platforms developed for 157 nm microlithography.....	17
1.14.	Pattern replication defect mechanisms in imprint lithography.....	20
2.1.	CO <sub>2</sub> phase diagram for changes in pressure and temperature.....	35
2.2.	Images obtained using a cyclic olefin terpolymer.....	42
2.3.	Imaging capability of NBHFA-based addition polymer to 100 nm.....	43
2.4.	IUPAC numbering of a substituted norbornene molecule.....	48
2.5.	<sup>1</sup> H NMR spectrum of NBFOA.....	52
2.6.	<sup>19</sup> F NMR spectrum of NBFOA.....	53
2.7.	<sup>1</sup> H NMR spectrum of FAE.....	55

2.8. $^1\text{H}$ NMR spectrum of NBFAE.....	56
2.9. $^1\text{H}$ NMR of NBHFA and NBHFA-BOC.....	58
2.10. $^{19}\text{F}$ NMR of NBHFA and NBHFA-BOC.....	59
2.11. $^1\text{H}$ NMR of poly(NBFOA).....	61
2.12. Thermogravimetric analysis of poly(NBFOA) and poly(NBFAE).....	63
2.13. Differential scanning calorimetry of poly(NBFOA) and poly(NBFAE).....	64
2.14. Optical absorbance of poly(NBFOA) and poly(NBFAE).....	65
2.15. $\text{CO}_2$ solubility of poly(NBFOA) and poly(NBFAE).....	66
2.16. Oxygen plasma etch rates of norbornyl copolymers.....	67
2.17. $^{19}\text{F}$ NMR of poly(NBFOA/NBHFA) and poly(NBFOA/NBHFA-BOC).....	69
2.18. $^1\text{H}$ NMR of poly(NBFOA/NBHFA) and poly(NBFOA/NBHFA-BOC).....	70
2.19. Thermogravimetric analysis of poly(NBFOA/NBHFA) and poly(NBFOA/NBHFA-BOC).....	71
2.20. Differential scanning calorimetry of poly(NBFOA/NBHFA-BOC).....	72
2.21. $\text{CO}_2$ solubility curves of poly(NBFOA/NBHFA-BOC) and poly(NBFOA/NBHFA)..	73
2.22. Infrared spectra of poly(NBFOA/NBHFA-BOC) and poly(NBFOA/NBHFA).....	74
3.1. Selective etching to form high aspect ratio images.....	84
3.2. Multilayer resists for high aspect ratio etching.....	91
3.3. Polymer platforms containing silane side groups.....	94
3.4. UV absorbance and photobleaching of an example polysilane.....	96
3.5. Porous images due to outgassing of tBOC-Sty functionalized polysiloxane.....	99
3.6. Different architectures of silsesquioxanes.....	100
3.7. Polycondensation of a negative tone SSQ resist.....	101

3.8. Synthesis of NBPOSS-NBFAE copolymer.....	107
3.9. IUPAC numbering of a substituted norbornene molecule.....	108
3.10. <sup>1</sup> H NMR of poly(NBFAE/NBPOSS).....	110
3.11. RIE data for copolymers of NBFAE and NBPOSS.....	111
4.1. Available starting materials for POSS-based molecular resists.....	120



## LIST OF ABBREVIATIONS

157i	157 nm immersion lithography
193i	193 nm immersion lithography
Allyl-Pd	Allylpalladium chloride dimer
bisBOC	Di- <i>tert</i> -butyldicarboxylate
BLR	Bilayer resist
CA	Chemical amplification
CD <sub>min</sub>	Minimum critical dimension
CO <sub>2</sub>	Carbon dioxide
COMA	Cyclic olefin-maleic anhydride
DBP	Di- <i>tert</i> -butylphenol
DCP	Dicyclopentadiene
DMAP	N,N-dimethylaminopyridine
DNQ	Diazonaphthoquinone
DOF	Depth of focus
DSC	Differential scanning calorimetry
DUV	Deep ultraviolet
ESCAP	Environmentally stable chemically amplified photoresist
EUV	Extreme ultraviolet
FAE	(1H,1H-Perfluorooctyloxy)-propene
FOMA	1H,1H-perfluorooctyl methacrylate
FOA	1H,1H-perfluorooctyl acrylate
HMDS	Hexamethyldisilazane

IC	Integrated circuit
IR	Infrared spectroscopy
ISP	Incremental structural parameter
ITRS	International Technology Roadmap for Semiconductors
IUPAC	International Union of Pure and Applied Chemistry
LER	Line edge roughness
$M_{CR}$	Mass of carbon atoms in ring structures
MeOH	Methanol
MMA	Methyl methacrylate
$M_n$	Number average molecular weight
MSC	Monomer structural contribution
$M_{TOT}$	Total mass
MW	Molecular weight
NA	Numerical aperture
NB	Norbornene
NBFAE	5-(1H,1H-Perfluorooctyloxymethyl)-norborn-2-ene
NBFOA	Norborn-5-ene-2-carboxylic acid 1H, 1H-perfluorooctyl ester
NBPOSS	1-[dimethyl[2-(Norbornen-2-yl)ethyl]siloxy]-3,5,7,9,11,13,15-heptacyclopentyl[9.5.1.1 <sup>3,9</sup> .1 <sup>5,15</sup> .1 <sup>7,13</sup> ] octasiloxane
$N_C$	Number of carbon atoms in a resist monomer
$N_{C-C}$	Number of carbon-carbon bonds in a resist monomer
$N_{C-N}$	Number of carbon-nitrogen bonds in a resist monomer
$N_{C-O}$	Number of carbon-oxygen bonds in a resist monomer
NGL	Next generation lithography

N <sub>H</sub>	Number of hydrogen atoms in a resist monomer
NBHFA	3-((Norbornyl)-1,1,1-trifluoro-2-trifluoromethyl)propan-2-ol
NBHFABOC	Carbonic acid 1-norborn-5-en-2-ylmethyl-2,2,2-trifluoro-1-trifluoromethyl-ethyl ester tert-butyl ester
NBTBE	Norborn-5-ene-2-carboxylic acid <i>tert</i> -butyl ester
NBtBOC	norbornyl-2- <i>tert</i> -butoxycarbonate
NCSU	North Carolina State University
NIL	Nanoimprint lithography
NMR	Nuclear magnetic resonance spectroscopy
PAB	Post applied bake
PAG	Photoacid generator
PDMS	Polydimethylsiloxane
PEB	Post exposure bake
PED	Post exposure delay
PFO	1H,1H-perfluorooctan-1-ol
PFPE	Perfluoropolyether
PGMEA	Propylene glycol methyl ether acetate
PHOST	Polyhydroxystyrene
PMMA	Polymethylmethacrylate
POSS	Polyhedral oligomeric silsesquioxane
PPMS	Plasma polymerized methylsilane
PTFE	Polytetrafluoroethylene
RIE	Reactive ion etch
ROMP	Ring opening metathesis polymerization

RT	Room temperature
SEM	Scanning electron microscopy
SFC	Supercritical fluid chromatography
SFIL	Step-and-flash imprint lithography
SLR	Single layer resist
SSQ	Silsesquioxane
Sty	Styrene
TBAH	Tetrabutylammonium hydroxide
TBAHS	tetrabutylammonium hydrogen sulfate
TBMA	<i>tert</i> -butylmethacrylate
t-BOC	<i>tert</i> -Butoxycarbonate
Td	Decomposition temperaure
TEOS	Tetraethylorthosilicate
TFE	Tetrafluoroethylene
TFT	$\alpha,\alpha,\alpha$ -Trifluorotoluene
Tg	Glass transition temperature
TGA	Thermal gravimetric analysis
THF	Tetrahydrofuran
THPMA	Tetrahydropyranyl methacrylate
TMAH	Tetramethylammonium hydroxide
TPS-Tf	Triphenylsulfonium triflate
UV	Ultraviolet
VASE	Variable angle scanning ellipsometer

WPAG

Diphenyl-*p*-tolylsulfonium triflate

# REVIEW OF PHOTORESISTS FOR MICROLITHOGRAPHY

# 1. Review of photoresists for microlithography

## 1.1. Introduction

### 1.1.1. The Technology Roadmap

In microelectronics, “the technology roadmap”, or Moore’s Law, is a prediction that the number of transistors on an integrated circuit (IC) will double every 18 months.<sup>2</sup> While this

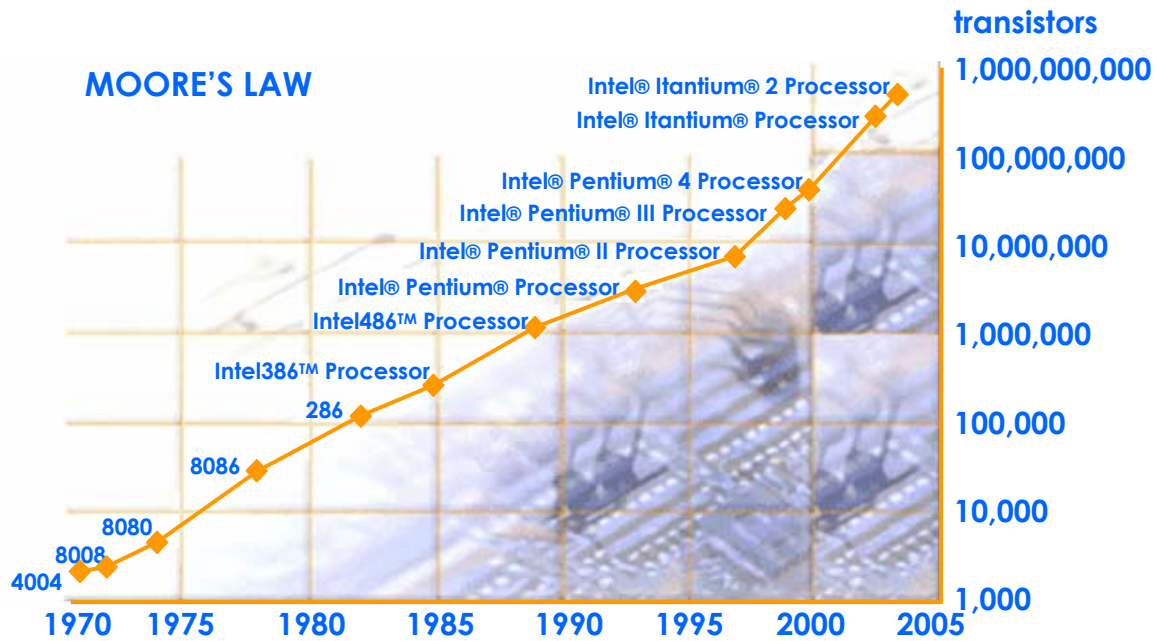


Figure 1.1. The rapid increase of transistors on a microchip is reflected by Moore’s Law.<sup>3</sup>

prediction was made in 1965, it has, remarkably, held true for the past four decades (Fig. 1.1). The size of a transistor is determined by the smallest image that can be made on the silicon wafer substrate. Smaller images, made using microlithographic techniques, enable more transistors to be placed on an IC in the same amount of space on the wafer. (Fig. 1.2.) This also results in faster chips, as electronic signals have a shorter distance to travel. The smallest image possible in optical lithography, for each exposure wavelength, is given by the Rayleigh equation,

$$CD_{\min} = (k_1 \times \lambda) / NA, \quad [1]$$

where  $CD_{\min}$  is the minimum feature resolution, or critical dimension,  $k_1$  is an optical constant,  $\lambda$  is the exposure wavelength, and  $NA$  is the numerical aperture of the lens.<sup>4</sup> The IC industry is constantly looking for ways to obtain an ever smaller resolution. This can be

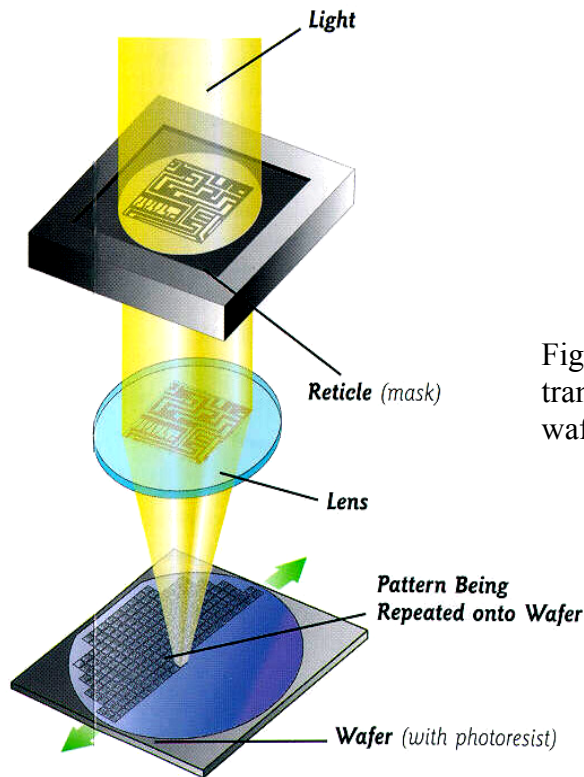


Figure 1.2. Photolithography: the transfer of an image onto a silicon wafer.<sup>1</sup>

attained by either decreasing the wavelength or increasing the numerical aperture. Decreasing the wavelength involves changing the photoresist materials used and replacing the lithography equipment for usage at these smaller wavelengths. The most advanced microchips currently available are manufactured with 193 nm lithography.

### 1.1.2. Microlithography process

The microlithography process consists of various steps, the net goal of which is to transfer an image onto a silicon wafer. The wafer is initially spin-coated at 2000-5000 rpm with a photoresist solution containing a polymeric photoresist and a photoacid generator (PAG).



According to the International Technology Roadmap for Semiconductors (ITRS) requirements for 2005, photoresist coatings on wafers should be approximately 160 – 280 nm thick, with no more than 0.01 defects per square centimeter.<sup>5</sup> Once a thin film of the photoresist has been cast, the wafer is placed beneath a mask and exposed to UV light (Fig. 1.3.). This step activates the PAG in exposed regions, as determined by the mask. Next, the

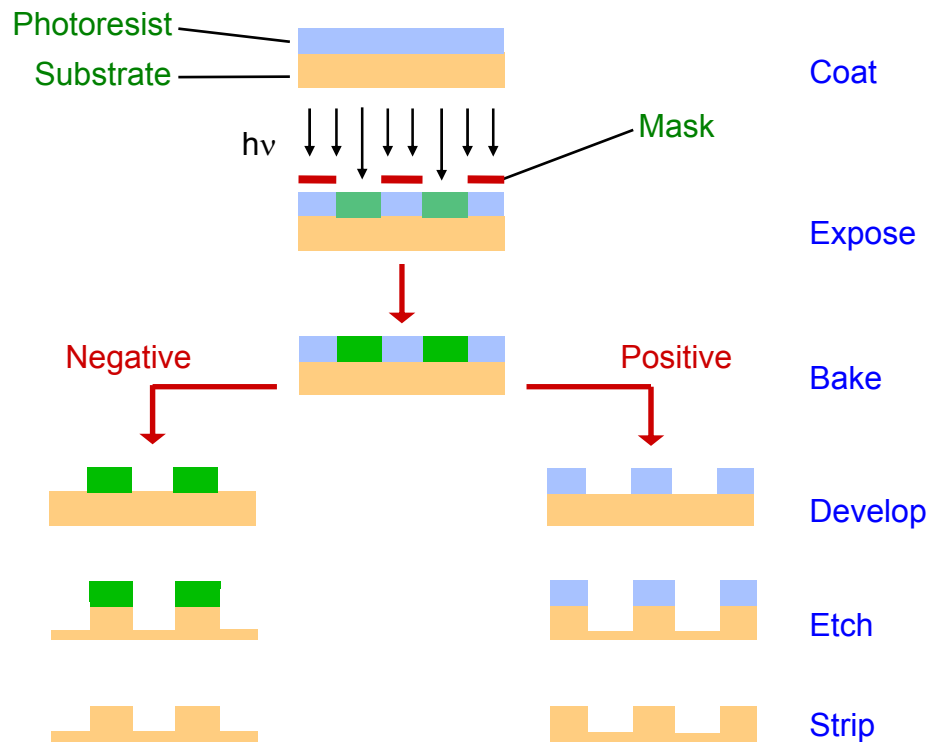


Figure 1.3. The basic steps of the lithography process.<sup>3</sup>

wafer is subjected to a post-exposure bake step (PEB), which allows the photo-generated acid to diffuse and react with an acid-sensitive group on the photoresist polymer. This creates a solubility contrast in the polymer between the exposed and unexposed regions, as two different polymers are now present. An appropriate solvent can then be used to wash away, or develop, one portion of the polymer such that either the exposed region is removed

(positive-tone resist), or the unexposed region is removed (negative-tone resist). Once part of the resist has been dissolved away, the wafer is subjected to an etchant that will remove exposed regions of the silicon wafer. Etchants typically consist of either a dry plasma, or an aqueous acidic solution. Photoresists need to be highly resistant to the etchant. After the image has been etched, the remaining photoresist is stripped away with an appropriate solvent, and the wafer is ready for later steps in the manufacturing process, such as further lithography, doping the wafer with conducting material, or chemical mechanical planarization.

## 1.2. Photoresist requirements

As indicated in the previous section, photoresists are critical to the manufacture of microchips. As such, the photoresist must have a number of specific properties in order to function. First, to obtain smooth, defect-free films, the resist must be highly soluble in the spin-coating solution. The resist must also have good adhesion to the silicon wafer. However, poor adhesion can be remedied through the use of an adhesion promoter, such as hexamethyldisilazane (HMDS). HMDS forms a hydrocarbon monolayer on the wafer, allowing for better adhesion of the organic photoresist. During exposure, the resist must also have low outgassing. Outgassing, or the vaporization of small molecules from the resist film during exposure, is deleterious to the final lenses used in microlithography tools. These outgassing products could adsorb to the lenses, requiring costly cleaning, repair, or even replacement. The resist must also have low absorbance at the exposure wavelength. If the resist absorbs at this wavelength, the UV light cannot penetrate the film, and meniscus-like latent images will form in the resist (Fig. 1.4.), ultimately leading to incomplete development. However, at the same time, the PAG must absorb at the exposure wavelength

to generate the acid. Further, the generated acid must be able to react with the resist in order to achieve the necessary contrast. Therefore, acid-cleavable functional groups must be present in the polymer. During the PEB step, a large solubility contrast will arise due to reaction of these groups with the acid. A high glass transition temperature ( $T_g$ ), permits a range of PEB temperatures without polymer flow and allows the acid to diffuse and react with acid-labile portions of the resist. This is important as such flow during the PEB step could destroy the images. Development then removes the new soluble portion (or the unexposed portion, as appropriate). Finally, high etch resistance is important as the resist must remain intact to protect the underlying wafer.

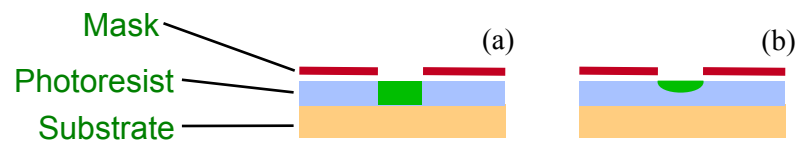


Figure 1.4. A photoresist with low absorbance (a) or high absorbance (b) at the exposure wavelength. A photoresist that absorbs the light will not form latent images that reach the underlying substrate.

### 1.3. Previous photoresist platforms and technology nodes

#### 1.3.1. G-line and I-line microlithography

The formation of integrated circuits using optical exposures was first implemented using a mercury arc lamp, with wavelength filters for the G-line (436 nm) or the I-line (365 nm) emissions. The photosensitive materials initially used as resists functioned differently than described above. The resin was made of novolac, a condensation polymer of formaldehyde and m- or p-cresol (Fig. 1.5). A solubility contrast was attained by formulating novolac with a diazonaphthoquinone (DNQ). DNQ will act as a solubility inhibitor, but upon exposure, the DNQ will undergo Wolff rearrangement to a highly polar solubility promoter (Fig. 1.6).<sup>6</sup>

While this system worked very well for images greater than 0.5  $\mu\text{m}$ , it was widely acknowledged that further miniturization would eventually require imaging at smaller wavelengths. The known light sources at these deep ultraviolet (DUV) wavelengths necessitated the development of a new resist, as novolac could not exhibit the desired sensitivity and was not transparent enough at DUV.

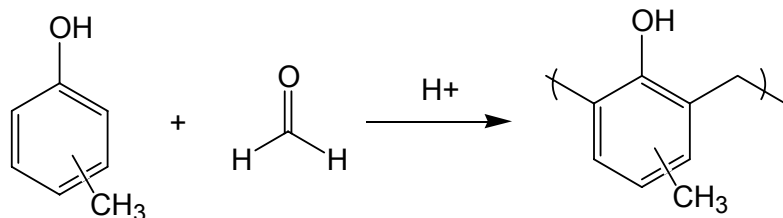


Figure 1.5. Acid-catalyzed synthesis of novolac.

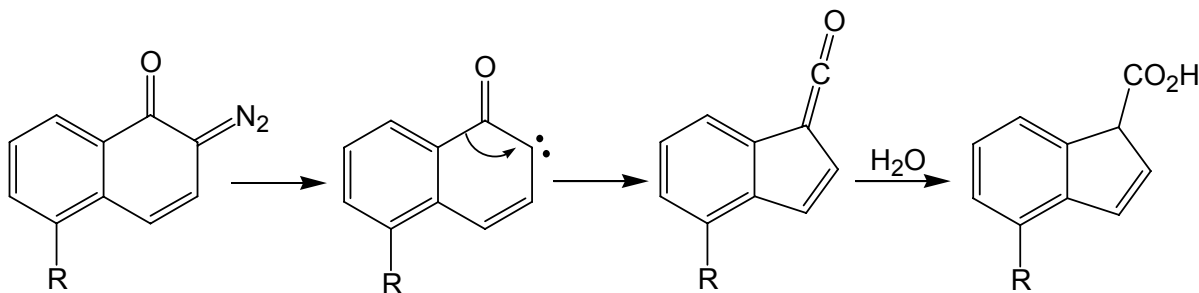


Figure 1.6. Wolff rearrangement of a solubility-inhibiting diazonaphthoquinone into a solubility-promoting molecule.

### 1.3.2. 248 nm Microlithography

The current paradigm of microlithography using acid-sensitive groups on the photoresist, known as chemical amplification, made its commercial debut in 1997 with 248 nm lithography. Two related polymer platforms have been used as photoresists at this wavelength. Polymers based on poly(*p*-hydroxystyrene) (PHOST) were the first successful CA resist platform (Fig. 1.7).<sup>7</sup> IBM commercialized these materials under the name APEX. These polymers have low absorbance at 248 nm and the aromatic ring imparts dry etch

resistance. PHOST resists exhibit very high glass transition temperatures ( $\geq 150$  °C), which prevent polymer flow during the PEB, thus maintaining the integrity of the images to be developed.<sup>8</sup> A portion of the phenolic hydroxyl groups are protected with *tert*-butoxycarbonate groups. This group can be cleaved by organic acids derived from the PAG

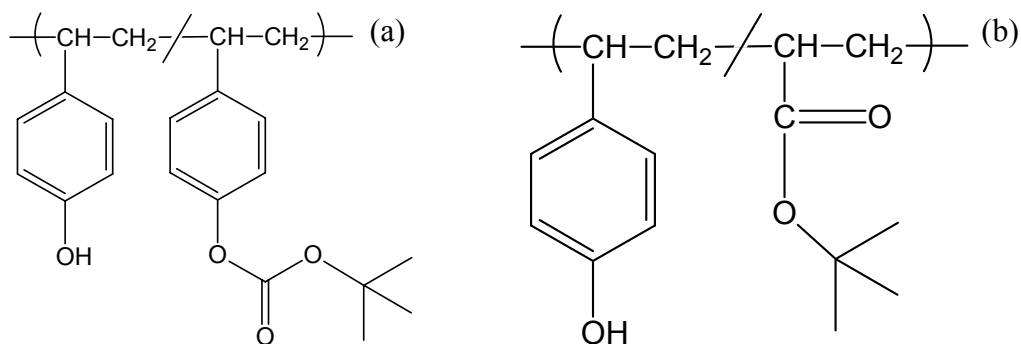


Figure 1.7. Chemical amplification polymer platforms for 248 nm lithography: PHOST (a) and ESCAP (b).

during the post-exposure bake, allowing for a higher solubility of the cleaved polymer in the tetramethyl ammonium hydroxide developing solution (Figs. 1.8 and 1.9). A primary concern that quickly arose with this platform was the formation of an insoluble “skin” layer that formed at the top surface of images. It was determined that this phenomenon, known as “T-topping,” resulted from the PAG interacting with trace atmospheric bases, and becoming deactivated (Fig. 1.10). This problem was largely resolved by substituting *t*-butyl acrylate for the *t*-BOC-protected styrene. This new platform, called ESCAP, or Environmentally Stable Chemical Amplification Photoresist, could be baked above its  $T_g$ , which reduces the free volume of the film, and dramatically lowers the diffusion rate of airborne contaminants. Unlike PHOST resists, ESCAP polymers have a significant gap between the glass transition temperature and the cleaving temperature of the acid-sensitive group. This window allows for

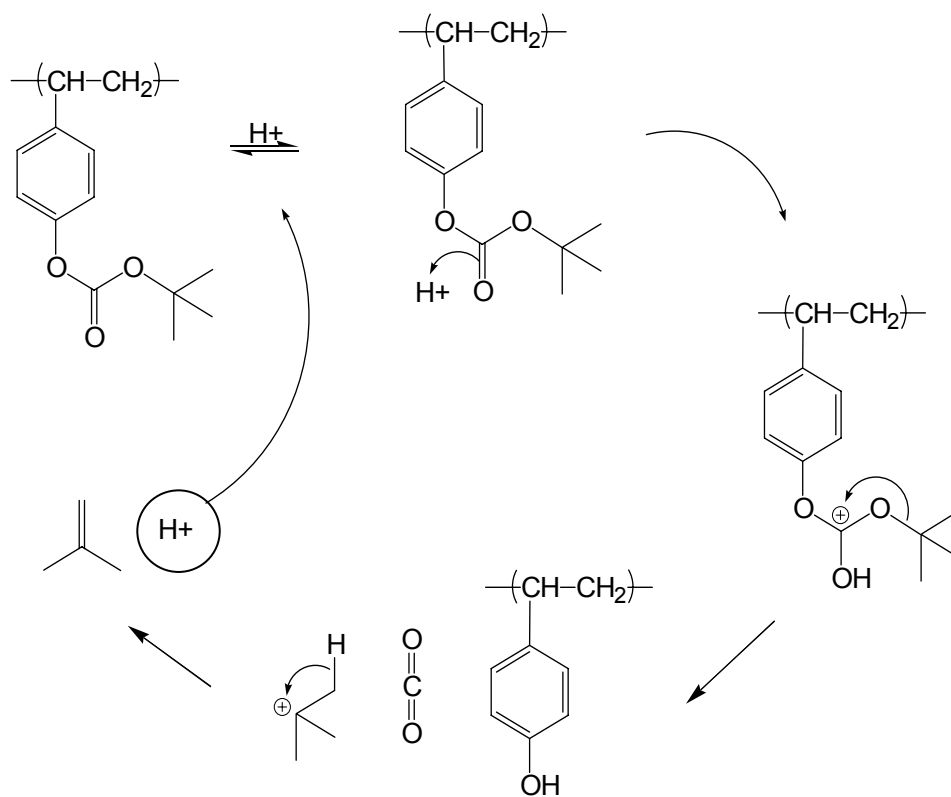


Figure 1.8. Mechanism of acid-catalyzed deprotection of PHOST-tBOC.

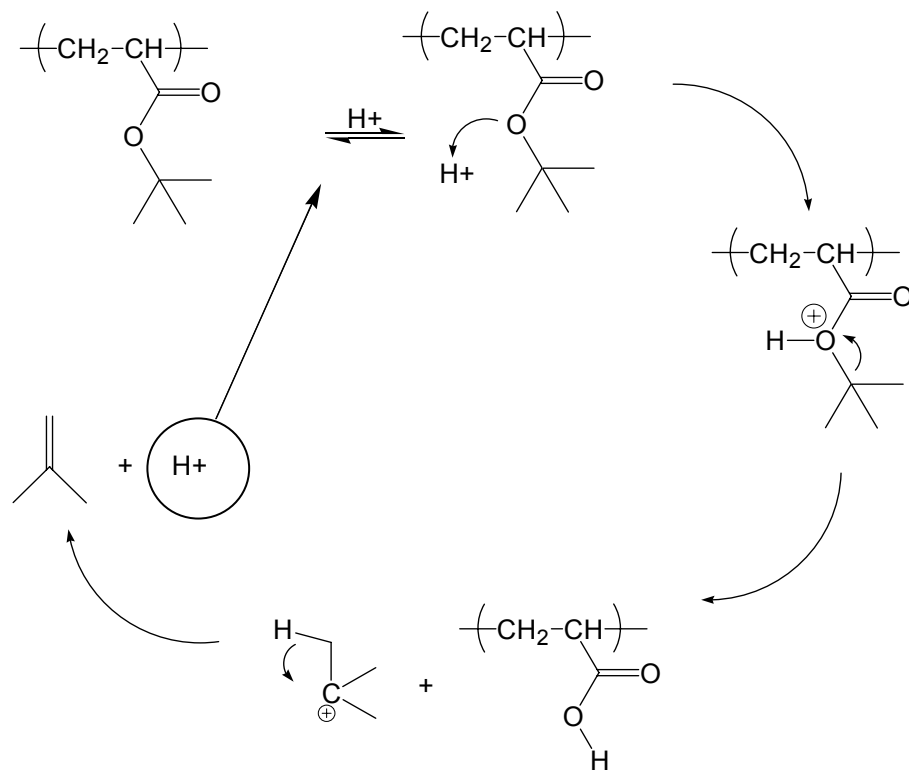


Figure 1.9. Mechanism of acid-catalyzed deprotection of poly(*tert*-butyl acrylate).

a PAB temperature above the  $T_g$ . A PAB temperature above the  $T_g$  is not possible for PHOST, as its  $T_d$  is in the same temperature range as its  $T_g$ .

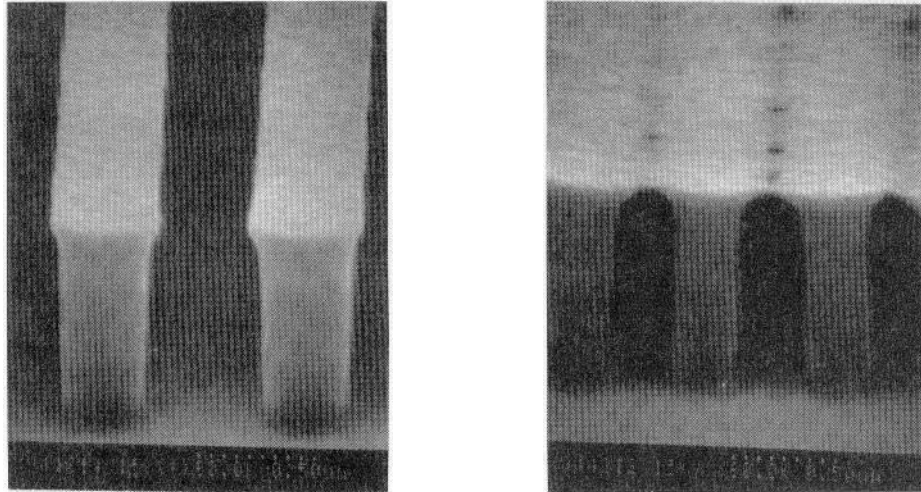


Figure 1.10. Lithographic images exhibiting T-topping, due to surface deactivation of the photoacid generator prior to exposure.<sup>9</sup>

The first commercially available IC materials made using 248 nm lithography had feature sizes of 350 nm.<sup>6</sup> Today, through the use of various resolution-enhancement techniques, including the use of an immersion fluid and interferometric exposure, 248 nm lithography has been demonstrated to produce images as small as 79 nm.<sup>10</sup> The IC industry continues to use 248 nm lithography, but the smallest linewidths are now made using 193 nm lithography. Earlier this year, Intel announced the commercial production of flash memory products using 90 nm technology, manufactured using 193 nm lithography.<sup>11</sup>

### 1.3.3. 193 nm Microlithography

The state-of-the-art of lithography, using a 193 nm ArF excimer laser, cannot use the same resists used for 248 nm lithography: the aromatic portion of phenolic resists absorbs too

strongly at 193 nm for use at this wavelength.<sup>12</sup> Two polymer platforms have been commercialized as resists for this wavelength: methacrylate-based resists and cyclic olefin-

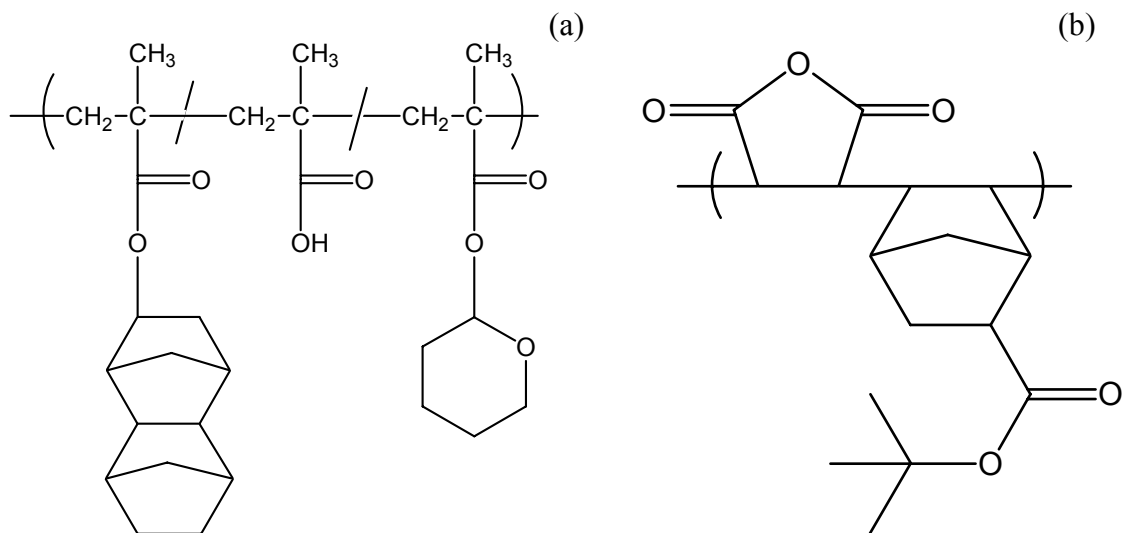


Figure 1.11. Examples of the polymer platforms for 193 nm lithography: acrylates (a) and COMA (b).

maleic anhydride (COMA) resists. Methacrylate-based resists have extremely low absorbance at 193 nm. However, since the aromatic group – used for etch resistance in phenolic resists – is absent, etch resistance must be attained through pendant alicyclic groups, such as norbornyl or adamantyl groups (Fig. 1.11). While this has successfully been shown to increase the etch resistance of these polymers, post-etch surface roughness and insufficient etch resistance continue to hinder these materials.<sup>13,14</sup> As seen in the ESCAP resist for 248 nm lithography, *t*-butyl (meth)acrylate can easily be incorporated into this platform as the contrastable group. Other acid sensitive groups have been investigated for contrast in methacrylate resists, especially groups with a lower activation energy to acid cleavage, such as the tetrahydropyranyl group in Fig. 1.11(a). Such groups allow for lower PAG loading, lower PEB temperatures, and lower exposure doses. A low sensitivity, as indicated by the



exposure dose needed, is beneficial to the lifetime of the exposure tool. Methacrylic acid may also be included in a methacrylate resist to balance the hydrophobicity of the resist. It is desirable for the resist to be somewhat hydrophobic to exclude water from the film. However, the resist must also be somewhat hydrophilic so the developer can wet the material. The  $\alpha$ -methyl group of methacrylates impart a significant barrier to rotation along the backbone, which enables this class of photoresist to have a sufficiently high  $T_g$ , typically above 110 °C. The design flexibility of acrylate resists has allowed the incorporation of etch resistant and acid-cleavable moieties, and further improvements to this platform can easily be attained. The other major polymer platform commercialized as a 193 nm photoresist is COMA. Resists based on COMA are free-radically polymerized copolymers of maleic anhydride with a cyclic olefin. The cyclic olefins typically used are norbornenes or tetracyclododecenes. The electron-rich olefin of norbornene forms a perfectly alternating copolymer with the electron-poor olefin of maleic anhydride, resulting in a 50/50 mol composition of the two monomers. While these materials lack the excellent transparency of acrylic resists, their moderate transparency is offset by a high RIE resistance.<sup>15</sup> The highly strained backbone of these materials imparts a high  $T_g$ , typically greater than 180 °C, if it can be measured below the decomposition temperature.<sup>16</sup> Imagable groups in COMA resists are typically pendant to the cyclic olefin, and are otherwise identical to the contrastable groups of acrylate resists. The acid anhydride of COMA resists is highly susceptible to hydrolysis, thus these materials must be protected from water and have a limited shelf life.<sup>14,17</sup>

The 193 nm lithography tool was introduced in manufacturing at the sub-200 nm node. Current research has demonstrated images as small as 31 nm, with the aid of a sapphire prism for solid immersion lithography of a high-refractive index resist, and interference exposure of

a phase grating mask.<sup>18</sup> In order to achieve smaller feature sizes beyond the limits of 193 nm lithography, the IC industry has several potential paths. The forerunner of these options is an extension of the current 193 nm lithography, using a high NA immersion fluid. Other contenders include 157 nm, imprint, e-beam, and EUV lithographies.

#### 1.4. Potential future lithographic technologies and related materials

##### 1.4.1. 193 nm Immersion lithography

Immersion 193 nm (193i) lithography uses a fluid placed between the photoresist and the final lens during exposure. Akin to oil-immersion microscopy used in biology, 193i uses a high-refractive index (NA) fluid to effectively shorten the exposure wavelength to achieve a higher resolution. A greater depth of focus (DOF) is also attained, as the angle of propagation of the light between the final lens and the resist ( $\theta$ ) is smaller in an immersion fluid than in air, resulting in the light being less sensitive to vertical displacement of the resist (Fig. 1.12).<sup>19</sup> The leading fluid of choice for 193i lithography is water, with a very low absorption coefficient at 193 nm and an index of refraction of 1.44. However, major challenges still exist in the implementation of water-based immersion lithography, as the absorption coefficient of water is highly sensitive to impurities. Also, microbubble formation can distort the image as it is patterned onto the resist.<sup>20,21</sup> Minor fluctuations in the flow rate or temperature of the immersion fluid as it is passed over the wafer could also impact imaging performance. Changes in flow rates could introduce inaccuracies in the position of the wafer stage, leading to inaccurate overlay of the images. Temperature fluctuations in the immersion fluid could potentially distort images, as well. Another major concern with the implementation of 193i has been the leaching of small photoresist components into the

immersion fluid.<sup>22</sup> The leaching of a PAG could deactivate the top portion of the photoresist, and any organic contaminant in contact with the final lens could foul or damage the lens.

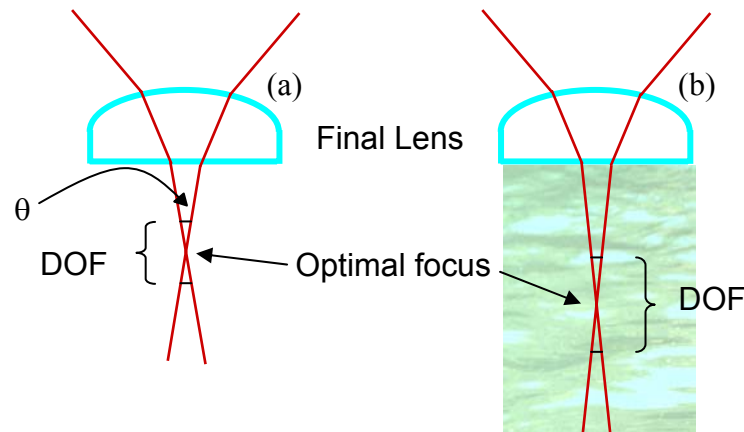


Figure 1.12. DOF advantages in immersion lithography. Red lines indicate the light path. In the presence of a high NA fluid (b), the light is diffracted more, resulting in a greater depth of focus.

Despite these challenges to 193i lithography, it is the leading choice for next generation lithography. The resolution enhancement possible through the use of an immersion fluid can be attained with the current photoresists used for dry 193 nm lithography. Specifically, the methacrylate platform of 193 nm dry lithography resists has performed remarkably well, though modifications will be needed in order to optimize imaging performance.<sup>21</sup> Such modifications include increasing the hydrophobicity of the resist to minimize water uptake into the film, and compensating for confinement effects in very thin films (<80 nm), such as diffusion and glass transition temperature changes.<sup>23</sup>

#### 1.4.2. 157 nm (Immersion) lithography

Once the leading candidate of the IC industry to succeed 193 nm lithography, dry 157 nm lithography has since been largely abandoned. Much exciting, active research in the search for viable photoresists at this node was accomplished between the years 2000 – 2003. However, with Intel's announcement to eliminate its 157 nm lithography program in 2003, and the 2004 update of the International Technology Roadmap for Semiconductors (ITRS) which sidelined 157 nm dry technology in favor of 193 nm immersion,<sup>5</sup> many researchers have since turned their focus to other, more viable technology nodes. The major shortcoming of 157 nm lithography was economics. This technology had high costs in the development of photoresists, which must be highly fluorinated to attain acceptable absorbance. The CaF<sub>2</sub> lenses needed were also quite expensive and difficult to manufacture and maintain defect-free. Another issue related to the implementation of 157 nm lithography has been the development of a robust, transparent pellicle. The pellicle is a thin polymer film mounted near the mask to prevent any particulate contaminants from depositing on the mask. The pellicle is mounted at a sufficient distance from the mask so that any particulates on the pellicle will be sufficiently out of focus from the mask, and will not distort the projected image. Nitrocellulose and Teflon® based membranes are used for 193 nm lithography, but no leading candidates have yet emerged for 157 nm polymeric soft pellicles. Current “high-performance” soft pellicles exhibit low stability toward 157 nm exposure, up to 20 J/cm<sup>2</sup>, but a pellicle with a lifetime an order of magnitude greater is needed for practical use.<sup>24</sup> Hard pellicles made of modified fused silica have been explored as a temporary solution, though these pellicles are quite expensive, and are subject to stringent requirements, as the exposure beam must pass through the silica plate pellicle. Particularly troubling is the unresolved

issue of flatness of the pellicle with respect to the reticle. Edge distortions and overlay issues resulting from this problem must be resolved through improvements in pellicle mounting techniques. In light of less-expensive manufacturing options, 157 nm lithography could not survive. However, 157 nm lithography still has potential to be used as a future immersion technology, and is projected for introduction at the 32 nm node, beyond the expected resolution limit of 193i lithography.<sup>25</sup> The advantages and issues discussed for 193i lithography also apply to 157i lithography. The choice of immersion fluid for 193i lithography cannot be applied to 157i lithography, as water absorbs 157 nm light too strongly. Instead, perfluoropolyethers have been investigated as potential immersion fluids.<sup>26</sup> Fortunately, all the work in designing photoresists for dry 157 nm lithography has not gone to waste, as these resists can also be used toward the immersion technology. Some of the leading 157 nm resist platforms include norbornene addition polymers, tetrafluoroethylene (TFE) copolymers, and trifluoromethacrylates (Fig. 1.13).

Norbornene-based polymers, synthesized utilizing a late transition metal catalyst, have been examined as 157 nm photoresists. This catalytic synthesis is known to yield polymers with the norbornene unit intact, which results in a highly strained backbone, which easily provides glass transition temperatures around 150 °C. In addition, the alicyclic groups on the polymer backbone provide plasma etch resistance, as the carbon/hydrogen ratio is greater than in a linear material.<sup>27</sup> Moderate 157 nm absorbances have been reported for materials of this platform.<sup>28</sup> The absorbance has been shown to be sensitive to fluorine location and content, especially on the norbornene unit. Unfortunately, fluorine directly bound to the norbornene has been shown to inhibit polymerization. Figure 1.13(a) is an example of a copolymer that exhibited a particularly low absorbance for these materials, at  $2.17 \mu\text{m}^{-1}$  at

157 nm. Ideally, the absorbance of a photoresist should be less than  $1.0 \mu\text{m}^{-1}$  at the exposure wavelength, so further work is needed to make these materials compliant for 157 nm lithography.

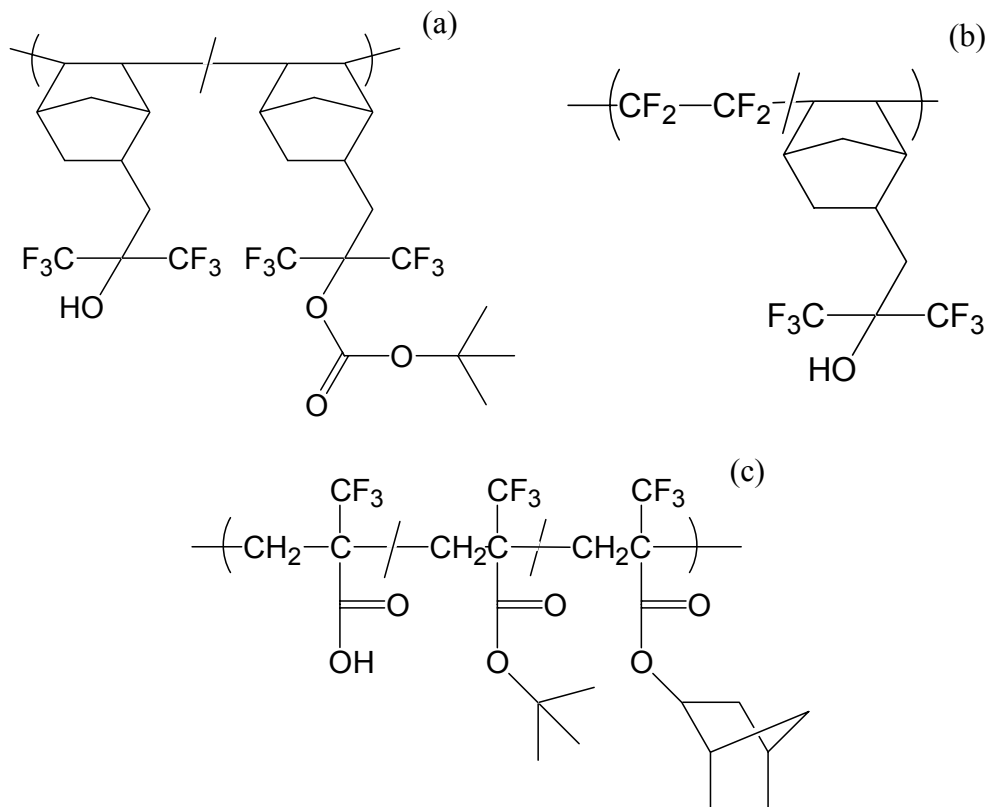


Figure 1.13. Several of the leading photoresist platforms developed for 157 nm microlithography: (a) norbornene addition polymers, (b) TFE copolymers, and (c) trifluoromethacrylates.

Much research has also centered on the investigation of copolymers of TFE with alicyclic monomers. A fluorinated backbone is advantageous to both lowering the DUV absorbance and increasing the plasma etch resistance.<sup>29</sup> Comonomers must be included in the TFE-based polymer to break up the crystallinity of PTFE and to incorporate a contrastable group. Coupling an electron-poor olefin, such as TFE, with an electron-rich olefin, such as that of norbornene, is a useful match for making an alternating copolymer by free radical

polymerization.<sup>29</sup> In practice, though, these copolymers do not always result in perfectly alternating copolymers with the expected 50/50 monomer incorporation.<sup>30,31</sup> These materials exhibit excellent absorbance at 157 nm. However, the absorbance was found to be a strong function of the endgroup identity, as the molecular weights of these polymers tend to be low (~5000 g/mol).<sup>29</sup> For example, the polymer shown above in Figure 1.13(b) was shown to have an absorbance as low as  $0.4 \mu\text{m}^{-1}$  when polymerized with a fluorinated initiator, but the absorbance increased to  $0.9 \mu\text{m}^{-1}$  when polymerized with a hydrocarbon initiator.<sup>29</sup> The  $T_g$  of this class of polymers (140 – 150 °C, typically) is suitable for thermal lithographic processing.<sup>30</sup> The dry etch rate of poly(TFE/NB) is slightly faster than novolac under oxygen plasma conditions, but increases with the incorporation of functional norbornenes.<sup>31</sup> While this class of polymers has potentially excellent properties as 157 nm photoresists, the synthesis of these polymers is somewhat challenging and is not as flexible as the synthesis of acrylates. TFE is a highly explosive, toxic, reactive gas<sup>32</sup> and must be polymerized in a high pressure stainless steel cell. In addition, a mixture of products is often obtained when phase separation occurs during polymerization.

Trifluoromethacrylate copolymers combine the ease of processing acrylates with the low absorbance obtained from fluorine near the polymer backbone. Work on homopolymers and copolymers of these materials has been described as early as 1978, though for e-beam resist applications.<sup>33</sup> Renewed interest in these polymers for 157 nm lithography has produced a number of novel materials, including a fluorinated analog to the 248 nm ESCAP resists,<sup>34</sup> and a methacrylate copolymer containing pendant polyhedral oligomeric silsesquioxane (POSS) groups.<sup>35</sup> Both of these classes of materials exhibited high glass transition temperatures (up to 160 °C). The fluorinated ESCAP had a relatively high absorbance at 3.2

–  $4.2 \mu\text{m}^{-1}$ .<sup>34</sup> The POSS terpolymer with *t*-butyltrifluoromethacrylate and trifluoromethacrylic acid was primarily designed to optimize etch resistance.<sup>35</sup> Even with 20% overetching, the POSS copolymer exhibited excellent etch resistance and low roughness (0.3 nm). Unfortunately, this material exhibited an unacceptably high absorbance at 157 nm, at  $4.5 - 5.5 \mu\text{m}^{-1}$ . This resist could be imaged using 157 nm lithography, and 100 nm lines/spaces were observed. Current trifluoromethacrylate polymers have mixed properties as 157 nm resists, though the ease of polymerization should facilitate ameliorations in less desirable properties.

As an analogy to 193i photoresists, the design of 157 nm resists specifically for immersion lithography only requires fine-tuning of existing materials to minimize interaction with the immersion fluid. An ESCAP-type resist formulated for 157 exposure, LUVR 99071, was found to neither swell nor dissolve into a PFPE immersion fluid.<sup>36</sup> Imaging with 157 nm lasers has produced images as small as 30 nm half-pitch dense lines, using interferometric exposure through an immersion layer.<sup>37</sup>

#### 1.4.3. Imprint lithography

Recent interest in imprint lithography has demonstrated the capability to replicate defect-free linewidths as small as 30 nm, with the potential to replicate 10 nm lines.<sup>38</sup> Several approaches to realizing this technology share the common use of a template to mechanically transfer an image into or onto an etch-resistant barrier material coated onto substrate. Templates are made from either rigid materials, such as quartz, or cross-linked elastomers, such as PDMS. Imprint lithography has an incredible capability of replicating large volumes of defect-free images, at a fraction of the cost of optical lithography. The ultimate resolution is not limited by optics, as is traditional lithography, although the ultimate resolution is



limited by the resolution capabilities of other technologies used for making the template. The templates (or master templates, for elastomeric templates) are typically patterned using e-beam lithography, as discussed in the following section. Another limitation experienced with imprint lithography has been difficulties in replicating patterns with varied feature densities, especially in a resist material with a moderate viscosity.<sup>39</sup> Image deformation can be caused by: (a) insufficient flow of the resist from large features, (b) insufficient flow of the resist, coupled with deformation of the template, and (c) inadequate penetration of resist into small, dense features (Fig. 1.14). Further details of the leading imprint technologies are described.

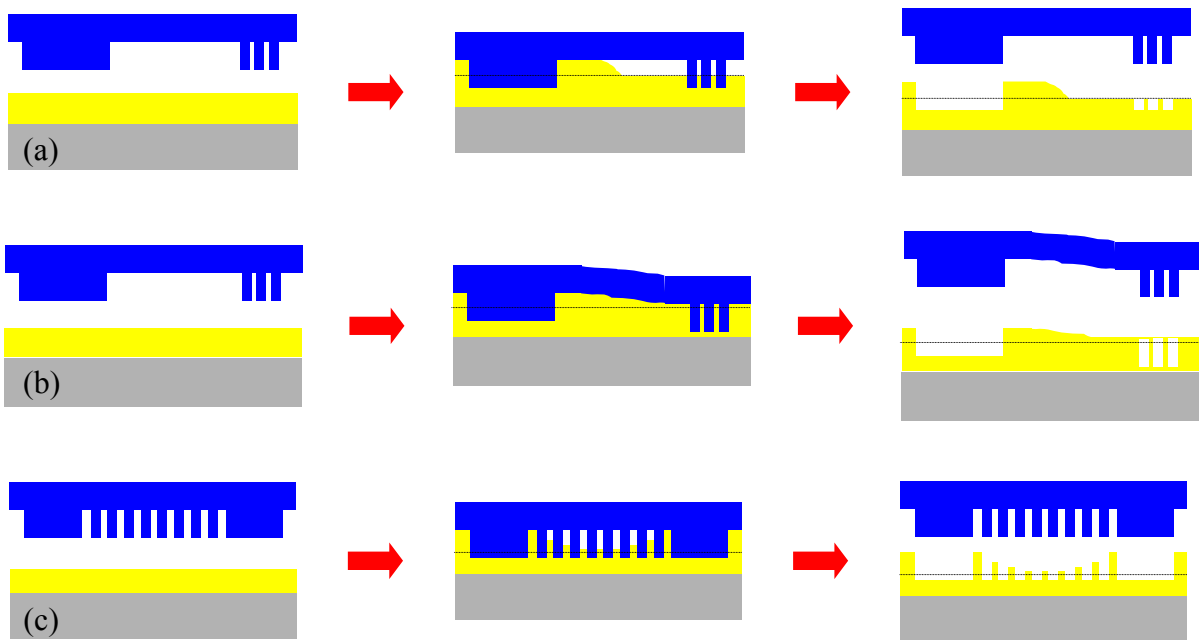


Figure 1.14. Pattern replication defect mechanisms in imprint lithography: (a) insufficient flow of the resist from large features, (b) insufficient flow of the resist, coupled with deformation of the template, and (c) inadequate penetration of resist into small, dense features. Dashed lines indicate original film height of etch barrier.<sup>39</sup>

Nanoimprint lithography (NIL) and step-and-flash imprint lithography (SFIL) are two established imprint methods for the transfer of nano-scale images, using rigid templates.<sup>40</sup> In

these two processes, the template is coated with a release layer to ensure complete release of the patterned etch barrier. The release layer is often fluorinated; such coatings are known to have very low surface tension. In addition, there are several important properties needed for an effective etch barrier.<sup>41</sup> First, adhesion to the underlying substrate is important. Should the etch barrier have poor adhesion, a pattern will collapse or lift off with removal of the template. The kinetics of imprinting must be fast, to ensure image formation in a reasonable time period. The etch barrier must exhibit low shrinkage to prevent CD changes in the etched image. As with photoresists in traditional optical lithography, a high etch selectivity must exist between the etch barrier and the substrate to be etched. Finally, it is desirable for the etch barrier to completely wet the template pattern, but have excellent release properties, as well. Once patterned, a thin film of the etch barrier will remain over the entire substrate surface. This film can be removed from relief areas with a short halogen breakthrough etch, then the substrate is exposed for subsequent pattern transfer by oxygen etch.<sup>41</sup> Although this adds an extra etch step, the residual etch barrier film serves to protect the template from damage by contact with the hard substrate. These two methods differ in the mechanism of patterning in the etch barrier. In NIL, a thermopolymer, such as PMMA, is heated above its glass transition temperature in order to stamp the template into the softened material.<sup>42</sup> Subsequent cooling of the etch barrier locks in the relief image of the template. Uneven mass flow of the thermopolymer, especially in non-periodic patterns, is a continuing issue for this method.<sup>39,43</sup> The SFIL method differs from NIL by replacing the thermopolymer etch barrier with a photocurable monomer mixture. This monomer mixture consists of a free-radical initiator dissolved in a silylated monomer. The template is pressed into the monomer mixture, and irradiated with broadband UV light. The light activates the initiator, which

polymerizes and crosslinks the monomer. The lower viscosity of the monomer mixture, as opposed to the heated polymer resist in NIL, allows for faster flow and better image fidelity. A single SFIL template has been demonstrated to replicate defect-free images more than 500 times, indicating a very robust template and process.<sup>40</sup>

Interesting work has been accomplished using elastomeric templates, as well. Microcontact printing uses a PDMS template, coated with a alkylthiol “ink” to imprint images as small as 1  $\mu\text{m}$ . The template is stamped onto a gold-coated substrate, to which the thiol groups adhere. The alkylthiol serves as a wet etch barrier, while the exposed gold is removed. Subsequent dry etching transfers the pattern into the substrate. Conversely, this method has also been used to stamp gold from a GaAs template onto an alkylthiol-coated substrate to resolve 75 nm images.

In an effort to combine the advantages of a rigid template with the advantages of an elastomeric template, PFPE stamps have recently been investigated.<sup>44</sup> The process for replicating images with these stamps is identical to that of SFIL. PFPE templates exhibit the robustness and solvent resistance seen in rigid templates, as well as the gas permeability and ease of fabrication of soft templates. Unlike NIL and SFIL, no release layer is needed to prevent delamination or damage to the patterned etch barrier material. The surface energy of PFPE is  $\sim 12$  mN/m, which is comparable to that of the release layer coated onto rigid quartz masks. Perfluoropolyether templates have also been shown to completely eliminate the residual film of the etch barrier, which eliminates the additional etch step of NIL and SFIL. The template protection provided by the residual film layer in the latter methods is unnecessary when using a high modulus elastomeric stamp, such as PFPE, that is less

susceptible to damage. With these novel PFPE materials, the smallest resolution obtained so far has been 2 nm in single-walled nanotubes.<sup>45</sup>

The replication of patterns for microlithography using imprint technologies has great potential to provide submicron images, with much lower expenditures than with the current optical lithography techniques. At present, the only resolution limit for this technique is the limitations of the complementary imaging technologies required to generate template masters.

#### 1.4.4. Electron beam lithography

The greatest strength of e-beam lithography is its very high resolution. In fact, the templates for 30 nm NIL images described in the previous section were made using e-beam lithography.<sup>38</sup> Structures as small as 10 nm are routine, and e-beam lithography has been used to construct AuPd electrodes with a 4 nm gap!<sup>40</sup> E-beam lithography can be carried out by either a projection or direct-write process.<sup>46</sup> In projection e-beam, a relatively large beam is passed through a mask with the desired pattern, and focused through the objective lens onto the substrate. In the commonly used direct-write process, no mask is used. Instead, the beam is only focused through the objective lens, and the beam spot size determines the minimum feature size. A high-energy electron beam is needed to obtain a highly focused spot size. Typical acceleration voltages for the beam are 25 – 100 keV. The drawback of using high voltages, though, is the inelastic scattering of electrons, which could expose the resist as far as 1  $\mu\text{m}$  from the primary beam.<sup>47</sup> Known as the proximity effect, this can be reduced through the use of a lower-energy beam—but at the expense of resolution.<sup>40</sup> Other solutions include the use of retarding optics to slow the beam as it approaches the target, or the use of a miniaturized beam column. Of course, a direct-write process, such as e-beam, is

inherently slow. The rate of writing a pattern using e-beam lithography has held this technique back from large-scale manufacturing of integrated circuits. The greatest promise for e-beam in IC manufacturing will be in conjunction with imprint lithography, which can provide high-throughput replication.

The photoresists for e-beam must exhibit very high resolution, so that the imaging capability of this tool can be attained. In addition, as the writing method is quite slow, a high speed (low sensitivity) resist is needed to avoid slowing the process further. Other important properties are similar to the desired properties of a photoresist for optical lithography, including thermal stability and dry etch resistance. Both positive-tone and negative-tone resists have been developed for e-beam applications.<sup>46</sup> Poly(methylmethacrylate / methacrylic acid) is widely used as a positive tone resist for its excellent resolution (<10 nm).<sup>48</sup> The polymer undergoes chain scission when interacting with the electron beam. The lower molecular weight material then has a greater solubility in a developer solution. The sensitivity and etch resistance of this material are poor, although much improved over the homopolymer of MMA. Another positive-tone resist used is poly(1-butene sulfone). The perfectly alternating copolymer of sulfur dioxide and 1-butene will depolymerize when exposed to the e-beam. This polymer has a better sensitivity than poly(MMA / MAA), but with inferior resolution.<sup>49</sup> Recently, calixarenes have also been examined as positive-tone e-beam resists.<sup>50</sup> Calixarenes are small molecules that exhibit a glass transition temperature, and are a well-defined alternative to polymers. This resist, formulated and developed identical to a resist for optical lithography, could be imaged to 50 nm. The primary negative tone resist used for e-beam lithography is Shipley's SAL, which is a copolymer of glycidyl methacrylate and ethyl acrylate. In the presence of an electron beam, this polymer cross-

links to form a latent image that is insoluble in developer solution. SAL is more robust to changes in the critical dimension (bias) than seen in the PMMA copolymer resist, but it suffers from imaging defects such as scum, swelling, and bridging between features.

#### 1.4.5. EUV lithography / X-Ray lithography

Since the early 1980's, a substantial amount of research has been invested into the potential use of 13 nm light to form lithographic images.<sup>51</sup> This technology, uses soft x-rays, or "extreme ultraviolet" light at 13 nm, to pattern images into a photoresist film. The radiation is generated by either a laser bombarding a target, or a Xe gas discharge plasma. The latter source has been used in various  $\alpha$ -tools for EUV.<sup>52,53</sup> The radiation is collected and filtered through a series of reflective mirrors, then illuminates a reflective reticle, and is finally focused and reduced onto a resist-coated wafer.<sup>54</sup> As a long extension of optical lithography, EUV can be seen as the ultimate reduction in wavelength to attain smaller images. A large depth of focus (DOF) is expected for EUV imaging, as high NA tools are not needed to attain <100 nm images. DUV lithography tools have required increases in NA in order to decrease resolution, according to the Rayleigh equation (Eq. [1]), however, this is to the detriment of the DOF, where:

$$\text{DOF} = (k_1 \times \lambda) / (\text{NA})^2. \quad [2]$$

The DOF determines the process latitude for imaging. A greater DOF allows for less-stringent requirements to image the desired CD and higher aspect ratio images.<sup>54</sup> When using  $\lambda = 13$  nm to image 100 nm lines, a NA of 0.1 – 0.3 is sufficient, while imaging 100 nm lines with  $\lambda = 193$  nm requires NA to be at least 0.65, with a significant reduction in DOF.<sup>52</sup> Production of ICs using EUV is expected no earlier than the 32 nm node. This delay

is advantageous to EUV technology, as substantial engineering issues remain unresolved.<sup>54</sup> The design of an inexpensive, reliable, high-intensity radiation source for EUV continues to be the subject of much research.<sup>55</sup> The manufacture of the aspherical mirrors is difficult and accurate metrology techniques have not been well-developed. Furthermore, the mirrors require precise interference coatings with high reflectivity with <3 nm precision.<sup>54</sup> Currently, Mo/Si composites are used to achieve 50-60 % reflectivity. At this rate, few mirrors can be used in EUV lithography before the radiation intensity is too low for effective imaging. As another shortcoming, most liquids, solids, and gases will absorb or scatter 13 nm radiation. This requires the entire stepper to be maintained under ultra high vacuum (<10<sup>-6</sup> mbar) conditions.<sup>52</sup> Such conditions greatly complicate normal maintenance operations, and increase tool downtime. Furthermore, the photoresists required for this technology, need continued development. Active research for adequate photoresists has focused on needs for low absorbance at 13 nm, low sensitivity, and low line edge roughness (LER). Other requirements include good chemical stability and high thermal stability. Photoresist suppliers have approached the design of EUV resists through the modification of existing DUV resists. For example, Rohm and Haas Electronic Materials manufactures an ESCAP-type resist, EUV-2D, for EUV applications.<sup>56</sup> Experimentally determining the absorbance of a photoresist candidate has proven difficult, with the lack of a reliable light source. Recent work at Intel determined the absorbance of EUV-2D by two reflective methods, obtaining good agreement with theoretical modelling, at 4.20  $\mu\text{m}^{-1}$  (1.83  $\mu\text{m}^{-1}$ , base 10).<sup>57</sup> The absorbance is greater than desirable, but it serves as a good starting point for optimized resist formulations. Other EUV resist designs have started from the photoabsorption cross-section of individual atoms at 13.4 nm (92.7 eV).<sup>58,59</sup> This has led to novel resist designs

incorporating carborane units on a vinyl backbone and polysilanes, with acid sensitive and solubilizing groups.<sup>59</sup> The sensitivity of EUV resists must be low (2-5 mJ/cm<sup>2</sup>) in order to maximize wafer throughput.<sup>60</sup> The requirement for low LER ( $3\sigma = 1.1$  nm, 32 nm node) promotes imaging performance.<sup>53</sup> Poor LER could lead to local CD variations or changes in the effective gate length of the device. Resists have been successfully developed to achieve either of these requirements, but not both. Brainard studied the relationship between these two parameters to determine that LER follows a Poisson (random noise) distribution:

$$\text{LER} \propto (\text{Dose})^{-1/2}, \quad [3]$$

though further understanding of why this occurs and how to minimize both LER and dose is ongoing.<sup>61</sup>

The challenges to EUV lithography remain formidable, both in the chemistry and engineering of this technology, despite many years of research. In light of more reliable and economical alternatives for NGL, integration of EUV lithography into manufacturing may be pushed back another generation or two, or eliminated entirely.

### 1.5. Research objectives

With the continual drive for advanced integrated circuits, many materials research opportunities exist. In the present body of work, we have set out to design photoresists for next-generation imaging. The resists studied herein contain norbornyl backbones, which are expected to enhance the etch resistance and elevate the glass transition temperatures of the resultant polymers. Furthermore, these resists have been designed to incorporate highly fluorinated groups (up to 58 wt% of the polymer) in an effort to decrease optical absorbance at the DUV wavelengths used in modern imaging. These highly fluorinated materials also



enable solubility of the polymers in condensed carbon dioxide. Chapter Two will describe how compressed carbon dioxide (CO<sub>2</sub>) can be used to prevent image collapse during development, specifically, in reference to the photoresists we have designed for this purpose. Chapter Three discusses a multilayer resist approach, and related resist materials designed to dramatically increasing the plasma etch resistance through the incorporation of a silicon-containing monomer. Finally, Chapter Four will delve into possible future directions for this work.

## 1.6. Conclusion

Although Moore's Law was written over 40 years ago, the microelectronic industry has continually accelerated the research needed to keep up with this prediction of smaller and faster devices. With each current generation of device size, there has been an ongoing prediction for a failure to achieve the requirements for 2-3 device generations ahead. One researcher said this has almost become a running joke.<sup>62</sup> There certainly will be a limitation to the fabrication of advanced devices. However, the short summary of lithographic advances and future challenges described here gives a glimpse of the possibilities for future generations of devices that may be realized.

## 1.7. References

- 1) McAdams, C. L.; Flowers, D.; Zannoni, L.; DeSimone, J. M.; Hoggan, E.; Carbonell, R. *All CO<sub>2</sub>-processed fluorine-containing photoresist materials*; University of North Carolina: Chapel Hill, NC, April 23, 2001.
- 2) Moore, G. E., *Electronics* **1965**, *38*, 1-4.
- 3) intel.com.
- 4) Levinson, H. J., *Principles of Lithography*; SPIE Press: Bellingham, WA, 2001; p373.
- 5) *International Technology Roadmap for Semiconductors. 2004 Update: Lithography*; public.itrs.org.
- 6) Levinson, H. J.; Arnold, W. H., Optical Lithography. In *Microlithography, Micromachining, and Microfabrication*, Rai-Choudhury, P., Ed. SPIE Press: Bellingham, WA, **1997**; *1*, 11-138.
- 7) Stewart, M. D.; Patterson, K.; Somervell, M. H.; Willson, C. G., *J. Phys. Org. Chem.* **2000**, *13*, 767-774.
- 8) Ito, H., *J. Polym. Sci. A* **2003**, *41*, 3863-3870.
- 9) Levinson, H. J., *Principles of Lithography*; SPIE Press: Bellingham, WA, 2001; p78.
- 10) Smith, B. W.; Fan, Y.; Jianming, Z.; Bourov, A.; Zavyalova, L.; Lafferty, N.; Cropanese, F.; Estroff, A., *J. Vac. Sci. Technol. B* **2004**, *22*, 3439-3443.
- 11) Intel Press Release: Intel discloses new NOR flash memory technologies, Sets stage for 2005 [http://www.intel.com/pressroom/archive/releases/20050302net\\_a.htm](http://www.intel.com/pressroom/archive/releases/20050302net_a.htm).
- 12) Pasini, D.; Klopp, J. M.; Frechet, J. M. J., *Chem. Mater.* **2001**, *13*, 4136-4146.
- 13) Kaimoto, Y.; Nozaki, K.; Takechi, S.; Abe, N., *Proc. SPIE* **1992**, *1672*, 66-73.
- 14) Kajita, T.; Nishimura, Y.; Yamamoto, M.; Ishii, H.; Soyano, A.; Kataoka, A.; Slezak, M.; Shimizu, M.; Varanasi, P. R.; Jordahamo, G.; Lawson, M. C.; Chen, R.; Brunsvold, W. R.; Li, W.; Allen, R. D.; Ito, H.; Truong, H.; Wallow, T., *Proc SPIE (Adv. Resist Tech. Proc.)* **2001**, *4345*, 712-724.
- 15) Uedono, A.; Ohdaira, T.; Suzuki, R.; Mikado, T.; Fukui, S.; Kimura, S.; Miyamoto, H.; Nemoto, H., *J. Polym. Sci. B* **2004**, *42*, 341-346.
- 16) Amblard, G.; Byers, J.; Domke, W.-D.; Rich, G.; Graffenburg, V.; Patel, S.; Miller, D.; Perez, G., *Proc SPIE (Adv. Resist Tech. Proc.)* **2000**, *3999*, 32-50.

- 17) Dammel, R. R.; Bae, J.-B.; Kim, W.-K.; Kudo, T.; McKenzie, D.; Padmanaban, M.; Rahman, M. D., *PMSE Prepr.* **2001**, *84*, 283.
- 18) Smith, B. W.; Fan, Y.; Slocum, M.; Zavyalova, L., *Proc SPIE (Opt. Microlith.)* **2005**, *5754*, 141-147.
- 19) Rothschild, M.; Bloomstein, T. M.; Kunz, R. R.; Liberman, V.; Switkes, M.; Palmacci, S. T.; Sedlacek, J. H. C.; Hardy, D.; Grenville, A., *J. Vac. Sci. Technol. B* **2004**, *22*, 2877-2881.
- 20) (a) Nakano, H.; Hata, H.; Takahashi, K.; Arakawa, M.; Chibanan, T.; Honda, T.; Chiba, K.; Mori, S., *Proc SPIE (Opt. Microlith.)* **2005**, *5754*, 693-700; (b) DeBisschop, P.; Erdmann, A.; Rathsfeld, A., *Proc SPIE (Opt. Microlith.)* **2005**, *5754*, 243-253.
- 21) Owa, S.; Nagasaka, H., *Proc SPIE (Opt. Microlith.)* **2003**, *5040*, 724-733.
- 22) Taylor, J. C.; LeSuer, R. J.; Chambers, C. R.; Fan, F.-R. F.; Bard, A. J.; Conley, W. E.; Willson, C. G., *Chem. Mater.* **2005**, *17*, 4194-4203.
- 23) Dammel, R. R.; Houlihan, F. M.; Sakamuri, R.; Rentkiewicz, D.; Romano, A., *J. Photopolym. Sci. Technol.* **2004**, *17*, 587-602.
- 24) Ronse, K.; DeBisschop, P.; Goethals, A. M.; Hermans, J.; Jonckheere, R.; Light, S.; Okoroanyanwu, U.; Watso, R.; McAfferty, D.; Ivaldi, J.; Oneil, T.; Sewell, H., *Microelectron. Eng.* **2004**, *73-74*, 5-10.
- 25) Fujii, K.; Hagiwara, T.; Matsuura, S.; Ishimaru, T.; Matsubara, Y.; Wakamiya, W., *Proc SPIE (Opt. Microlith.)* **2005**, *5754*, 226-236.
- 26) Rothschild, M.; Bloomstein, T. M.; Fedynyshyn, T. H.; Liberman, V.; Mowers, W.; Sinta, R.; Switkes, M.; Grenville, A.; Orvek, K., *J. Fluorine Chem.* **2003**, *122*, 3-10.
- 27) Gokan, H.; Esho, S.; Ohnishi, Y., *J. Electrochem. Soc.* **1983**, *130*, 143-146.
- 28) Trinqué, B. C.; Chambers, C. R.; Osborn, B. P.; Callahan, R. P.; Lee, G. S.; Kusumoto, S.; Sanders, D. P.; Grubbs, R. H.; Conley, W. E.; Willson, C. G., *J. Fluorine Chem.* **2003**, *122*, 17-26.
- 29) Toriumi, M.; Ishikawa, T.; Kodani, T.; Koh, M.; Moriya, T.; Yamashita, T.; Araki, T.; Aoyama, H.; Yamazaki, T.; Furukawa, T.; Itani, T., *J. Vac. Sci. Technol. B* **2004**, *22*, 27-30.

- 30) Feiring, A. E.; Crawford, M. K.; Farnham, W. B.; Feldman, J.; French, R. H.; Leffew, K. W.; Petrov, V. A.; Schadt, F. L., III; Wheland, R. C.; Zumsteg, F. C., *J. Fluorine Chem.* **2003**, *122*, 11-16.
- 31) Zannoni, L. A. Fluoroolefin copolymerizations in supercritical carbon dioxide towards the development of a 157 nm photoresist. University of North Carolina, Chapel Hill, 2003.
- 32) *Material Safety Data Sheet for Tetrafluoroethylene*; 2001.
- 33) Ito, H.; Miller, D. C.; Willson, C. G., *Macromolecules* **1982**, *15*, 915-920.
- 34) Ito, H.; Okazaki, M.; Miller, D. C., *J. Polym. Sci. A* **2004**, *42*, 1506-1527.
- 35) Tegou, E.; Bellas, V.; Gogolides, E.; Argitis, P.; Eon, D.; Cartry, G.; Cardinaud, C., *Chem. Mater.* **2004**, *16*, 2567-2577.
- 36) Switkes, M.; Rothschild, M., *J. Vac. Sci. Technol. B* **2001**, *19*, 2353-2356.
- 37) Switkes, M.; Rothschild, M., *Proc SPIE (Opt. Microlith.)* **2002**, *4691*, 459-465.
- 38) Chou, S. Y.; Krauss, P. R.; Renstrom, P. J., *J. Vac. Sci. Technol. B* **1996**, *14*, 4129-4133.
- 39) Guo, L. J., *J. Phys. D: Appl. Phys.* **2004**, *37*, R123-R141.
- 40) Marrian, C. R. K.; Tennant, D. M., *J. Vac. Sci. Technol. A* **2003**, *21*, S207-S215.
- 41) Colburn, M.; Bailey, T.; Choi, B. J.; Ekerdt, J. G.; Sreenivasan, S. V.; Willson, C. G., *Solid State Technology* **2001**, *44*, 67-77.
- 42) Chou, S. Y.; Krauss, P. R.; Renstrom, P. J., *Appl. Phys. Lett.* **1995**, *67*, 3114-3116.
- 43) Scheer, H.-C.; Schulz, H.; Hoffmann, T.; Torres, C. M. S., *J. Vac. Sci. Technol. B* **1998**, *16*, 3917-3921.
- 44) (a) Rolland, J. P.; van Dam, M.; Hagberg, E. C.; Carter, K. R.; Quake, S. R.; DeSimone, J. M., *Polym. Prepr.* **2004**, *45*, 106-107; (b) Rolland, J. P.; Zhou, Z.; Kelly, J. Y.; Denison, G. M.; van Dam, M.; Hagberg, E. C.; Carter, K. R.; Quake, S. R.; DeSimone, J. M., *PMSE Prepr.* **2004**, *91*, 254-255; (c) Rolland, J. P.; Maynor, B. W.; Exner, A. E.; DeSimone, J. M., *PMSE Prepr.* **2005**, *92*, 393-394; (d) DeSimone, J. M.; Rolland, J. P.; Quake, S. R.; Schorzman, D. A.; Yarbrough, J.; van Dam, M. Photocurable perfluoropolyethers as patterned layers and solvent-resistant microfluidic devices containing the same. WO 2005030822, **2005**; (e) Rolland, J. P.; Hagberg, E. C.; Carter, K. R.; DeSimone, J. M., *Proc SPIE (Emer. Litho. Tech.)* **2005**, *5751*, 410-414.

- 45) Maynor, B., Personal communication, **2005**.
- 46) Tseng, A. A.; Chen, K.; Chen, C. D.; Ma, K. J., *IEEE Trans. Electr. Packag. Man.* **2003**, *26*, 141-149.
- 47) Heuberger, A.; Brunger, W., *Microelectron. Eng.* **1996**, *34*, 39-50.
- 48) Khoury, M.; Ferry, D. K., *J. Vac. Sci. Technol. B* **1996**, *14*, 75-79.
- 49) (a) Gozdz, A. S.; Carnazza, C.; Bowden, M. J., *Proc SPIE (Adv. Resist Tech. Proc.)* **1986**, *631*, 2-7; (b) Reichmanis, E.; Wilkins, Chemistry of Microelectronic Polymers. In *Microelectronic Polymers*, Htoo, M. S., Eds. Marcel Decker: New York, **1989**; 1-66; (c) DeSimone, J. M.; York, G. A.; McGrath, J. E.; Gozdz, A. S.; Bowden, M. J., *Macromolecules* **1991**, *24*, 5330-5339.
- 50) Chang, S. W.; Felix, N.; Yang, D.; Ramakrishnan, A.; Ober, C. K., *PMSE Prepr.* **2005**, *92*, 131-132.
- 51) Haelbich, R. P.; Silverman, J. P.; Grobman, W. D.; Maldonado, J. R.; Warlaumont, J. M., *J. Vac. Sci. Technol. B* **1983**, *1*, 1262-1266.
- 52) (a) Brunton, A.; Cashmore, J.; Elbourn, P.; Elliner, G.; Gower, M.; Grunewald, P.; Harman, M.; Hough, S.; McEntee, N.; Mundair, S.; Rees, D.; Richards, P.; Truffert, V.; Wallhead, I.; Whitfield, M., *Proc SPIE (Emer. Litho. Tech.)* **2004**, *5374*, 869-880.
- 53) Meiling, H.; Banine, V.; Kurz, P.; Harned, N., *Proc SPIE (Emer. Litho. Tech.)* **2004**, *5374*, 31-42.
- 54) Wolf, S., *Microchip manufacturing*; Lattice Press: Sunset Beach, CA, 2003; p375-376.
- 55) (a) Stamm, U.; Kleinschmidt, J.; Gaebel, K.; Birner, H.; Ahmed, I.; Bolshukhin, D.; Brudermann, J.; Chinh, T. D.; Flohrer, F.; Goetze, S.; Hergenhan, G.; Kloepfel, D.; Korobotchko, V.; Mader, B.; Muller, R.; Ringling, J.; Schriver, G.; Ziener, C., *Proc SPIE (Emer. Litho. Tech.)* **2004**, *5374*, 133-144; (b) Endo, A., *Proc SPIE (Laser Prec. Microfab.)* **2003**, *5063*, 269-273; (c) Schuermann, M. C.; Missalla, T.; Mann, K. R.; Kranzusch, S.; Klein, R. M.; Scholze, F.; Ulm, G.; Lebert, R.; Juschkin, L., *Proc SPIE (Emer. Litho. Tech.)* **2003**, *5037*, 378-388; (d) Hassanein, A.; Burtseva, T.; Brooks, J. N.; Konkashbaev, I. K.; Rice, B. J., *Proc SPIE (Emer. Litho. Tech.)* **2003**, *5037*, 358-369.
- 56) Brainard, R. L.; Henderson, C.; Cobb, J.; Rao, V.; Mackevich, J. F.; Okoroanyanwu, U.; Gunn, S.; Chambers, J.; Connolly, S., *J. Vac. Sci. Technol. B* **1999**, *17*, 3384-3389.

- 57) Chandhok, M.; Cao, H.; Yueh, W.; Gullikson, E.; Brainard, R.; Robertson, S., *Proc SPIE (Emer. Litho. Tech.)* **2004**, 5374, 861-868.
- 58) Ober, C. K.; Dai, J.; Yang, D.; Chang, S. W., *PMSE Prepr.* **2004**, 91, 140.
- 59) Ober, C. K.; Kwark, Y.-J.; Bravo-Vasquez, J.-P.; Dai, J.; Hamad, A., *PMSE Prepr.* **2004**, 90, 22.
- 60) Cao, H.; Roberts, J.; Dalin, J.; Chandhok, M.; Meagley, R.; Panning, E.; Shell, M.; Rice, B., *Proc SPIE (Adv. Resist Tech. Proc.)* **2003**, 5039, 484-491.
- 61) Brainard, R. L.; Trefonas, P.; Lammers, J. H.; Cutler, C. A.; Mackevich, J. F.; Trefonas, A.; Robertson, S. A., *Proc SPIE (Emer. Litho. Tech.)* **2004**, 5374, 74-85.
- 62) Mack, C. A., *Proc SPIE (Emer. Litho. Tech.)* **2004**, 5374, 1-8.

SINGLE-LAYER RESISTS FOR DEVELOPMENT IN COMPRESSED CO<sub>2</sub>

## 2. Single-layer resists for development in compressed CO<sub>2</sub>

### 2.1. Introduction

#### 2.1.1. Performance enhancement using compressed carbon dioxide

As the smallest lithographic images on a silicon wafer diminish, more transistors can be placed on the resultant integrated circuit in the same amount of space on the wafer. This also results in faster chips, as electronic signals have a shorter distance to travel. In the drive for smaller image sizes in microelectronic devices, the lithography industry has reached a point where the solvents traditionally used for development are potentially damaging to the images formed. Further, the high aspect ratio photoresist structures, needed to protect the underlying

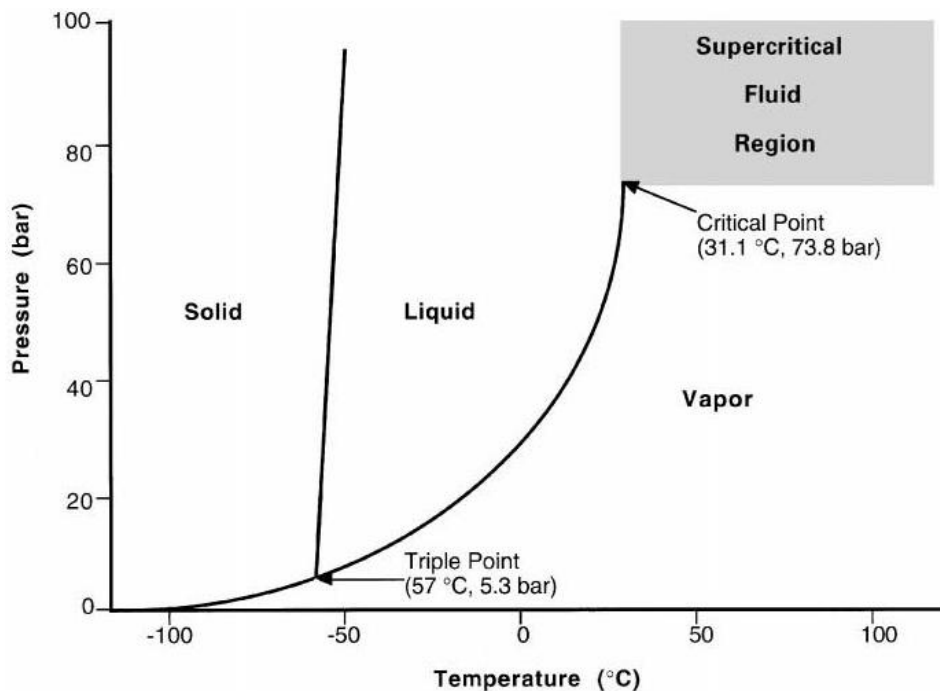


Figure 2.1. CO<sub>2</sub> phase diagram for changes in pressure and temperature.<sup>1</sup>

substrate, are susceptible to damage from the high surface tension of typical aqueous developers. The use of a more gentle solvent, such as condensed carbon dioxide (CO<sub>2</sub>), has been shown to alleviate this problem.<sup>2-4</sup> Interest in the use of CO<sub>2</sub> as an alternative,



environmentally benign solvent stems from its low viscosity, low surface tension and high diffusivity compared to other solvents.<sup>5</sup> The high diffusivity of CO<sub>2</sub> ensures complete wetting of the images in a microelectronic device, while the low viscosity and low surface tension prevents the image collapse observed in high aspect ratio structures developed using traditional aqueous-based development solutions. Supercritical CO<sub>2</sub> is readily accessible, as its critical point is at moderate conditions: 73.8 bar and 31.1 °C. Furthermore, liquid CO<sub>2</sub> is attained at even lower temperatures and pressures (Fig. 2.1). Carbon dioxide has been successfully used to develop resists in conjunction with surfactants in order to remove aqueous-based developers without causing image collapse.<sup>2</sup> It has also been used in the absence of aqueous developer to obtain residue-free, high aspect ratio images.<sup>4</sup> Post-etch stripping has also been accomplished with CO<sub>2</sub>-philic resists.<sup>6</sup> Carbon dioxide is an environmentally benign and easily recyclable alternative to the solvents currently used in microlithography for the solvent-intensive steps of processing a photoresist. The use of condensed CO<sub>2</sub> in lithography could greatly reduce the costs of toxic waste disposal, as well as the costs of complying with environmental and health regulations.

#### 2.1.2. Previous work on CO<sub>2</sub>-based microelectronics processing

Previously, condensed CO<sub>2</sub> has been successfully used as a processing solvent for microlithography at 193 nm. Ober and Allen, *et al.*<sup>4</sup> successfully resolved 0.2 μm lines, using a block copolymer of 1H,1H-perfluorooctyl methacrylate (FOMA) and tetrahydropyranyl methacrylate developed in supercritical CO<sub>2</sub> (Table 2.1). This resist system had a sensitivity (23 mJ/cm<sup>2</sup>) comparable to that of commercial resists using non-ionic photoacid generators (PAGs), and while the contrast of this system appeared good, it was not quantified. The glass transition temperature (T<sub>g</sub>) was measured, but not indicated,

and the etch properties of this system were not measured. Due to this material's similarities to the following system designed by DeSimone, it is possible that these properties are similar.

DeSimone, *et al.*<sup>7</sup> used a related resist consisting of a random copolymer of the same monomers used by Ober and Allen, but with a greater mol percent of FOMA, to demonstrate a lithographic process using only CO<sub>2</sub> as the processing solvent in development, as well as in

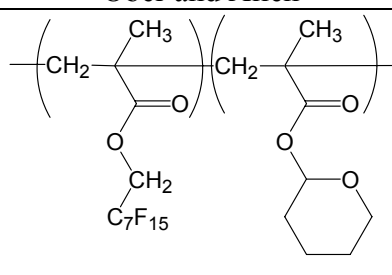
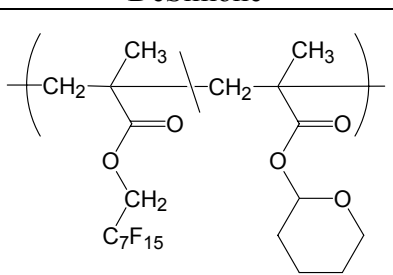
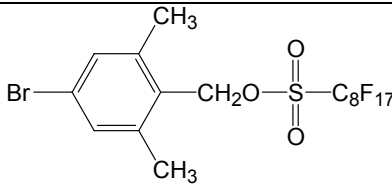
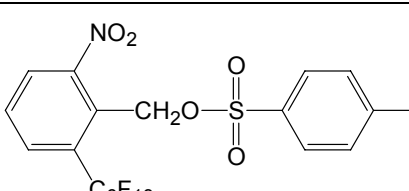
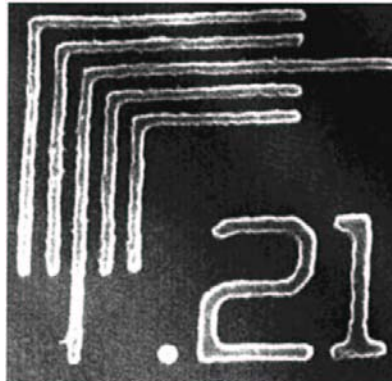
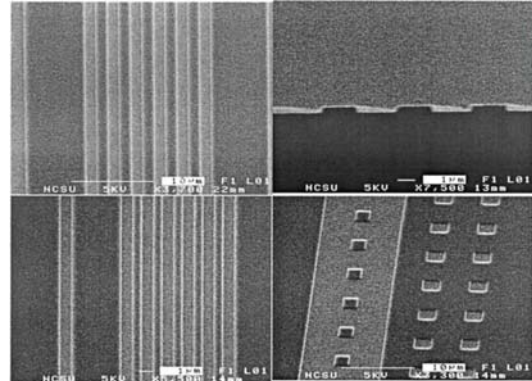
	Ober and Allen	DeSimone
Polymer resin		
Mol ratio of FOMA:THPMA	43:57	65:35
Molecular weight (M <sub>n</sub> )	6600	Not indicated
PAG		
SEM micrographs		

Table 2.1. Comparison of photoresists processed in condensed CO<sub>2</sub> from Ober and Allen,<sup>4</sup> and DeSimone.<sup>7,8</sup>

spin coating and the stripping of the resist. This system exhibited a sensitivity ( $21 \text{ mJ/cm}^2$ ) similar to that of Ober and Allen's polymer, and had a high contrast of 10.8. Unfortunately, this material resolved images to only  $1 \text{ }\mu\text{m}$ . This resolution may be due to a higher molecular weight or a larger polydispersity. The difference in resolving capability in these two very similar resist systems demonstrates just how sensitive a material is to the processing conditions. The low  $T_g$  of the random copolymer at  $48 \text{ }^\circ\text{C}$  likely prevented smaller resolutions.<sup>8</sup> In addition, the etch rate of this material was 2.5 times the etch rate of Shipley's S1813 Novolac resist under oxygen plasma conditions.

While the resist system described above use only condensed  $\text{CO}_2$  for development, other work has focused on using traditional developers, and gently removing the developer with a  $\text{scCO}_2$  drying step.<sup>2</sup> In an important example of this, a commercially-available APEX-E 2408 photoresist, exposed by e-beam lithography, was developed in 0.21 N TMAH solution, followed by DI water rinse. This water was then replaced with rinsing in a *n*-hexane solution, containing a surfactant to sequester the water. A fresh hexane rinse removed the surfactant and water, and finally the hexane layer was removed by supercritical drying with  $\text{CO}_2$ . Between each rinse step, much care was taken to prevent solvent drainage from the resist surface to prevent image collapse from capillary forces. From this development process, 140 nm lines with a 6.8 aspect ratio were successfully printed, showing no evidence mechanical failure. Furthermore, retreatment of these imaged lines with water or hexanes resulted in catastrophic image collapse. Although the development process described contains numerous steps, this process has the advantage of using commercially-available resists, which have already been optimized for small critical dimensions.

### 2.1.3. Addition polymers of norbornene / Alicyclic resist formulations

Cyclic olefin-maleic anhydride (COMA) photoresists were discussed in the previous chapter. Another class of photoresist materials that has gained significant interest is based on the addition polymerization of norbornene-based monomers. These polymers are typically synthesized with a Group VIII transition metal catalyst. Unlike the ROMP polymers of these materials, the norbornene unit remains intact, resulting in a highly strained alicyclic polymer. The next sections briefly describe recent work on the development of catalysts for addition polymerization of norbornene-based monomers, and lithographic results from such polymers.

Since the late 1980's palladium (II) catalysts have been investigated for the polymerization of alicyclic monomers, such as norbornene.<sup>9</sup> One of the early catalysts,  $[\text{Pd}(\text{CH}_3\text{CN})_4](\text{BF}_4)_2$ , was found to readily polymerize norbornene to high yields at ambient temperatures. Although this material was insoluble in a variety of solvents, the mechanism of this polymerization warranted further inquiry, in order to obtain more tractable materials. Using a similar catalyst containing a more non-coordinating anion, Sen made polymers of norbornene derivatives in high yields with moderate – though not well-controlled – molecular weights.<sup>10</sup> Mechanistic studies revealed a preference for incorporation of exo norbornene derivatives.<sup>11</sup> The less-hindered olefin of the exo isomer presents two possible faces for the metal catalyst to bind. However, the substituent on the endo isomer sterically prevents approach from this face of the olefin, thus offering a diminished opportunity of binding to the polymerization catalyst. Research by Sen also elucidated that polymerizations occur slower with ester-functionalized monomers in the presence of a cationic catalyst.<sup>12</sup> The carbonyl of the ester functionality was found to coordinate with palladium, and occupied a coordination site that would otherwise be used to insert a second norbornene monomer.

Later work showed that norbornene polymerizations using neutral Pd(II) catalysts were not inhibited by ester functionality.<sup>13</sup>

As early as 1991, Risse<sup>14</sup> described efforts toward the addition polymerization of norbornene using a Pd(II) catalyst. The authors did not perform lithographic imaging experiments on these polymers, though the catalysts demonstrated potential for making norbornene-based photoresists along the same lines as the previously described work. It was also noted the linear relationship between molecular weight and an increase in the  $[M]/[I]$  ratio, where  $[M]$  is the monomer concentration, and  $[I]$  is the catalyst concentration. Further, they observed a decrease in catalyst activity with the addition of triphenylphosphine, suggesting that the triphenylphosphine coordinates to the palladium and prevents the coordination of norbornene by an insertion type mechanism. Risse further tested the mechanism by polymerizing endo-dicyclopentadiene.<sup>15</sup> The product was entirely endo, suggesting no cationic rearrangement at the cyclopentene ring, which would have occurred in a cationic mechanism. Based on the narrow polydispersity of the resultant product, Risse also surmised a fast initiation with minimal chain transfer and chain termination, akin to a living polymerization. By 1996, Risse found that an  $\eta^3$ -allyl ligand on the palladium catalyst, rather than coordinated  $\text{CH}_3\text{CN}$ , provided greater functional group tolerance without impairing catalyst activity.<sup>16</sup> Notably, a key advantage to using the allyl palladium catalyst included a greater activity toward endo-substituted norbornenes. Risse also found that the use of a bulkier non-coordinating anion increased catalytic activity, as the monomer had greater access to the metal.<sup>17</sup> In collaboration with Goodall, this new catalyst enabled the synthesis of a host of polymers with a highly strained norbornyl backbone.<sup>18</sup> Unfortunately, this catalyst did not exhibit the same near-living polymerization of its precursor. Most

recently, Risse has examined the role of steric substitution on the allyl ligand and the use of different counter ions on the polymerization activity.<sup>19</sup> Unsurprisingly, he found that bulky substituents yield lower MW polymers, with a slower polymerization rate, and more nucleophilic counter ions also decrease the polymerization rate.

In the 1990's, Goodall's work at B. F. Goodrich focused on the addition polymerization of highly strained monomers, such as norbornene. This interest stemmed from possible thermal applications for such materials, which could exhibit Tg's in excess of 300 °C. The first generation of catalysts developed by Goodall included multicomponent<sup>20</sup> and single-component<sup>21</sup> nickel catalysts with labile ligands. These catalysts were known as "naked" nickel catalysts, as the ligands dissociated from the metal center completely during polymerization.

Further studies of a large number of nickel and palladium catalysts elucidated several attributes that contribute toward the activity of a norbornene addition catalyst, including the requirements that (1) the only bonds to the transition metal center are  $\sigma$  metal-carbon bonds and  $\pi$ -metal-olefin bonds, and that (2) the cationic metal center must have a weakly coordinating counter ion.<sup>22</sup> These studies also established that nickel-based catalysts typically have a higher activity than their palladium analogs. However, the palladium catalysts exhibit a greater functional group tolerance. While the first generation catalysts yielded polymers with very high molecular weights (>1,000,000 g/mol), the molecular weight of polymers from later catalysts could be well-controlled through the addition of  $\alpha$ -olefin chain transfer agents for Ni-based catalysts,<sup>23</sup> or the use of bulky phosphine ligands for Pd-based catalysts.<sup>24</sup> Through careful examination of structure-property relationships,

Goodall determined various Group VIII catalysts that could be used to obtain desired properties for the resultant polymer.

With such control over the polymer properties, one application that was examined was the use of these polymers as photoresists. Using a cyclic olefin terpolymer, Goodall obtained 160 nm dense lines using 193 nm exposure of 15 mJ/cm<sup>2</sup> (Fig. 2.2.).

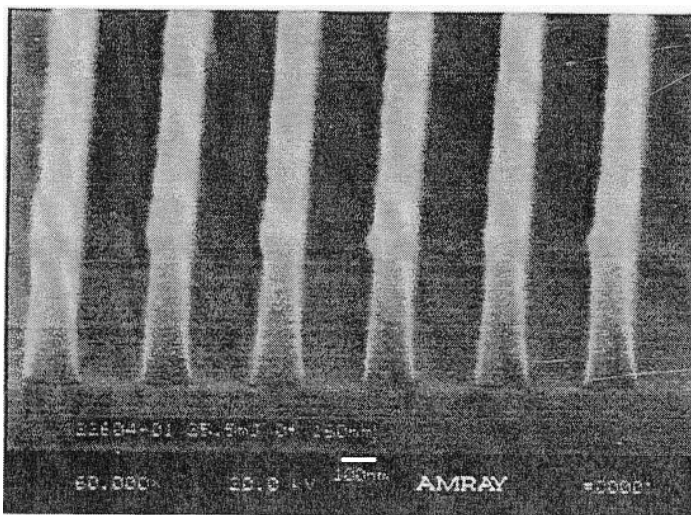
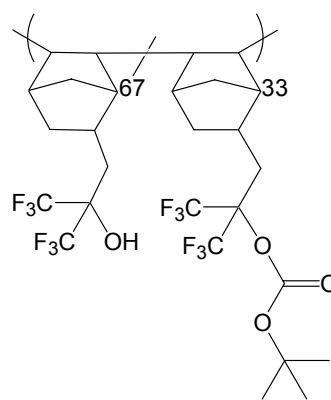
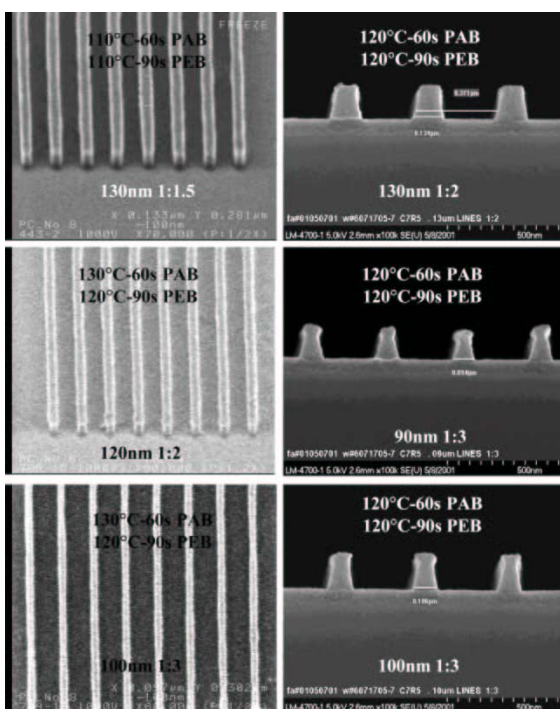


Figure 2.2. Images obtained using a cyclic olefin terpolymer.<sup>25</sup> Scale bar is 100 nm.

Unlike Goodall's work that focused on optimizing the addition polymerization catalyst, the Willson group focused on optimizing the polymers as photoresists. Willson's early work on alicyclic addition polymers used Risse's [Pd(CH<sub>3</sub>CN)<sub>4</sub>](BF<sub>3</sub>)<sub>2</sub> catalyst. This resulted in low yields of polymer, however, the materials exhibited good thermal stability and low optical densities (<0.5 μm<sup>-1</sup> at 193 nm).<sup>26</sup> The high etch resistance relative to APEX-E and the good contrast of these materials warranted further investigation of this class of materials as 157 nm photoresists.

Exploratory work on the viability of 157 nm lithography suggested that promising resists for this technology would need to be hydrofluoropolymers.<sup>27</sup> As the incorporation of

fluorine would be necessary for a functional 157 nm resist, various norbornene-based copolymers were synthesized to include strategically-placed fluorinated moieties.<sup>28</sup> Willson synthesized 157 nm photoresists using one of two catalysts: ( $\eta^6$ -toluene)-bis(pentafluorophenyl)nickel(II) or allyl palladium chloride dimer.<sup>29</sup> Initial copolymers of NBHFA and NBTBE made with the nickel catalyst had very high molecular weights. However, these could not be easily controlled and resulted in swollen images. However, the



**Formulation:** Poly(NBHFA/NBHFABOC), 6 wt% TPS-T<sub>f</sub>, 0.3 wt% TBAH in PGMEA.  
**Conditions:** 157 nm exposure (0.6 NA-0.7 $\sigma$ , 17.3 mJ/cm<sup>2</sup>), binary mask, 160 nm thick resist on 82 nm anti-reflective layer (AR19), 20 sec 0.26N TMAH development

Figure 2.3. Imaging capability of NBHFA-based addition polymer to 100nm<sup>29</sup>.

molecular weights of parallel materials made using the allyl palladium catalyst could be controlled with increased catalyst loading. Unfortunately, it was found that this catalyst cleaved the tert-butyl ester group of NBTBE, presumably due to trace acid formation during polymerization. This could be circumvented through polymerization in the presence of a proton sponge. In an effort to further lower the 157 nm absorbance, Willson used the allyl palladium catalyst to synthesize a homopolymer of NBHFA, and subsequently protected 33%



of the hydroxy groups with t-BOC post-polymerization. This resist could be imaged down to 100 nm 1:3 lines, using 157 nm exposure (Fig. 2.3.).

#### 2.1.4. Present approach

Building on the work from Ober and Allen<sup>4</sup> and DeSimone,<sup>7</sup> photoresists for CO<sub>2</sub>-based lithography with adequate thermal and etching properties were still desired. These original resists had a T<sub>g</sub> of 48 °C, which is too low for typical baking steps in lithography. In addition, the etch rate for this polymer, under oxygen plasma conditions, showed poor RIE resistance as compared to Novolac materials.

With these issues in mind, an addition polymer of norbornene-based monomers was pursued as a new photoresist material for CO<sub>2</sub>-based lithography. In an addition polymer, the norbornene unit should remain intact through the polymerization, resulting in a highly strained backbone, which is expected to impart a high glass transition temperature. Furthermore, work by Kunz and Allen<sup>30</sup> suggested that cyclic structures are advantageous to plasma etch resistance. An alicyclic group, such as norbornene, provides a ring structure appropriate to lowering the etch rate. The norbornyl monomers were designed with side groups to effect the desired properties for a CO<sub>2</sub>-based lithography process. This included the incorporation of a monomer with a high fluorine content to allow CO<sub>2</sub> solubility, as well as the incorporation of a monomer that could be chemically protected and later deprotected with acid.

## 2.2. Experimental

### 2.2.1. Synthesis

#### 2.2.1.1. Materials

1H, 1H-perfluorooctyl acrylate (FOA) was kindly received from 3M Co. It was distilled to remove inhibitor, then stored at 0°C. Methylene chloride (CH<sub>2</sub>Cl<sub>2</sub>, 99.5% Fisher) was dried over 4Å molecular sieves and degassed with argon. Diphenyl-*p*-tolylsulfonium triflate (WPAG) was kindly received from Wako Chemicals and used as received. Allyl bromide (Aldrich), allylpalladium chloride dimer (allyl-Pd, 99% Strem), argon (Ar, Fisher), carbon black (Fisher), carbon dioxide (CO<sub>2</sub>, SFC purity, Air Products), celite (Aldrich), di-*tert*-butyldicarboxylate (bisBOC, Aldrich), di-*tert*-butylphenol (DBP, Aldrich), hexanes (Fisher), N,N-dimethylaminopyridine (DMAP, Aldrich), magnesium sulfate (MgSO<sub>4</sub>, Fisher), methanol (MeOH, Fisher), 3-((norbornyl)-1,1,1-trifluoro-2-trifluoromethyl)propan-2-ol (NBHFA, Central Glass Corporation), 1,1,1,3,3-pentafluorobutane (Solkane, Solvay Fluorides), 1H,1H-perfluorooctan-1-ol (Fluorosolutions), 50 w/w% potassium hydroxide (KOH) solution (Fisher), silver hexafluoroantimonate (AgSbF<sub>6</sub>, 98% Strem), sodium chloride (NaCl, Fisher), sodium hydride (NaH, 60 w/w% dispersed in mineral oil, Aldrich), 50 w/w% sodium hydroxide (NaOH) solution (Fisher), tetrabutyl ammonium hydrogen sulfate (TBAHS, Aldrich), tetrahydrofuran (THF), and  $\alpha,\alpha,\alpha$ -trifluorotoluene (TFT, Aldrich) were used as received. Allyl-Pd and AgSbF<sub>6</sub> were stored in a dry box prior to use. AgSbF<sub>6</sub> was stored away from light. Dicyclopentadiene (DCP, Aldrich) was cracked immediately prior to use.

#### 2.2.1.2. Equipment

Schlenk flasks and a custom-made fritted funnel, bearing a 14/20 male ground glass joint and a 14/20 female ground glass joint were made by Walt Boger of the University of North Carolina Chemistry Department glass shop. Reactions were heated in a mineral oil bath

(Fisher) on a heater/stir plate from Fisher Scientific. Air and moisture-sensitive reagents were prepared in an oxygen-free glove box from Vacuum Atmospheres Company.

### 2.2.1.3. Monomer synthesis

#### 2.2.1.3.1. Norborn-5-ene-2-carboxylic acid 1H, 1H-perfluorooctyl ester (NBFOA)

A pressure tube was charged with cyclopentadiene (4.40 g, 66.57 mmol), FOA (29.71 g, 65.42 mmol), and DBP (68.4 mg, 0.33 mmol). The vessel was closed and heated to 170°C for 2 days. Vacuum distillation at 80 °C afforded a colorless liquid product in 91% yield.

#### 2.2.1.3.2. (1H,1H-Perfluorooctyloxy)-propene (FAE)

A round bottom flask was charged with 1H,1H-perfluorooctan-1-ol (19.83 g, 62.75 mmol) and TBAHS (2.15 g, 6.34 mmol). Addition of 50 mL of a 50 w/w% aqueous KOH solution resulted in the formation of a fluffy white precipitate. The mixture was stirred at RT for 10 minutes, followed by the addition of allyl bromide (21.36 g, 176.53 mmol) in 50 mL CH<sub>2</sub>Cl<sub>2</sub>. The reaction mixture was gently heated at 40°C for 18h. The CH<sub>2</sub>Cl<sub>2</sub> layer was dried over MgSO<sub>4</sub>, filtered, and dried. Vacuum distillation afforded a colorless liquid product at 30°C (62%).

#### 2.2.1.3.3. 5-(1H,1H-Perfluorooctyloxymethyl)-norborn-2-ene (NBFAE)

A pressure tube was charged with cyclopentadiene (2.70 g, 40.90 mmol), FAE (12.16 g, 27.60 mmol), and DBP (27.4 mg, 0.13 mmol). The vessel was closed and heated to 170°C for 2 days. Vacuum distillation afforded a colorless liquid product at 55°C in 40% yield.

#### 2.2.1.3.4. Carbonic acid 1-norborn-5-en-2-ylmethyl-2,2,2-trifluoro-1-trifluoromethyl-ethyl ester tert-butyl ester (NBHFA-BOC)

The synthesis was carried out with a modified procedure from literature.<sup>31</sup> A solution of NBHFA (9.37 g, 34.20 mmol) in 10 mL THF was slowly added to a mixture of NaH (1.11 g,

46.25 mmol) in 40 mL THF, cooled in an ice bath. The ice bath was removed when H<sub>2</sub> gas no longer evolved. The resultant slurry changed in color from orange to green to blue. A solution of bisBOC (7.49 g, 34.32 mmol) in 10 mL THF was then added slowly, changing the reaction mixture to pink. The reaction was allowed to stir at RT overnight, then washed with water and saturated aqueous NaCl solution until the aqueous portion was at neutral pH. The organic layer was dried over MgSO<sub>4</sub> and filtered. The solvent was removed *in vacuo*, yielding 70% of a colorless liquid.

#### 2.2.1.4. Polymer synthesis

##### 2.2.1.4.1. Addition polymerization

A typical polymerization using a palladium catalyst was carried out in an inert atmosphere, similar to literature procedures.<sup>32</sup> A solution of allyl-Pd (16.6 mg, 45.3 μmol) and AgSbF<sub>6</sub> (45.17 mg, 131.5 μmol) in 5 mL CH<sub>2</sub>Cl<sub>2</sub> was stirred for 10 min. The catalyst solution was transferred *via* cannula onto a fitted ground glass frit and allowed to filter into a flask containing a mixture of NBFOA (1.65 g, 3.18 mmol) and NBHFA (0.37 g, 1.36 mmol). The yellow reaction mixture was heated gently overnight at 30 – 35 °C. The resultant gelatinous yellow solid was isolated *via* precipitation into hexanes. The polymer was redissolved in Solkane, treated with Celite and carbon black, then precipitated into methanol yielded a white powder in 51% yield.

##### 2.2.1.4.2. Post-polymerization protection of NBHFA

The method described above for the t-BOC protection of the NBHFA monomer was not effective at protecting poly(NBFOA/NBHFA). Therefore, the following procedure was employed. Two equivalents of DMAP (399.4 mg, 3.27 mmol) were added to a solution of poly(70% NBFOA / 30% NBHFA) (2.59 g polymer, 1.74 mmol –OH) and bis-BOC (662.5

mg, 3.04 mmol) in 30 mL Solkane. The brown reaction mixture was stirred at RT overnight, then precipitated into methanol. The white powder was filtered, dried *in vacuo*, and collected in 75% yield.

#### 2.2.1.5. Spin coating of resist formulations

A formulation of 10 wt% protected copolymer and 0.5 – 5.0 wt% of a photoacid generator in TFT was spin coated onto 100-oriented silicon wafers at 4000 rpm for 40s using a Headway spin coater, followed by a post-applied bake (PAB) at 90 – 105°C for 120s.

#### 2.2.2. Characterization

##### 2.2.2.1. Nuclear Magnetic Resonance Spectroscopy (NMR)

$^1\text{H}$  and  $^{19}\text{F}$  NMR spectra were collected on a Bruker Avance 400 MHz spectrometer and analyzed using Mestre-C 2.3 software. Approximately 5 mg of each monomer sample was dissolved in 1 mL deuterated chloroform ( $\text{CDCl}_3$ , Cambridge Isotope Labs), with a TFT internal reference for  $^{19}\text{F}$  NMR. Polymer samples were dissolved in TFT, with a  $\text{CDCl}_3$  external lock solvent.  $^1\text{H}$  chemical shifts were referenced to  $\text{CHCl}_3$  at 7.24 ppm and  $^{19}\text{F}$  chemical shifts were referenced to TFT -63.72 ppm or fluorobenzene at -113.15 ppm. The labelling of carbon atom positions in norbornyl materials is in accordance with IUPAC definitions (Fig. 2.4.).

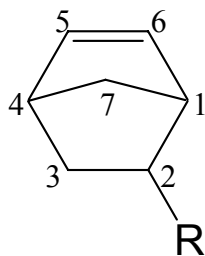


Fig. 2.4. IUPAC numbering of a substituted norbornene molecule.

##### 2.2.2.2. Elemental Analysis

Elemental analysis of monomers and polymers for C, H, and F content was carried out by Atlantic Microlabs, Inc in Norcross, GA.

#### 2.2.2.3. Infrared Spectroscopy (IR)

Infrared measurements were performed on a Perkin Elmer Spectrum BX spectrometer from  $4000\text{ cm}^{-1}$  to  $400\text{ cm}^{-1}$ . Samples were cast onto sodium chloride (NaCl) plates from a Solkane solution and dried.

#### 2.2.2.4. Intrinsic Viscosity

Intrinsic viscosity measurements were obtained from polymer solutions in TFT immersed in a constant-temperature bath of  $25^{\circ}\text{C}$ . Flow times from a No. 50 Cannon-Fenske capillary were measured automatically with a photoelectric barrier meniscus detector. The intrinsic viscosity was determined from the linear curve of concentration versus Staudinger function, extrapolated to zero concentration.

#### 2.2.2.5. $\text{CO}_2$ solubility

$\text{CO}_2$  solubility measurements were determined using a stainless steel high-pressure variable-volume view cell with a sapphire window. Pressures up to 5000 psi were investigated, and temperatures investigated were between  $0 - 60^{\circ}\text{C}$ .

#### 2.2.2.6. Differential scanning calorimetry (DSC)

DSC was performed on a Seiko-Haake DSC 220. Samples ( $\sim 10\text{mg}$ ) were crimped shut in aluminum pans. All thermograms were collected from the second heat with a heating rate of  $10^{\circ}\text{C}/\text{min}$  under  $\text{N}_2$  up to  $250^{\circ}\text{C}$ .

#### 2.2.2.7. Thermal gravimetric analysis (TGA)

TGA measurements were made using a Seiko Instruments RTD 220. Samples ( $\sim 10\text{mg}$ ) were heated in aluminum pans, with a heating rate of  $10^{\circ}\text{C}/\text{min}$  under  $\text{N}_2$  up to  $580^{\circ}\text{C}$ .

#### 2.2.2.8. Optical Density Measurements

A J. A. Woolam VU301 variable angle scanning ellipsometer (VASE) was used to measure the Cauchy coefficients of the polymers as follows: A 10 w/w% polymer solution in TFT was filtered through a 0.45  $\mu\text{m}$  PTFE syringe filter. The filtered solutions were spin coated at 2000 rpm for 120 s on a Laurell Technologies WS-400A-6NPP/LITE spin coater onto 2-inch silicon wafers. The films were baked at 115  $^{\circ}\text{C}$  for 120 s, then shipped to International Sematech. Film thicknesses were determined to be approximately 250 nm thick, by VASE. The wafers were scanned on the VASE tool to measure the refractive index of the film as a function of wavelength from 150 to 1010 nm. Absorbance data reported are in base 10.

#### 2.2.2.9. Etching

Reactive ion etching (RIE) was performed at the NCSU Nanofabrication Facility, using a Semi Group RIE System 1000 TP tool. Samples with varying w/w% polymer in TFT were filtered through 0.45  $\mu\text{m}$  PTFE syringe filters. The filtered solutions were spin coated at 1100 rpm for 120 s on a Cookson Electronics Specialty Coating Systems G3P-8 spin coater onto 2-inch silicon wafers. The films were baked at 115  $^{\circ}\text{C}$  for 120 s. Films were etched for 1-8 minutes under an RIE plasma. The plasma used was a mixture of  $\text{CHF}_3$  (20 sccm) and  $\text{O}_2$  (5 sccm). The chamber pressure was 60 mTorr, the cathode configuration was  $\text{Al}_2\text{O}_3/\text{Al}$  and the power was 100W. Film thicknesses were measured before and after etching with interferometry.

#### 2.2.2.10. Interferometry

Interferometric measurements were obtained at the NCSU Nanofabrication Facility, using a Nanometrics NanoSpec AFT. The wavelength was scanned from 480 nm to 790 nm.

#### 2.2.2.11. 193 nm Exposure

Lithographic exposure experiments at 193 nm were made using an ASML PAS 5500/950B scanner at the Triangle National Lithography Center with NA = 0.63. Exposure doses up to 37 mJ/cm<sup>2</sup> were used either in the absence of a mask or using a test mask consisting of 1:1 dense and 1:3 semi-dense lines and spaces. The linewidths ranged from 0.18 μm to 10 μm.

#### 2.2.2.12. Optical microscopy

Optical images were obtained on a Carl Zeiss Axioskop 2 optical microscope.

#### 2.2.2.13. Scanning Electron Microscopy (SEM)

SEM samples were sputter-coated with Au-Pd prior to imaging. SEM images were obtained on a Hitachi S-4700 field emission instrument operated at relatively low acceleration voltages of 1 keV to 5 keV to minimize charging effects.

### 2.3. Results and discussion

#### 2.3.1. Monomer characterization

The synthesis of CO<sub>2</sub>-soluble norbornene-based monomers was needed to enable CO<sub>2</sub> solubility of the subsequent polymers. Given the well-known high solubility of fluorinated materials in CO<sub>2</sub>, highly fluorinated, norbornene-based monomers were synthesized. These monomers were identified by <sup>1</sup>H and <sup>19</sup>F NMR. Elemental analysis was used to confirm the expected composition and to indicate the purity of products.

##### 2.3.1.1. NBFOA

<sup>1</sup>H NMR results for the NBFOA monomer (Fig. 2.5.) showed a number of resonances, which can be assigned to the expected structure. The resonances at 5.87 – 6.19 ppm are due



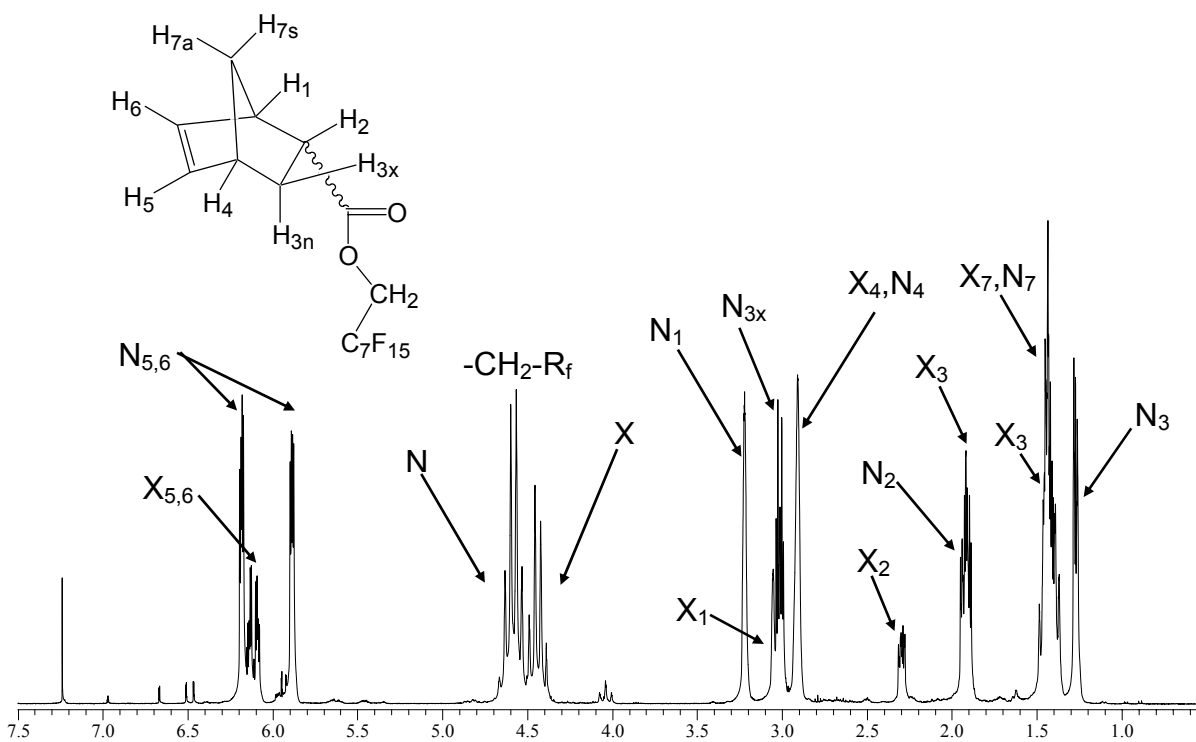


Figure 2.5.  $^1\text{H}$  NMR spectrum of NBFOA, with complete assignment of peaks for the endo (N) and exo (X) isomers.

to the vinyl protons. Although the two sets of resonances overlap somewhat, the exo:endo ratio can be calculated by separately integrating the lone peak at 5.87 ppm and the remaining vinylic resonances. The lone peak at 5.87 ppm represents one endo vinyl proton, so subtraction of this from the other integration value is the integration of the exo vinyl protons. This method indicated a 2:5 exo:endo ratio of isomers. The methylene group adjacent to the fluorinated tail was assigned the resonances at 4.39 – 4.67 ppm. These peaks are expected to be downfield due to the electron withdrawing effect of the fluorinated alkyl group. Assignment of the remaining resonances was aided with cross reference to the assigned  $^1\text{H}$  NMR spectrum of a mixture of the endo and exo isomers of norborn-5-enyl-2-methyl octanoate.<sup>16</sup> These resonances were assigned to protons expected in the product, and are

shown in Figure 2.5 in detail. Based on relative integrations, peak locations, and splitting patterns, all protons in both the exo and endo isomers of the NBFOA product.

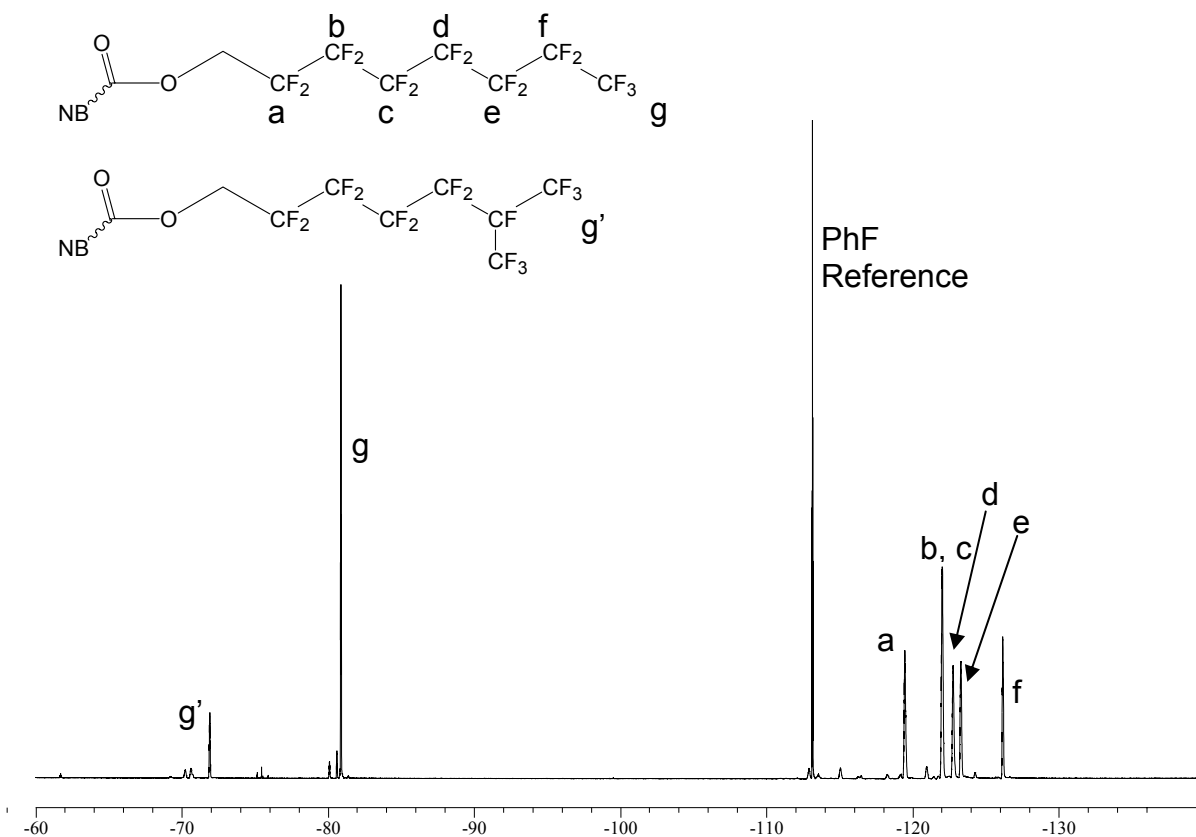


Figure 2.6.  $^{19}\text{F}$  NMR spectrum of NBFOA.

The  $^{19}\text{F}$  NMR spectrum of NBFOA (Fig. 2.6) was identical to that of FOA. Previous reports have indicated that FOA is a mixture of two isomers.<sup>33</sup> Approximately 80% of the material has a linear fluorinated chain, while the remaining 20% contains a methyl branched chain. The methyl branching is a result of the electrochemical process used to fluorinate octanoyl fluoride, a reagent in the manufacture of FOA.<sup>34</sup> This branching was evidenced in the  $^{19}\text{F}$  NMR spectrum of NBFOA. The peak at -80.89 ppm, assigned to the linear terminal  $\text{CF}_3$  group, and the peak at -71.90 ppm, assigned to the branched  $\text{CF}_3$ , had a relative integration of 1.0:0.2, respectively. This indicates that 17% of the fluorinated chain in this

sample has a methyl branch. The CF<sub>2</sub> group adjacent to the methylene group is a triplet at -119.46 ppm. The peaks upfield of -119.46 ppm have been assigned to the remaining CF<sub>2</sub> groups linearly, with the most upfield peaks assigned to the CF<sub>2</sub> groups closest to the terminal CF<sub>3</sub>.

Elemental analysis of purified NBFOA (Table 2.2.) indicated a high degree of purity, with less than 0.5 % difference between the calculated and found quantities of C, F, and H.

Element	Calculated	Found
C	36.92	37.16
H	2.12	2.19
F	54.81	54.49

Table 2.2. Elemental analysis results for NBFOA.

Based on NMR and elemental analysis results, it is reasonable to conclude that the material formed by the reaction of FOA with cyclopentadiene was the desired norbornyl product, containing 71% endo and 29% exo isomers.

#### 2.3.1.2. FAE

FAE was synthesized as an alternative material to FOA for making a highly-fluorinated monomer. In FAE, a methylene group replaces the carbonyl in FOA. Identification of the product was accomplished with <sup>1</sup>H NMR.

The <sup>1</sup>H NMR spectrum of FAE (Fig. 2.7.) exhibited peaks which could be assigned to each of the protons present in the molecule, based on relative integrations, chemical shift, and splitting patterns. The multiplets centered at 5.86, 5.31, and 5.26 ppm, and each integrating to one proton were due to the vinyl protons in FAE. The doublet at 4.12 ppm,

with an integration of two, was designated as the allylic protons. The methylene protons adjacent to the fluorinated tail were assigned to the triplet at 3.91 ppm. The splitting of the

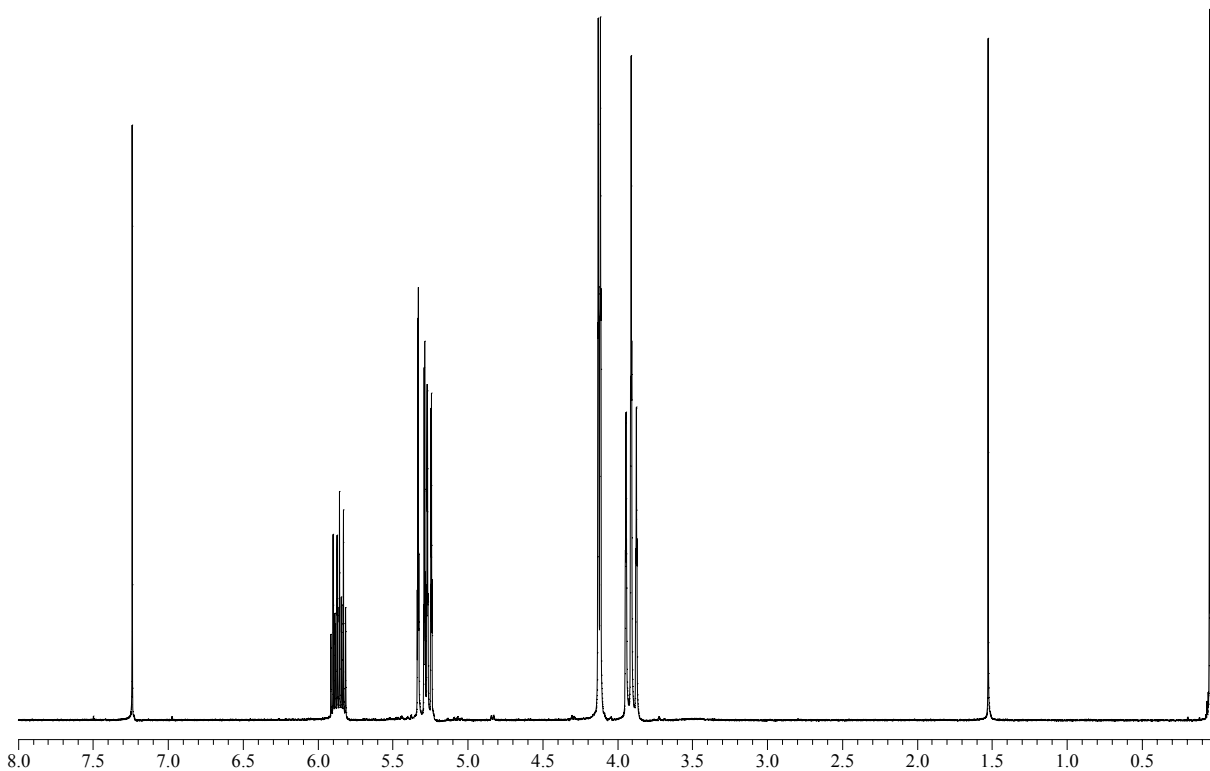


Figure 2.7. <sup>1</sup>H NMR spectrum of FAE.

latter resonance is due to spin-spin coupling with fluorines in the adjacent methylene group.

As the FAE product was merely an intermediate toward the desired NBFAE, <sup>1</sup>H NMR was deemed sufficient for product identification. A more detailed analysis of the NBFAE final product further confirmed that FAE was sufficient.

### 2.3.1.3. NBFAE

Using this initial product, the synthesis of NBFAE was accomplished using a Diels-Alder reaction with cyclopentadiene. As seen in the NBFOA <sup>1</sup>H NMR spectrum, this norbornyl material also exhibited a complex <sup>1</sup>H NMR spectrum (Fig. 2.8). The set of resonances at 5.89 – 6.13 ppm are due to the vinyl protons. Relative integration of this set of peaks

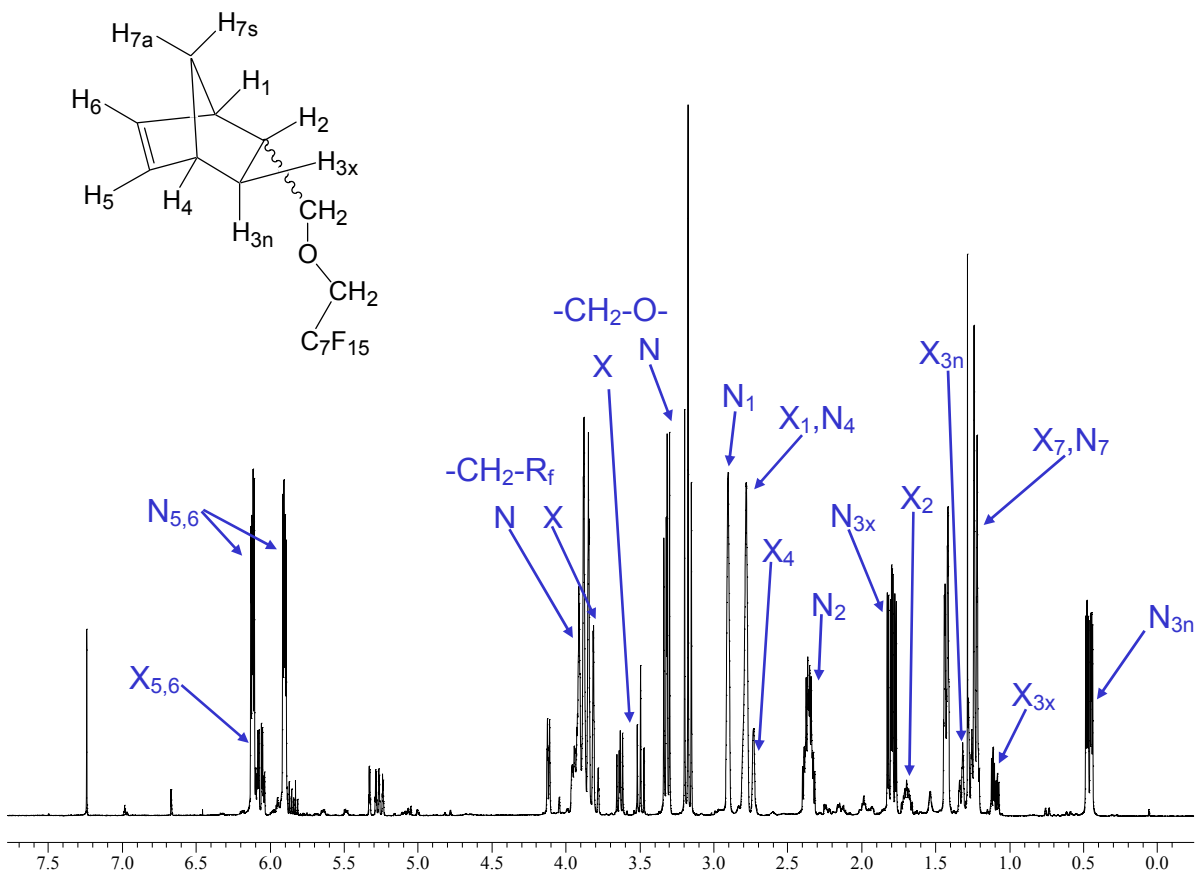


Figure 2.8.  $^1\text{H}$  NMR spectrum of NBFAE.

indicated a 1:5 exo:endo ratio of isomers. The methylene group adjacent to the fluorinated tail was assigned the multiplet centered at 3.86 ppm. The diastereotopic protons at the exo C8 were designated as the doublet of doublets at 3.64 ppm and the apparent triplet at 3.49 ppm, which may be an unresolved doublet of doublets. Similarly, the endo C8 protons were assigned to the doublet of doublets at 3.32 ppm and the triplet at 3.17 ppm. The remaining peaks are assigned in detail in Figure 2.8. A complete assignment of the  $^1\text{H}$  NMR structure was possible for NBFAE.

$^{19}\text{F}$  NMR was also used to identify the product of this material was nearly identical to that of NBFOA. However, the resonance of the branched  $\text{CF}_3$  group, present at -71.90 ppm in the NBFOA spectrum, was not present in the spectrum of NBFAE. This is expected, as the

1H,1H-perfluorooctan-1-ol, used as a starting material for the synthesis of FAE, contained only the linear isomer.

Element	Calculated	Found
C	37.94	38.85
H	2.57	2.67
F	56.32	55.90

Table 2.3. Elemental analysis results for NBFAE.

Elemental analysis of purified NBFAE (Table 2.3) indicated a high degree of purity, with less than 1.0 % difference between the calculated and found quantities of C, F, and H.

Based on this data of NBFAE, it appears that the product is the expected norbornene-based product. It was also found that this material did not contain the branching that was present in the NBFOA fluorinated chain. Elemental analysis confirmed a high purity monomer.

#### 2.3.1.4. NBHFA-BOC

NBHFA was incorporated into the photoresist polymer as a contrastable group. As such, the monomer was protected with a t-BOC group, which could later be cleaved with acid generated from a PAG. The protected monomer was identified by <sup>1</sup>H NMR, <sup>19</sup>F NMR, and elemental analysis.

The <sup>1</sup>H NMR spectrum of the t-BOC protected monomer was compared to that of the NBHFA spectrum (Fig. 2.9.). The assignments for each of the resonances could not be definitively identified, although certain assignments could be determined. As expected for any norbornenyl product, the vinylic resonances appeared downfield near 6.0 ppm. The exo sharp peaks due to the hydroxy proton in NBHFA, at 2.70 and 2.75 ppm for the endo and isomers respectively, were not present in the NBHFA-BOC spectrum, as expected. In

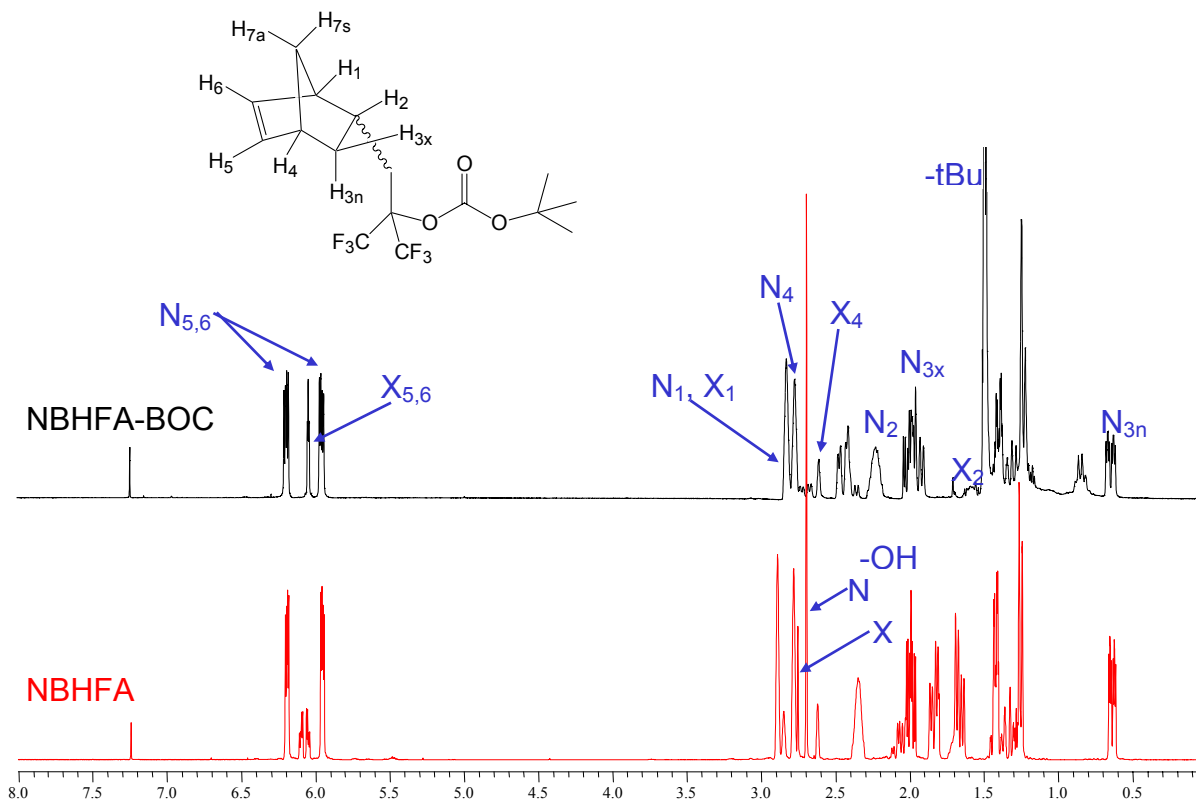


Figure 2.9.  $^1\text{H}$  NMR of NBHFA (red) and NBHFA-BOC (black).

addition, the NBHFA-BOC spectrum contained a sharp peak at 1.49 ppm, due to the *tert*-butyl protons. The integration of this peak could not be accurately determined, as other overlapping peaks were present in this region of the spectrum.

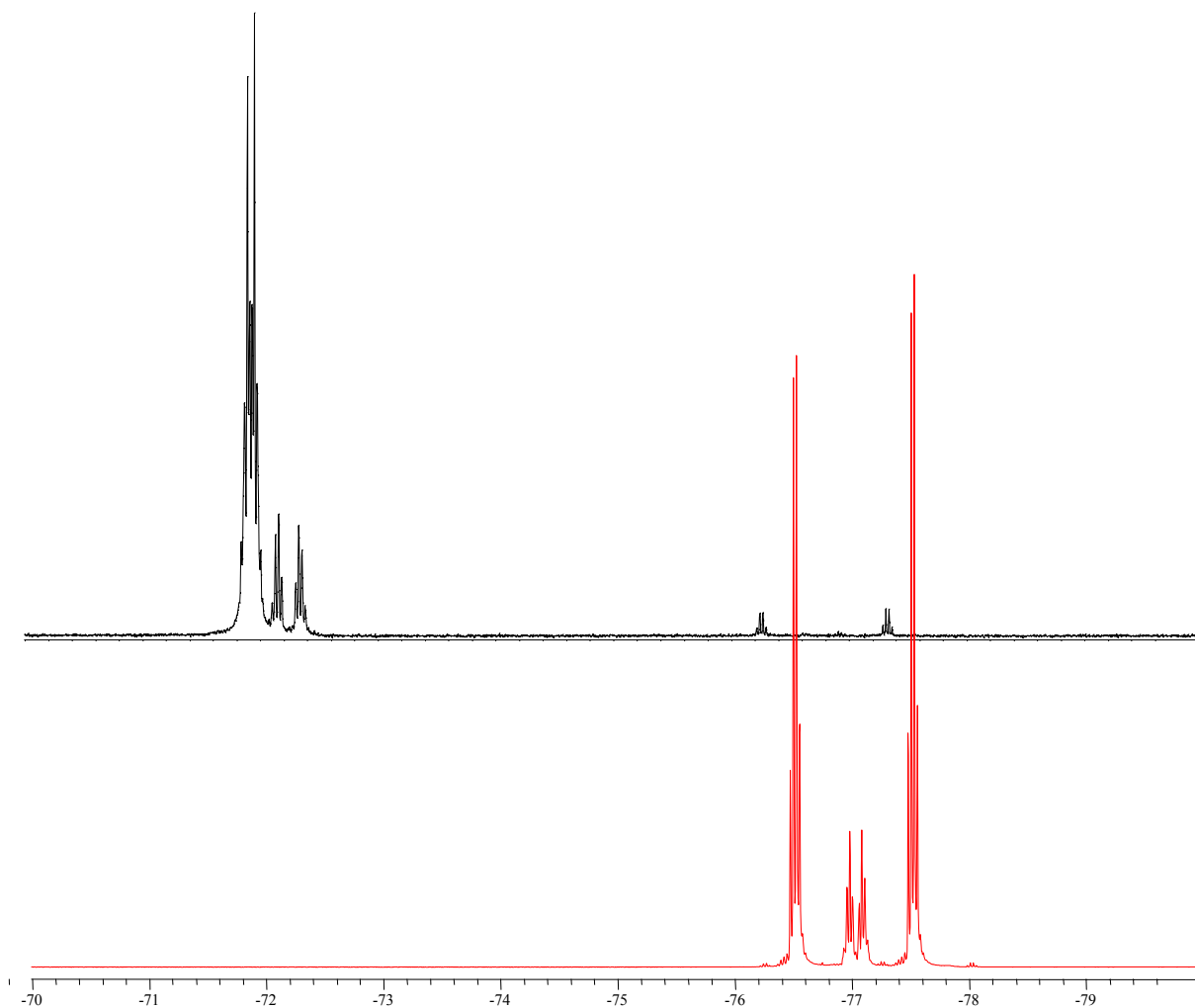


Figure 2.10.  $^{19}\text{F}$  NMR of NBHFA (red) and NBHFA-BOC (black).

Although each proton resonance in the latter spectrum could not be elucidated, the  $^1\text{H}$  NMR spectrum, in conjunction with the  $^{19}\text{F}$  NMR spectrum, presented a compelling case for the formation of the desired product. The  $^{19}\text{F}$  NMR spectra of NBHFA and NBHFA-BOC (Fig. 2.10.) each show two sets of multiplets corresponding to the  $\text{CF}_3$  groups in the endo and exo isomers. With the addition of t-BOC, these resonances shift downfield considerably from -77 ppm to -72 ppm. In the t-BOC-protected material, there is also evidence of 5.2 % residual NBHFA.



Element	Calculated	Found
C	51.34	53.06
H	5.35	5.93
F	30.48	29.21

Table 2.4. Elemental analysis results for NBHFA-BOC.

Elemental analysis of the purified NBHFA-BOC (Table 2.4.) indicated a purity of 96%, based on fluorine content. Impurities are most likely hydrocarbon-based.

The t-BOC-protected NBHFA monomer was successfully synthesized.  $^{19}\text{F}$  NMR showed a clear shift in the peak resonances,  $^1\text{H}$  NMR showed the loss of the  $-\text{OH}$  resonances, and elemental analysis agreed with the expected product.

### 2.3.2. Homopolymer characterization

Homopolymers of NBFOA and NBFAE were synthesized in order to gain understanding of the copolymers that would later be made from these materials. Characterization of the copolymers was also facilitated by examining the spectral data of the homopolymers.

#### 2.3.2.1. Poly(NBFOA)

$^1\text{H}$  NMR of poly(NBFOA) (Fig. 2.11.) contained several peaks that suggested the desired structure. Most notably was the absence of peaks at 5.5 – 6.5 ppm, indicating the absence of vinyl protons that were present in the monomer. The broad peak centered at 4.50 ppm corresponded well to the methylene protons adjacent to the perfluorinated group and the broad range at 1.0 – 3.3 ppm could be attributed to the remaining alicyclic  $\text{CH}_2$  and  $\text{CH}$  groups on the polymer. Resonances at 7.24 ppm and 2.15 ppm were due to chloroform and acetone, respectively.

The broadened polymer resonances indicate a short spin-spin relaxation time,  $T_2$ . This fast relaxation arises from the limited Brownian motion of the large, strained polymer, and

allows the local magnetic fields of other nuclei and electrons in the molecule to interfere with the primary external magnetic field, and thus the resonance frequency of the nucleus of interest, resulting in a broadened peak. In a highly mobile molecule, the local magnetic fields of other nuclei and electrons are averaged out and not observed in the NMR resonance.<sup>35</sup>

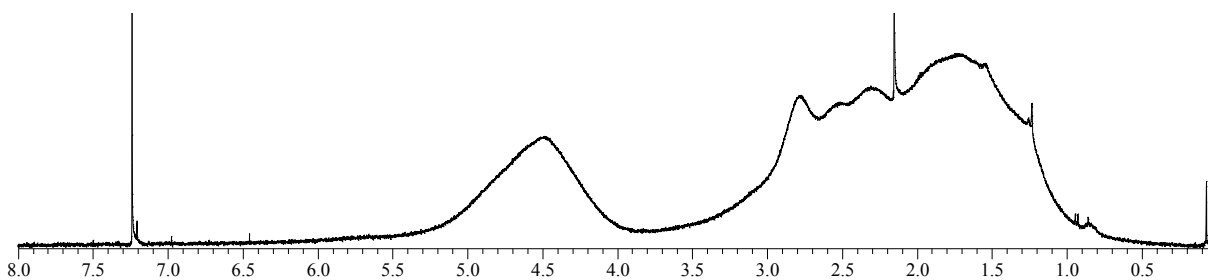


Figure 2.11. <sup>1</sup>H NMR of poly(NBFOA).

The polymer was also identified with <sup>19</sup>F NMR and elemental analysis. The <sup>19</sup>F NMR spectrum looked identical to that of the monomer, with the exception of peak broadening due to the strained structure. The elemental analysis of purified poly(NBFOA) (Table 2.5.) indicated a high degree of purity, with less than 0.5 % difference between the calculated and found quantities of C, F, and H.

Element	Calculated	Found
C	36.92	37.02
H	2.12	2.08
F	54.81	55.00

Table 2.5. Elemental analysis results for poly(NBFOA).

Based on NMR and elemental analysis, the poly(NBFOA) was successfully synthesized with the expected structure. Further analysis of this homopolymer provided baseline

information for the copolymers that would later be based on this material. This analysis is provided in section 3.3.4., alongside complementary analytical data for poly(NBFAE).

#### 2.3.2.2. Poly(NBFAE)

As observed in the poly(NBFOA)  $^1\text{H}$  NMR spectrum, the resonances broadened considerably from the monomer spectrum. The same is true for the poly(NBFAE)  $^1\text{H}$  NMR spectrum. The broad overlapping peaks centered at 3.51 and 3.85 ppm were assigned to the methylene protons at C8 and adjacent to the fluorinated chain, respectively. As seen in the NBFOA homopolymer spectrum, the most notable peaks are the ones not present: no resonances occur between 5.5 – 6.5 ppm, indicating the absence of vinylic protons from the monomer. As expected, the  $^{19}\text{F}$  NMR spectrum looked identical to that of the monomer, with the exception of peak broadening due to the strained structure.

Element	Calculated	Found
C	37.94	39.66
H	2.57	2.67
F	56.32	55.62

Table 2.6. Elemental analysis results for poly(NBFAE).

Elemental analysis of purified poly(NBFAE) (Table 2.6.) indicated a high purity of 99%, based on fluorine content. Impurities are most likely hydrocarbon-based, as the carbon and hydrogen contents are higher than expected.

#### 2.3.4. Homopolymer comparison

##### 2.3.4.1. Thermal analysis

Any material that is to be considered as a photoresist for microlithography must possess a range of properties. Among those desired properties is a high thermal stability. This requires that the polymer degrades at temperatures well above any baking steps that may be using

during lithographic processes. Typical PAB and PEB temperatures do not exceed 120 °C. Therefore, it is desirable to have degradation temperatures at or above 150 °C. Thermogravimetric analysis of poly(NBFOA) and poly(NBFAE) (Fig. 2.12.) indicates a very

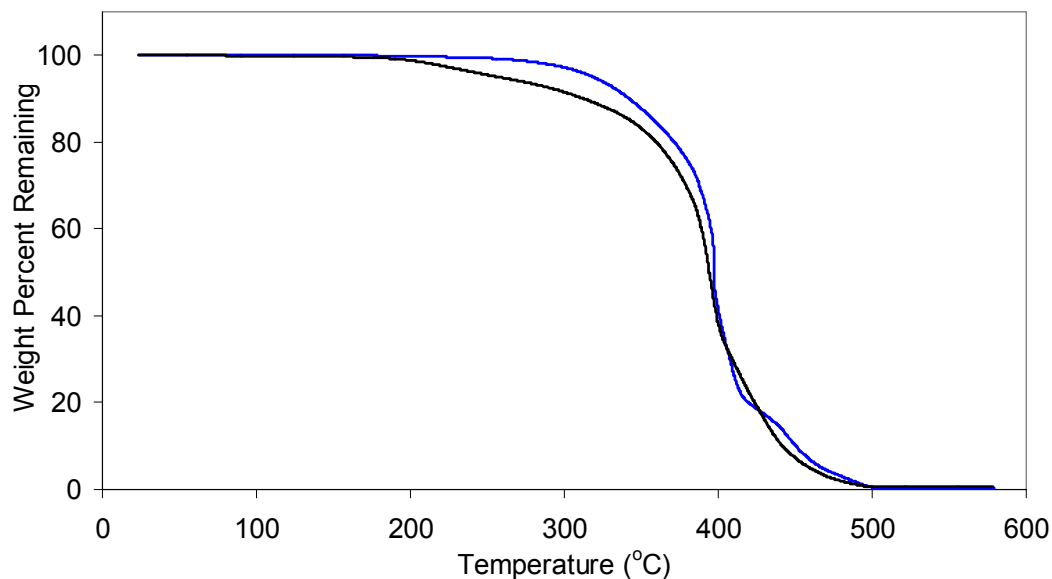


Figure 2.12. Thermogravimetric analysis of poly(NBFOA) (black) and poly(NBFAE) (blue).

high thermal stability. The 5 wt% decomposition temperature for poly(NBFOA) was measured to be 257°C, and for poly(NBFAE), this value was greater than 300 °C. Both of these polymers, therefore, exhibit exceptional stability toward degradation.

The glass transition temperature of a polymer is also important in the selection of a photoresist. As seen below (Fig. 2.13.), the Tg of both poly(NBFOA) and poly(NBFAE) is at 152°C, which is greater than the temperatures of baking steps in lithography.

The thermal properties of these homopolymers provide a good starting point for the synthesis of photoresists based on these polymers. Their high thermal stability ensures that

no polymer degradation or image loss will occur during the PAB and PEB steps in a microlithography process.

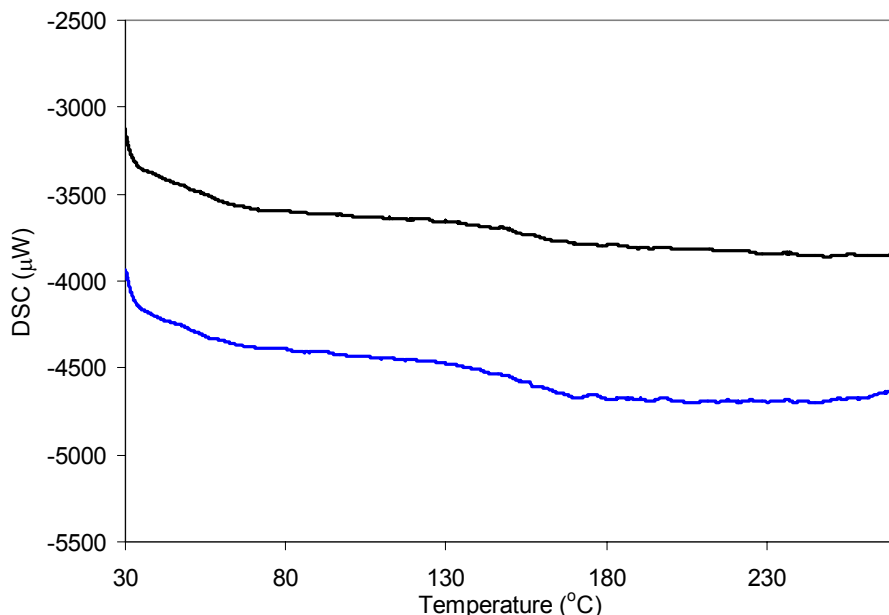


Figure 2.13. Differential scanning calorimetry of poly(NBFOA) (black) and poly(NBFAE) (blue).

#### 2.3.4.2. DUV absorbance

Both poly(NBFOA) and poly(NBFAE) exhibited absorbances of  $0.23 \mu\text{m}^{-1}$  at 193 nm (Fig. 2.14.), which is adequate for use as a platform for 193 nm resists. The absorbance of these materials at 157 nm – a potential future exposure wavelength – was unacceptably high at  $2.85$  and  $2.01 \mu\text{m}^{-1}$  for poly(NBFOA) and poly(NBFAE), respectively. However, some promise as a 157 nm lithography platform is apparent in the reduced absorbance of poly(NBFAE). The absence of the carbonyl group in this polymer dramatically reduces the absorbance, indicating the potential for other minor modifications that could further reduce the absorbance.

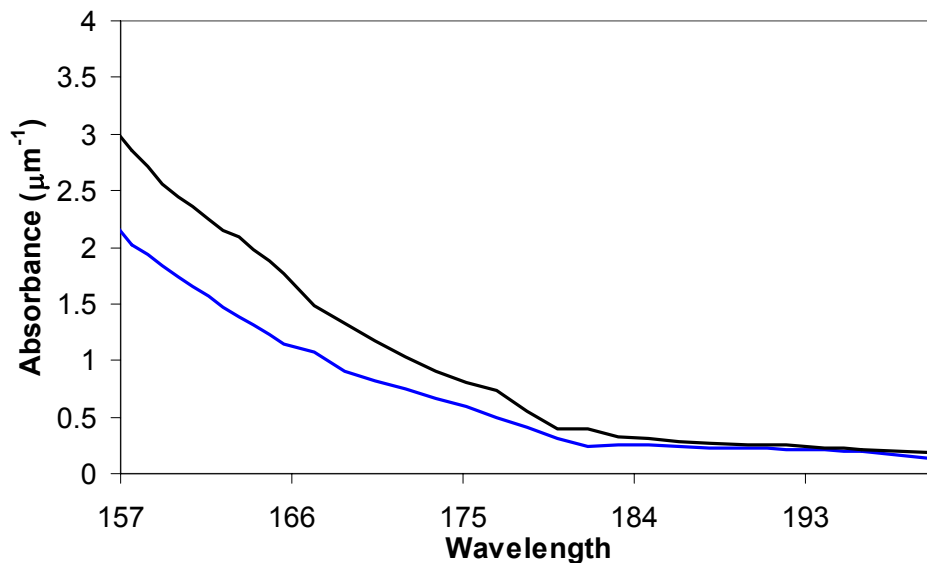


Figure 2.14. Optical absorbance of poly(NBFOA) (black) and poly(NBFAE) (blue) as a function of wavelength.

#### 2.3.4.3. CO<sub>2</sub> solubility

Highly fluorinated materials, such as the homopolymers described in this chapter, are expected to be soluble in condensed CO<sub>2</sub>. The cloud point of a material dissolved in CO<sub>2</sub>, at a given temperature, is the maximum pressure where the material begins to precipitate from solution. Conversely, at a given temperature, the cloud point is the minimum pressure that can sustain a stable solution. The previous definition is more accurate to this work, as the cloud points were measured at the first observation of precipitation. However, the latter definition may be easier to understand. The term “cloud point” refers to the opaque solution formed by initial precipitation from CO<sub>2</sub>. Since carbon dioxide has a variable density, a clearer understanding of a material’s solubility is attained by examining the cloud points over a range of temperatures. Based on the above definitions for a cloud point, one would expect a material to be soluble at CO<sub>2</sub> conditions above the curve and insoluble at conditions below the curve. The cloud point curves of the homopolymers, polymerized under identical

conditions, measured at 2.5 w/w%, was observed to be quite disparate (Fig. 2.15.). Poly(NBFOA) had a significantly higher CO<sub>2</sub> solubility than poly(NBFAE). This may be attributed to a specific interaction between CO<sub>2</sub> and the carbonyl group of poly(NBFOA), resulting in better solvation by CO<sub>2</sub>.<sup>36</sup> Also, there could be a molecular weight difference in these materials, resulting in an inaccurate comparison between these materials. The two polymers were polymerized under identical conditions, but as the molecular weight could not be determined, the possibility of different reactivity rates of each monomer with the palladium catalyst could contribute to a potential difference in molecular weight.

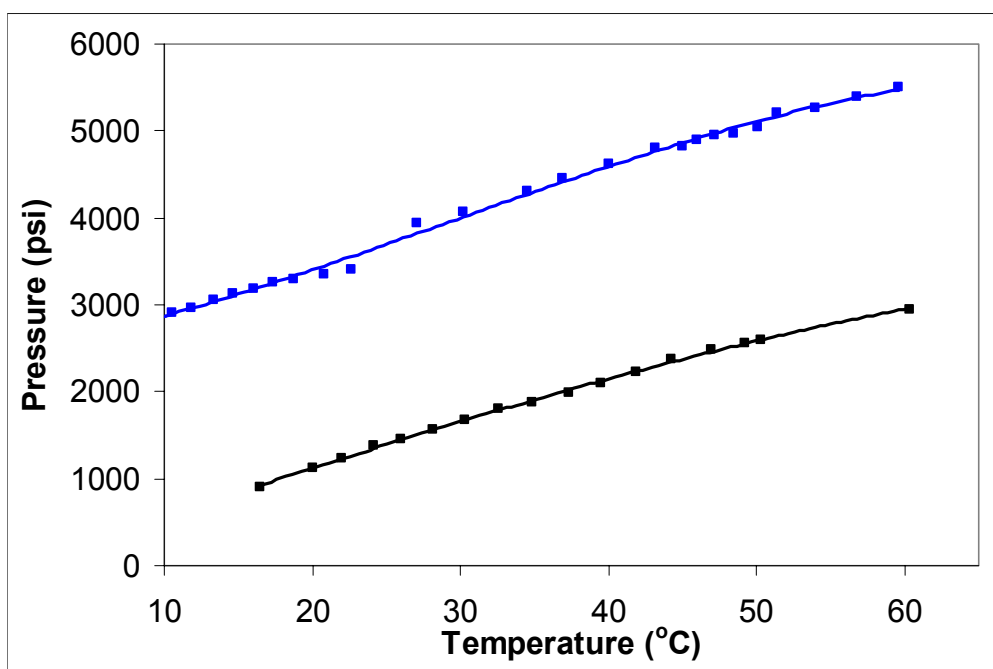


Figure 2.15. CO<sub>2</sub> solubility of poly(NBFOA) (black) and poly(NBFAE) (blue). Trendlines are third order polynomial fits.

#### 2.3.4.4. Etch resistance

Etch resistance studies of the homopolymers under oxygen plasma conditions indicated that these materials etched somewhat faster than a Shipley Novolac resin (Fig. 2.16.). It was

also observed that poly(NBFOA) etched significantly faster than p(NBFAE), despite their similar structures.

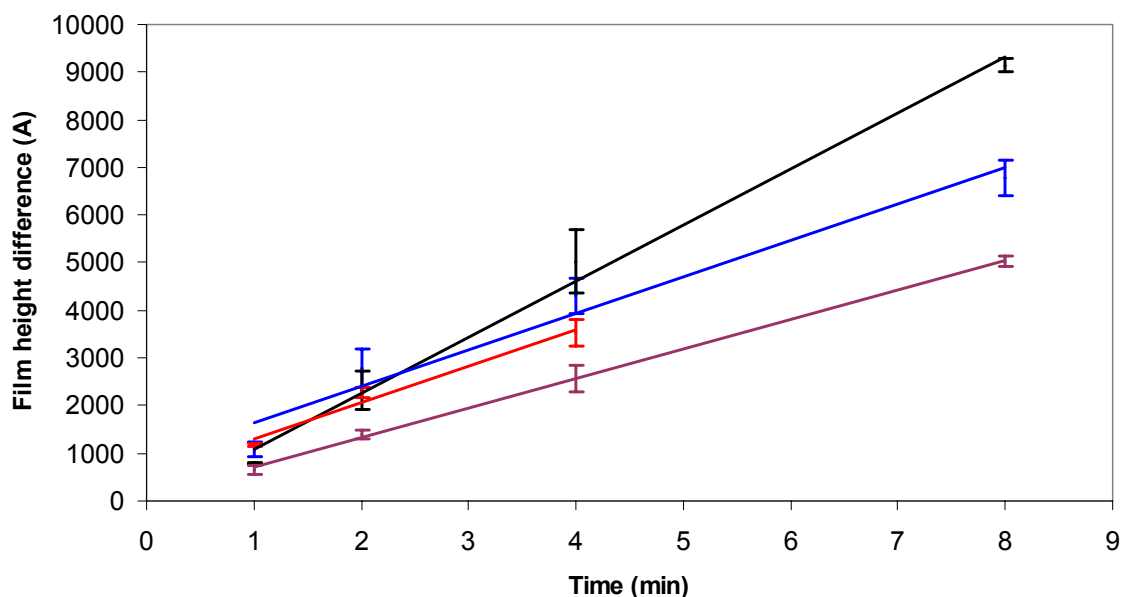


Figure 2.16. Oxygen plasma etch rates of poly(NBFOA) (black), poly(NBFAE) (blue), poly(NBFOA/NBHFA) (red) and Shipley 1813 Novolac (plum).

### 2.3.5. Copolymer characterization

#### 2.3.5.1. Poly(NBFOA/NBHFA)

Based on the higher CO<sub>2</sub> solubility and greater etch resistance, further work devoted to the synthesis of functional photoresists concentrated on NBFOA-based copolymers. Initially, a 70/30 mol/mol% copolymer of NBFOA and NBHFA was synthesized to evaluate the properties of the non-protected polymer. <sup>19</sup>F and <sup>1</sup>H NMR spectra (Figs. 2.17. and 2.18.) showed the expected resonances, with broadened peaks, as expected for a highly strained polymer. Elemental analysis of this polymer indicated the ratio of incorporated monomers to be in accordance with the monomer loading ratio (Table 2.7.).



Element	Calculated	Found
C	39.22	39.72
H	2.58	2.55
F	52.12	51.87

Table 2.7. Elemental analysis of poly(NBFOA/NBHFA).

As the NBFOA-NBHFA copolymer system is intended for use as a negative-tone resist using CO<sub>2</sub> development, any resist remaining on the wafer post-development will consist of the non-protected material. With this consideration, the non-protected copolymer was subjected to the same plasma etch conditions as previously tested on the homopolymers. (Fig. 2.16.) The etch rate of this material, at 1.6 times the rate of novolac, presented a significant improvement over the previous methacrylate platform, which etched at 2.5 times the rate of novolac.<sup>8</sup>

The non-protected copolymer of NBFOA and NBHFA was successfully identified by NMR. Furthermore, this copolymer exhibited a significantly slower etch rate compared to previous CO<sub>2</sub>-processable photoresists. The protected copolymer of this material was then synthesized and these materials were examined for lithographic properties, as described in the next sections.

#### 2.3.5.2. Poly(NBFOA/NBHFA-BOC)

Initial attempts to directly copolymerize NBFOA and NBHFA-BOC using the allylpalladium catalyst were unsuccessful. Trace amounts of acid, formed by the catalyst, deprotected the tBOC,<sup>29</sup> resulting in formation of the non-protected copolymer. However, post-polymerization protection of poly(NBFOA/NBHFA) produced the desired polymer in high yield. The polymer was primarily identified by <sup>19</sup>F NMR (Fig. 2.17.), where the bis-

trifluoromethyl group shifts from -78 ppm in the non-protected polymer to -72 ppm in the t-BOC protected polymer, as observed in the monomer.

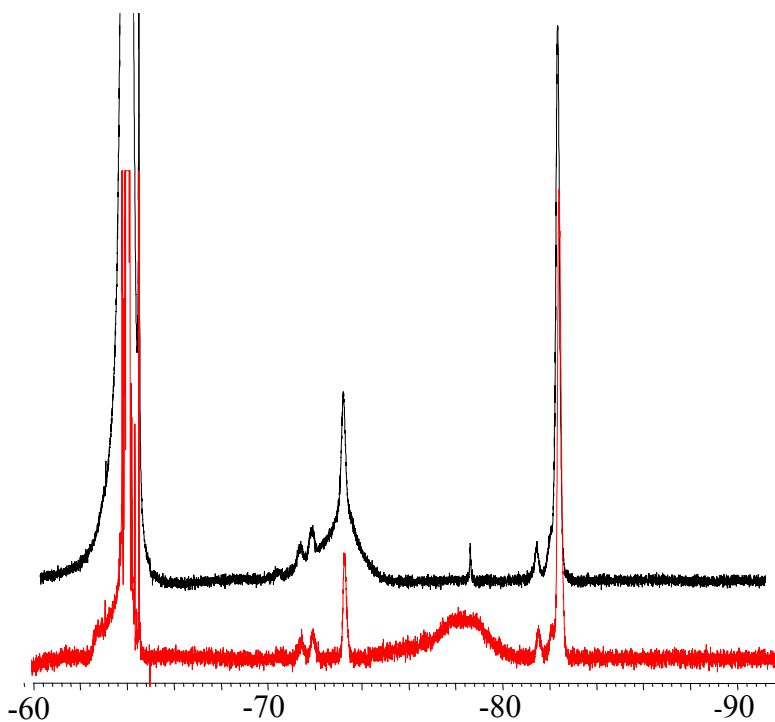


Figure 2.17.  $^{19}\text{F}$  NMR of poly(NBFOA/NBHFA) (red) and poly(NBFOA/NBHFA-BOC) (black).

The  $^1\text{H}$  NMR spectra of these polymers were most useful for the identification of the t-BOC group (Fig. 2.18.). The non-protected polymer spectrum showed impurities of acetone (2.15 ppm) and water (1.54 ppm). The protected polymer spectrum had a methanol impurity (3.32 and 2.77 ppm), and showed a large resonance at 1.46 ppm for the t-BOC protons.

Elemental analysis of purified poly(NBFOA/NBHFA-BOC) (Table 2.8.) indicated a high degree of purity, with less than 0.2 % difference between the calculated and found quantities of C, F, and H.

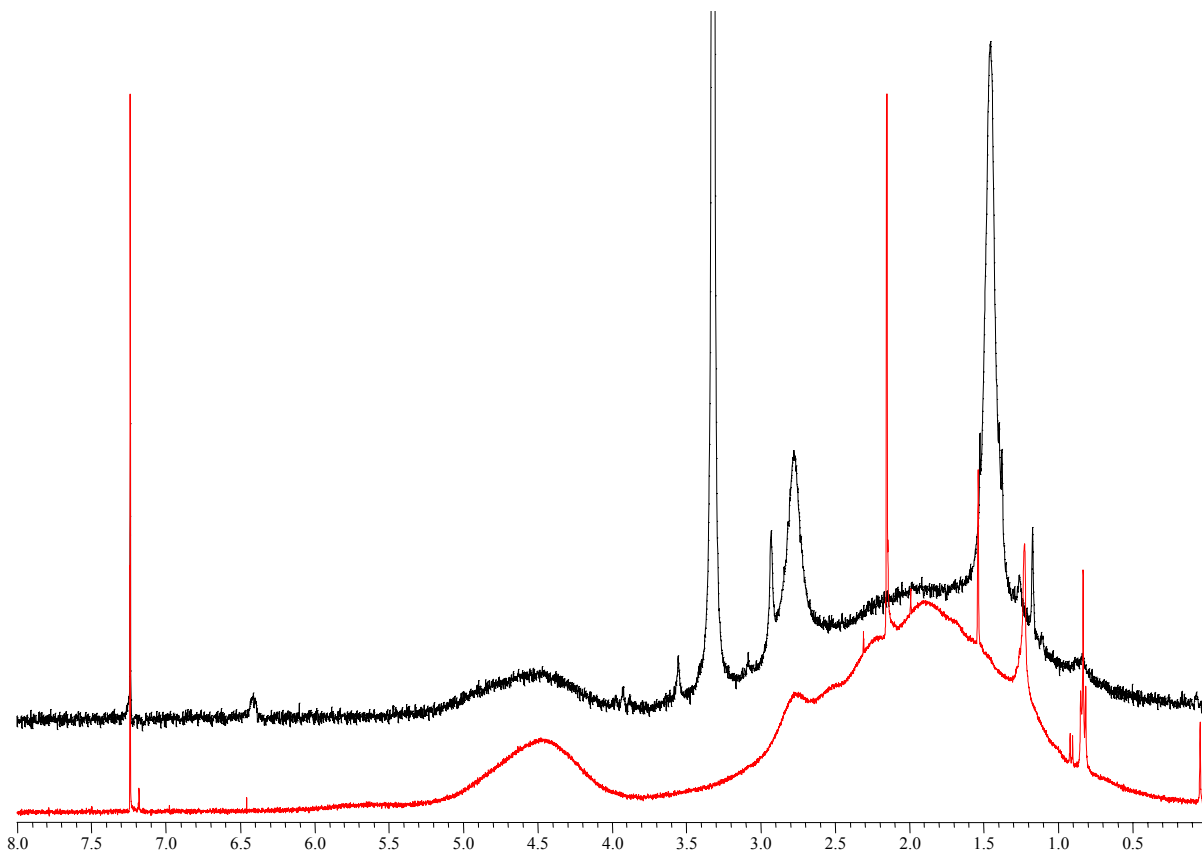


Figure 2.18.  $^1\text{H}$  NMR of poly(NBFOA/NBHFA) (red) and poly(NBFOA/NBHFA-BOC) (black).

Element	Calculated	Found
C	40.32	40.39
H	2.88	2.86
F	49.08	49.23

Table 2.8. Elemental analysis of poly(NBFOA/NBHFA-BOC).

In agreement with the expected thermal properties of these materials, the high decomposition and glass transition temperatures were found to be sufficient for the use of this material as a photoresist. In poly(NBFOA/NBHFA-BOC), an initial loss of 6.1 wt% was observed from 190°-228°C, which agrees with the calculated mass of t-BOC of 6.3 wt%. Thermal decomposition of the t-BOC occurred at 190 – 220 °C (Fig. 2.19.). Further

decomposition of poly(NBFOA/NBHFA-BOC), as well as decomposition of poly(NBFOA/NBHFA) occurred at temperatures in excess of 300 °C. The thermal phase

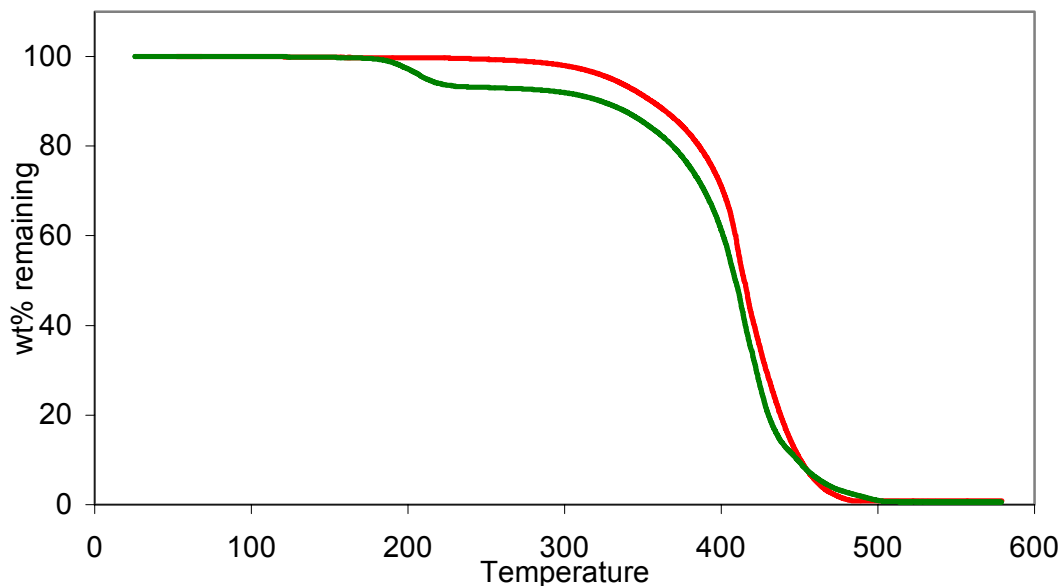


Figure 2.19. Thermogravimetric analysis of poly(NBFOA/NBHFA) (red) and poly(NBFOA/NBHFA-BOC) (green).

behavior, as measured by DSC, indicated a  $T_g$  at 120 °C (Fig. 2.20.). Further heating up to 220°C showed erratic behavior above 150°C, which might be attributed to melting of crystalline regions. The  $T_g$  was confirmed by slowly cooling, then reheating the sample. Notably, the erratic behavior previously observed was not reproduced upon further heating above 150°C, indicating a fully amorphous, non-crystalline material. The erratic thermal behavior in the second heat could be attributed to loss of the t-BOC group, in agreement with the TGA data. This thermal data suggest the polymer will be robust to typical baking steps in lithography.

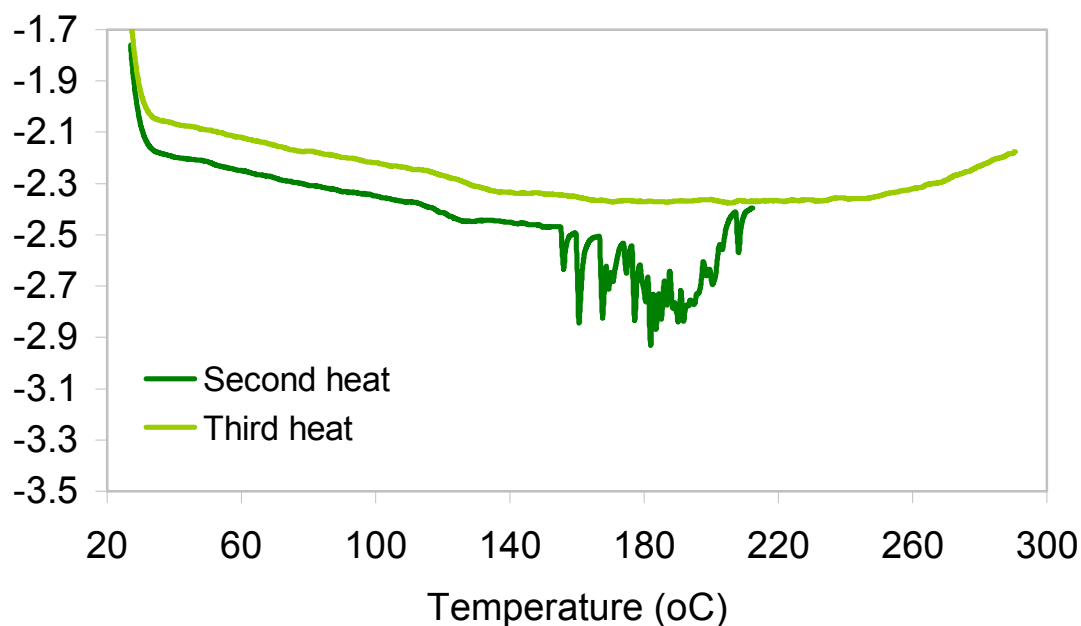


Figure 2.20. Differential scanning calorimetry of poly(NBFOA/NBHFA-BOC). A first heating to 150 °C (not shown) allowed the sample to anneal to the DSC pan. Second heating to 220 °C shows erratic behavior above 150 °C. Cooling the sample, followed by a third heating, shows no erratic behavior.

The polymers were soluble in liquid and compressed CO<sub>2</sub> as well as fluorinated solvents, with a significant difference in CO<sub>2</sub> solubility, thus providing an accessible region for CO<sub>2</sub> development (Fig. 2.21.). As stated earlier in section 2.3.4.3., the polymers are each soluble above the cloud point curve, and insoluble below the curve. The region between the protected and non-protected polymers represents CO<sub>2</sub> conditions that allow the solubility of only the protected material, and solubility of the resist decreases upon deprotection. Thus, this resist is expected to act as a negative tone resist in CO<sub>2</sub>. Nominal development conditions for this photoresist were found to be at 0-5 °C and 2000 psi.

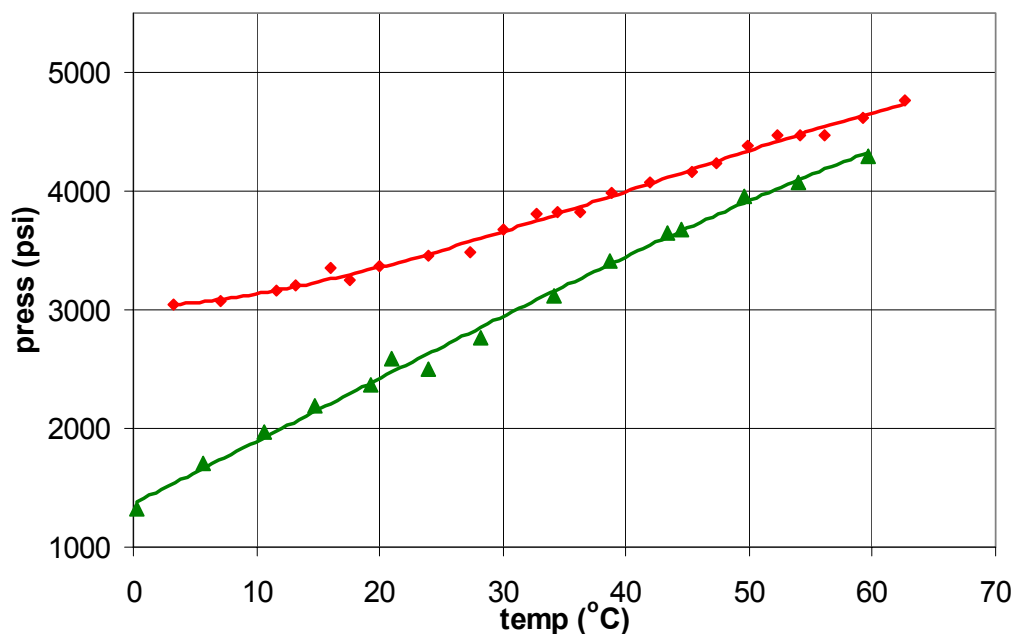


Figure 2.21. CO<sub>2</sub> solubility curves of poly(NBFOA/NBHFA-BOC) (green) and poly(NBFOA/NBHFA) (red). Both curves obtained at 2.5 wt% polymer in CO<sub>2</sub>. Trendlines are third order polynomial fits.

### 2.3.6. Lithographic evaluation

#### 2.3.6.1. Mercury arc lamp

Initial formulations of poly(NBFOA/NBHFA-BOC) with a photoacid generator were tested for photocleavage using a mercury arc lamp. A 10 w/w% solution of poly(NBFOA/NBHFA-BOC) in Solkane, containing 5 wt% WPAG was solvent-cast onto a NaCl plate and allowed to dry. The infrared spectrum of this film (Fig. 2.22.) contained the expected absorbances at 2955 cm<sup>-1</sup> for CH<sub>2</sub> stretching, 2880 cm<sup>-1</sup> for CH stretching, and overlapping carbonyl stretches at 1769 and 1751 cm<sup>-1</sup> for the t-BOC carbonyl and the NBFOA carbonyl. The film on NaCl was then exposed to UV light to test for photocleavage of the t-BOC group. The output of the Hg lamp is low at wavelengths less than 250 nm, extended exposure was necessary in order to activate the PAG. The film was exposed for 30

min, followed by a 10 min PEB at 105 °C. Infrared spectroscopic analysis of the resultant film showed no change in the methylene and methine C-H stretching absorbances. However, a broad OH stretching peak at 3550 – 3120  $\text{cm}^{-1}$  suggested the presence of the deprotected hexafluoroalcohol. Further, the carbonyl stretching region presented only a single absorbance at 1749  $\text{cm}^{-1}$ , indicating the loss of the t-BOC carbonyl.

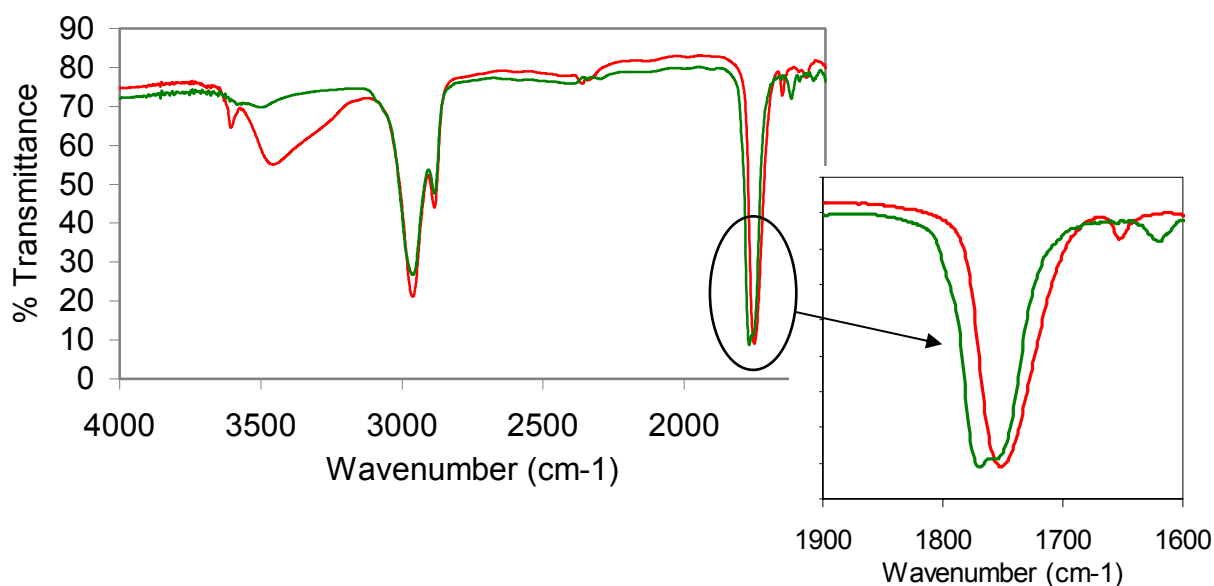


Figure 2.22. Infrared spectra of poly(NBFOA/NBHFA-BOC) (green) and poly(NBFOA/NBHFA) (red).

Initial photocleavage experiments showed that the t-BOC-protected copolymer could be cleaved with photo-generated acid. Using this information in conjunction with CO<sub>2</sub> solubility information, images were obtained from a test pattern in this photoresist.

#### 2.3.6.2. Imaging at 193 nm

A film of poly(NBFOA/NBHFA-BOC), containing 3 wt% WPAG, was exposed at 193 nm. Following exposure, the wafer was cleaved and placed in a CO<sub>2</sub> cell for development at 2000 psi and 0 – 5 °C for 5 min. The smallest images obtained for dense and semidense lines (Tables 2.9 and 2.10.) were 3  $\mu\text{m}$  and 1  $\mu\text{m}$ , respectively. The imaging of this photoresist

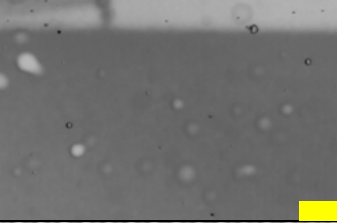
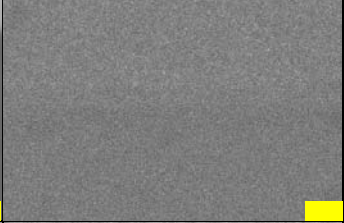
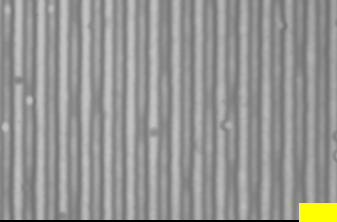
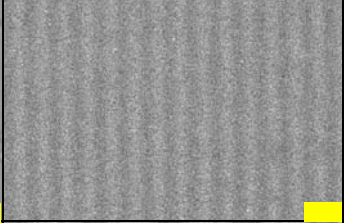
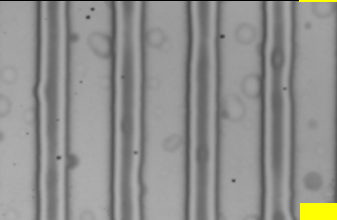
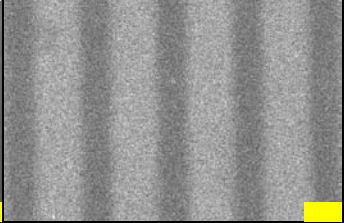
Expected Linewidth	Actual Linewidth	Optical Image	SEM
1 $\mu\text{m}$	NA		
3 $\mu\text{m}$	3 $\mu\text{m}$		
10 $\mu\text{m}$	9 $\mu\text{m}$		

Table 2.9. Optical and SEM micrographs of dense lines in poly(NBFOA/NBHFA) on Si. The scale bar is 10 $\mu\text{m}$ .

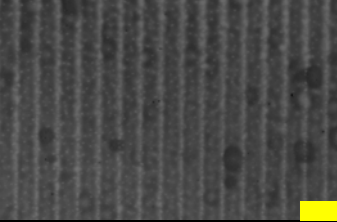

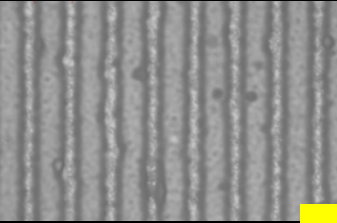
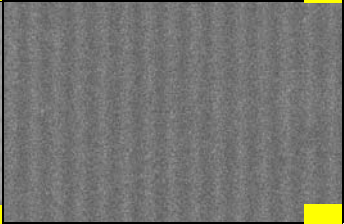
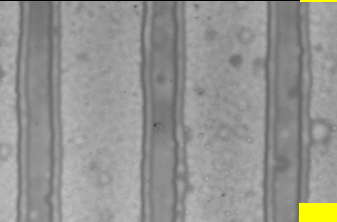

Expected Linewidth	Actual Linewidth	Optical Image	SEM
1 $\mu\text{m}$	1 $\mu\text{m}$		
3 $\mu\text{m}$	6 $\mu\text{m}$		
10 $\mu\text{m}$	9 $\mu\text{m}$		

Table 2.10. Optical and SEM micrographs of 1:3 semidense lines in poly(NBFOA/NBHFA) on Si. The scale bar is 10 $\mu\text{m}$ .



has not been optimized, and there are numerous ways this issue may be addressed.

Photolithography comprises several steps, each with a number of variables. Approaches toward obtaining smaller images are described below in terms of changing some of these variables. One obvious issue that has been present since the previous generation of CO<sub>2</sub>-soluble photoresists is the long PED before CO<sub>2</sub> development. A long PED allows acid to diffuse into non-exposed areas and destroys the latent image. Typical PED for this photoresist has been 2 – 24 h. PED could be minimized through the installation of a CO<sub>2</sub> development cell in the cleanroom, closer to the exposure location. In addition, PED could be controlled with the design of a low-volume CO<sub>2</sub> development cell that can contain a whole 6” wafer. This would enable development in one batch, rather than multiple batches, as is done now.

The optimization of PAB and PEB temperatures and times could also lead to smaller images. A higher temperature or longer time for PAB densifies the resist to a greater extent, which will result in denser and more robust images at smaller linewidths. However, bake temperatures and times that are excessive could lead to thermal acid generation or thermal photoresist cleavage, thus reducing selectivity. The PEB is a more critical parameter to fine tune. Higher temperatures and longer bake times allow acid to diffuse more through the resist. Both excessive and insufficient diffusion of the acid will prevent the formation of images.

Greater molecular weight control of the polymeric resist can help minimize non-uniform acid diffusion through polymer chains by regulating the chain length and distribution of lengths. A lower molecular weight material could promote acid diffusion, just as a higher molecular weight material could inhibit acid diffusion. Furthermore, development with a

higher molecular weight resist may have intrinsic difficulties in obtaining very small images, as the linewidth approaches the polymer's radius of gyration.

#### 2.4. Conclusion

Polymeric photoresists were synthesized and analyzed for their lithographic properties, using CO<sub>2</sub> as the processing solvent. As condensed CO<sub>2</sub> has numerous advantages over standard aqueous developers, the photoresists were designed for development using condensed CO<sub>2</sub>. These materials were improved upon the previous generation of materials for this application due to their higher plasma etch resistance and elevated glass transition temperature. Images were observed down to 1 μm, using 193 nm lithography and CO<sub>2</sub> development. Various processing parameters could be optimized to realize even smaller images.

## 2.5. References

- 1) Canelas, D. A.; DeSimone, J. M., Polymerizations in liquid and supercritical carbon dioxide. In *Advances in Polymer Science*, Springer-Verlag GmbH: **1997**; *133*, 103-140.
- 2) Goldfarb, D. L.; de Pablo, J. J.; Nealey, P. F.; Simons, J. P.; Moreau, W. M.; Angelopoulos, M., *J. Vac. Sci. Technol. B* **2000**, *18*, 3313-3401.
- 3) Ober, C. K.; Gabor, A. H.; Gallagher-Wetmore, P.; Allen, R. D., *Adv. Mater.* **1997**, *9*, 1039-1043.
- 4) Sundararajan, N.; Yang, S.; Ogino, K.; Valiyaveetil, S.; Wang, J.; Zhou, X.; Ober, C. K., *Chem. Mater.* **2000**, *12*, 41-48.
- 5) DeSimone, J. M., *Science* **2002**, *297*, 799-803.
- 6) Hoggan, E. N.; Kendall, J. L.; Flowers, D.; Carbonell, R. G.; DeSimone, J. M., *Polym. Mater. Sci. Eng.* **1999**, *81*, 47-48.
- 7) Hoggan, E. N.; Wang, K.; Flowers, D.; DeSimone, J. M.; Carbonell, R. G., *IEEE Trans. Semicond. Man.* **2004**, *17*, 510-516.
- 8) Flowers, D. Designing photoresist systems for dry microlithography in carbon dioxide. University of North Carolina, Chapel Hill, 2002.
- 9) Sen, A.; Lai, T.-W.; Thomas, R. R., *J. Organomet. Chem.* **1988**, *358*, 567-588.
- 10) Hennis, A. D.; Polley, J. D.; Sen, A., *Polym. Prepr.* **1999**, *40*, 782-783.
- 11) (a) Hennis, A. D.; Sen, A., *Polym. Prepr.* **2000**, *41*, 1933-1934; (b) Sen, A., *PMSE Prepr.* **2001**, *84*, 919; (c) Funk, J. K.; Andes, C. E.; Sen, A., *Organometallics* **2004**, *23*, 1680-1683.
- 12) (a) Hennis, A. D.; Polley, J. D.; Long, G. S.; Sen, A.; Yandulov, D.; Lipian, J.; Benedikt, G. M.; Rhodes, L. F.; Huffman, J., *Organometallics* **2001**, *20*, 2802-2812; (b) Andes, C.; Fischetti, L.; Hennis, A.; Sen, A., *Polym. Prepr.* **2002**, *43*, 963-964.
- 13) Kang, M.; Sen, A., *Organometallics* **2004**, *23*, 5396-5398.
- 14) Mehler, C.; Risse, W., *Makromol. Chem., Rapid Commun.* **1991**, *12*, 255-259.
- 15) Mehler, C.; Risse, W., *Macromolecules* **1992**, *25*, 4226-4228.
- 16) Mathew, J. P.; Reinmuth, A.; Melia, J.; Swords, N.; Risse, W., *Macromolecules* **1996**, *29*, 2755-2763.

- 17) Reinmuth, A.; Mathew, J. P.; Melia, J.; Risse, W., *Macromol. Rapid Commun.* **1996**, *17*, 173-180.
- 18) Goodall, B. L.; Risse, W.; Mathew, J. Addition polymers of polycycloolefins containing functional substituents. WO 96/37526, **1996**.
- 19) Peruch, F.; Risse, W., *Polym. Prepr.* **2000**, *41*, 1916-1917.
- 20) Goodall, B. L.; McIntosh, L. H., III; Barnes, D. A. Preparation of homopolymers and copolymers of cationically polymerizable monomers. WO 9637529, **1996**.
- 21) (a) Goodall, B. L.; Benedikt, G. M.; McIntosh, L. H., III; Barnes, D. A.; Rhodes, L. F. Addition polymers derived from norbornene-functional monomers and process therefor. WO 9514048, **1995**; (b) Goodall, B. L.; Benedikt, G. M.; McIntosh, L. H., III; Barnes, D. A.; Rhodes, L. F. Addition polymers and oligomers from norbornene-functional monomers using Group VIII metal compound catalysts and olefinic chain-transfer agents. US 5569730, **1996**.
- 22) Goodall, B. L., Cycloaliphatic polymers via late transition metal catalysis. In *Late transition metal polymerization catalysis*, Rieger, B.; Baugh, L. S.; Kacker, S.; Striegler, S., Eds. Wiley-VCH: Darmstadt, Germany, **2003**; 101-153.
- 23) Goodall, B. L.; Barnes, D. A.; Benedikt, G. M.; Jayaraman, S.; McIntosh, L. H.; Rhodes, L. F.; Shick, R. A., *Polym. Prepr.* **1998**, *39*, 216-217.
- 24) Lipian, J.; Mimna, R. A.; Fondran, J. C.; Yandulov, D.; Shick, R. A.; Goodall, B. L.; Rhodes, L. F.; Huffman, J. C., *Macromolecules* **2002**, *35*, 8969-8977.
- 25) Allen, R. D.; Opitz, J.; Wallow, T. I.; DiPietro, R. A.; Hofer, D. C.; Jayaraman, S.; Hullihan, K. A.; Rhodes, L. F.; Goodall, B. L.; Shick, R. A., *Proc SPIE (Adv. Resist Tech. Proc.)* **1998**, *3333*, 463-471.
- 26) (a) Okoroanyanwu, U.; Shimokawa, T.; Byers, J.; Willson, C. G., *Chem. Mater.* **1998**, *10*, 3319-3327; (b) Okoroanyanwu, U.; Byers, J. D.; Shimokawa, T.; Willson, C. G., *Chem. Mater.* **1998**, *10*, 3328-3333.
- 27) Kunz, R. R.; Bloomstein, T. M.; Hardy, D. E.; Goodman, R. B.; Downs, D. K.; Curtin, J. E., *J. Vac. Sci. Technol. B* **1999**, *17*, 3267-3272.
- 28) Trinque, B. C.; Chambers, C. R.; Osborn, B. P.; Callahan, R. P.; Lee, G. S.; Kusumoto, S.; Sanders, D. P.; Grubbs, R. H.; Conley, W. E.; Willson, C. G., *J. Fluorine Chem.* **2003**, *122*, 17-26.
- 29) Tran, H. V.; Hung, R. J.; Chiba, T.; Yamada, S.; Mrozek, T.; Hsieh, Y.-T.; Chambers, C. R.; Osborn, B. P.; Trinque, B. C.; Pinnow, M. J.; MacDonald, S. A.; Willson, C.

- G.; Sanders, D. P.; Connor, E. F.; Grubbs, R. H.; Conley, W., *Macromolecules* **2002**, *35*, 6539-6549.
- 30) Kunz, R. R.; Palmateer, S. C.; Forte, A. R.; Allen, R. D.; Wallraff, G. M.; DiPietro, R. A.; Hofer, D. C., *Proc SPIE (Adv. Resist Tech. Proc.)* **1996**, *2724*, 365-376.
- 31) Ito, H.; Miller, D. C.; Brock, P. J.; Wallraff, G. M. Norbornene fluoroacrylate copolymers and process for use thereof. US 2002/0146638, **2002**.
- 32) Okoroanyanwu, U.; Shimokawa, T.; Byers, J. D.; Willson, C. G., *J. Molec. Cat. A* **1998**, *133*, 93-114.
- 33) Kassis, C. M.; Steehler, J. K.; Betts, D. E.; Guan, Z.; Romack, T. J.; DeSimone, J. M.; Linton, R. W., *Macromolecules* **1996**, *29*, 3247-3254.
- 34) (a) Alsmeyer, Y. W.; Childs, W. V.; Flynn, R. M.; Moore, G. G. I.; Smeltzer, J. C., Electrochemical fluorination and its applications. In *Organofluorine Chemistry: Principles and commercial applications*, Banks, R. E.; Smart, B. E.; Tatlow, J. C., Eds. Plenum Press: New York, **1994**; 121-143; (b) Resnick, P., Personal communication, **2005**.
- 35) Levitt, M. H., Spin dynamics: Basics of nuclear magnetic resonance. In *Spin dynamics: Basics of nuclear magnetic resonance*, Eds. John Wiley & Sons: New York, **2001**; 528.
- 36) (a) Shieh, Y.-T.; Liu, K.-H., *J. Polym. Res.* **2002**, *9*, 107-113; (b) Blatchford, M. A.; Raveendran, P.; Wallen, S. L., *J. Phys. Chem. A* **2003**, *107*, 10311-10323; (c) Hong, L.; Thies, M. C.; Enick, R. M., *J. Supercrit. Fluids* **2005**, *34*, 11-16; (d) Sarbu, T.; Styranec, T.; Beckman, E. J., *Nature* **2000**, *405*, 165-168; (d) Kirby, C. F.; McHugh, M. A., *Chem. Rev.* **1999**, *99*, 565-602.

BILAYER RESISTS FOR DEVELOPMENT IN COMPRESSED CO<sub>2</sub>

### 3. Bilayer resists for development in compressed CO<sub>2</sub>

#### 3.1. Introduction

##### 3.1.1. Dry etch resistance of organic materials

Several portions of the lithographic process rely on dry plasma etching. Pattern transfer from the photoresist into the underlying substrate, as well as complete removal of residual resist (ashing) necessitate the use of plasmas. A plasma, or an ionized gas, consists of ions, electrons, and radicals and is formed by applying a high-power radio frequency discharge across a set of electrodes.<sup>1</sup> Electrons are then accelerated from the anode to the cathode and collide with gas molecules in between these electrodes. The applied voltage needs to be greater than the breakdown potential of the gas. This enables the accelerated electrons to collide inelastically with the gas molecules to break them down.

Though all plasmas are “glow discharges,” in so-called glow discharge methods, the plasma is confined to the region between the electrodes. Ordinary plasma etching places

<b>Plasma Component</b>	<b>Fraction</b>
Etch gas	0.5 – 0.8
Etch product	0.02 – 0.3
Radicals / neutral species	0.09 – 0.001
Charged particles	0.002 – 0.00001

Table 3.1. Fractional composition of a typical glow discharge RIE plasma.<sup>1</sup>

the substrate to be etched on the grounded electrode, which minimizes ion bombardment.<sup>2</sup> On the other hand, reactive ion etching places the substrate on the powered electrode and bombards the substrate with both charged and neutral particles (Table 3.1). In other important plasma etching techniques, including ion-beam and “beam” methods, the plasmas are generated remotely. In ion beam etching, a series of grids is used to selectively accelerate

ions to the substrate. In “beam” methods, radicals and other reactive neutral species are accelerated to the substrate surface through the use of magnetic fields and/or a pressure differential within the etching chamber.

For a successful etch transfer of lithographic patterns, several parameters are key to optimal performance. First, the etch process must yield a high fidelity transfer through vertical, anisotropic etching. A dominance of chemical etching effects, as exemplified in wet etching, is well-known to produce an isotropic etch.<sup>3</sup> Therefore, anisotropy is enhanced when chemical effects are suppressed, and physical etching effects dominate. A dry, parallel plate RIE process exhibits excellent anisotropy. The parallel plate reactor is advantageous over other configurations for selective etching, as lower pressures can be used, and vertical particle bombardment results in greater anisotropy than with other reactors.<sup>1</sup>

A second parameter that is key to pattern transfer is the etch rate, or, more specifically, the relative etch rate of the resist versus the substrate.<sup>3</sup> It is desirable for the photoresist to have a slow etch rate compared to the substrate, so that the substrate beneath the resist remains protected during the etch. For novel resist systems, this selectivity is often given as a ratio of etch rate for the new material versus the etch rate of an established photoresist, such as novolac or Apex-E. Significant differences in the thermodynamic driving force of the surface molecules or atoms reacting with the plasma is known to lead to enhanced selectivity.<sup>1</sup> Any selectivity adjustments based on thermodynamics for a resist and substrate will depend upon the chemical identity of these materials, as well as the choice of plasma etchant. In addition to the thermodynamic influences on the selectivity during plasma etch, if the plasma contains reactive gases that can form volatile products with the one of the substrate materials, then that material will etch faster. Conversely, low-volatile etch products



could form a passivating layer over the substrate or resist, to create a mask that enables high aspect ratio imaging with another etch composition.<sup>4</sup> This principle is used extensively in the ashing of a photoresist with an O<sub>2</sub> plasma, where volatile reactive products from oxidation of the photoresist may include CO, CO<sub>2</sub>, H<sub>2</sub>O, NO<sub>x</sub>, and SO<sub>x</sub>, while the underlying oxide layer remains intact. Additionally, O<sub>2</sub> plasmas are used to form a protective SiO<sub>2</sub> layer from a silylated photoresist. Further etching under other conditions has been shown to yield very high aspect ratio imaging into the substrate. For example, researchers at Selete made 80 nm 1:1 contact holes, using a fluorinated silsesquioxane (SSQ) resist, on top of an

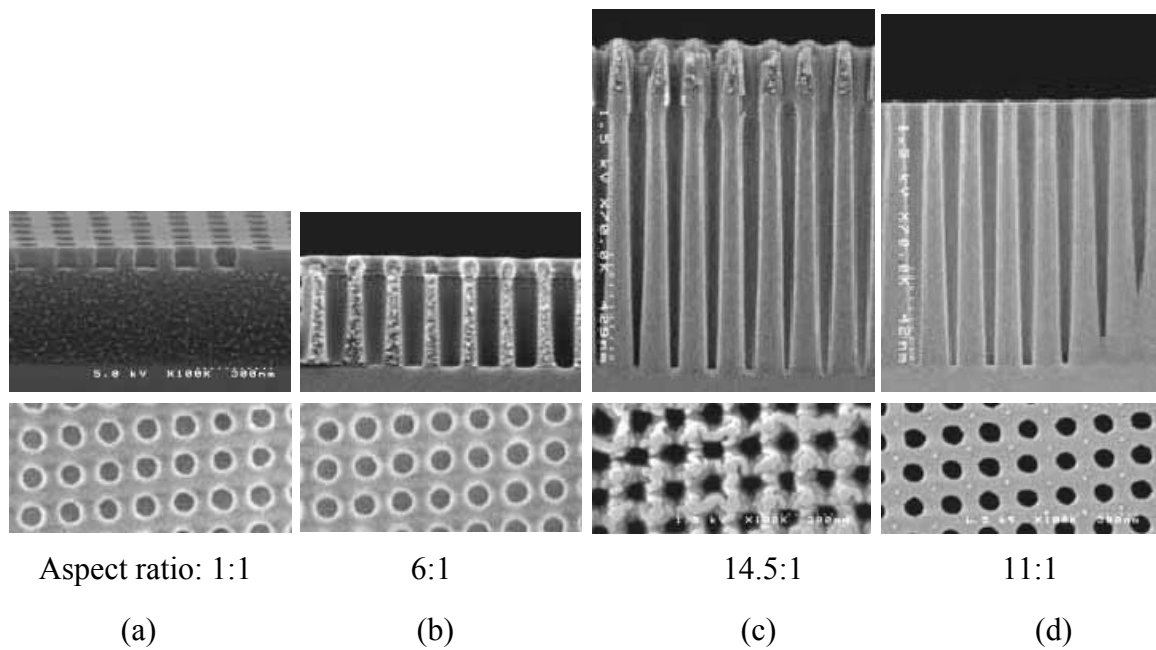


Figure 3.1. Selective etching to form high aspect ratio images in a SSQ/spin-on-carbon/TEOS/Si film stack. Images are shown after lithographic patterning and development of the SSQ (a), CO/O<sub>2</sub> etch into spin-on-carbon layer (b), C<sub>4</sub>F<sub>6</sub>/O<sub>2</sub>/Ar etch into TEOS layer (c), and final O<sub>2</sub> ashing of the mask. Side-on and top down images are shown.

antireflective layer, on tetraethyl orthosilicate (TEOS), on the Si substrate (Fig. 3.1).<sup>5</sup> The researchers patterned the SSQ resist, then used a CO/O<sub>2</sub> etch to transfer the pattern into the anti-reflective layer, which also served as a spin-on-carbon layer, to act as the etch mask in the following C<sub>4</sub>F<sub>6</sub>/O<sub>2</sub>/Ar etch. Finally, the etch mask was removed by O<sub>2</sub> ashing, to yield

11:1 aspect ratio contact holes. These multilayer photoresist compositions have proven to be a powerful tool in pattern transfer, and will be discussed in further detail in the following section. Both the volatility of etch products and thermodynamics at the surface are a function of the plasma species that reaches the substrate surface. Of course, the choice of gas composition used for the plasma is a strong parameter for variations in the selectivity. A dramatic example is the selective etching of polysilicon versus silicon dioxide. A 60/40%  $\text{CF}_4/\text{H}_2$  mixture can etch  $\text{SiO}_2$  over polysilicon at a ratio of 45:1, but if the etch gas composition is changed to 15:5 sccm  $\text{SF}_6/\text{Cl}_2$ , then polysilicon is etched at a ratio of 45:1 over  $\text{SiO}_2$ .<sup>3</sup> Furthermore, changes in the etchant composition can be a function of the etching chamber materials. The vacuum chamber walls often contain metals such as Fe, Ni, Cr, Al, Cu, and Zn, which could react with the plasma, depending on the process.<sup>1</sup> This will reduce the effective concentration of the plasma, and potentially change the plasma composition. On the other hand, an increase in the effective plasma concentration is also possible, depending on materials in the etch chamber. For example, one study used a polytetrafluoroethylene sample holder during an  $\text{O}_2$  etch process.<sup>6</sup> However, as PTFE is known to be a source of F radicals during plasma etching, the results resembled an  $\text{O}_2/\text{CF}_4$  etch more than a pure  $\text{O}_2$  etch.<sup>7</sup>

After the etching step, it is preferable to have minimal surface roughness in the remaining resist film. This allows the use of the thinnest resist layer needed in order to transfer the image to the desired depth, without the possibility of breakthrough etching of the protected regions. Minimal post-etch roughness also allows less stringent selectivity requirements.<sup>1</sup> Surface roughness can occur from two etching issues: non-uniform etching, and/or contamination or damage to the surface. Non-uniform etching can be a function of the gas inlet and outlet configurations. If the gas cannot be distributed uniformly over the substrate,

then the plasma, too, will not be evenly distributed. The gas flow rate and residence time in the etching chamber can also adversely affect the etch uniformity.<sup>8</sup> Insufficient gas flow rates can result in non-uniform coverage of the substrate, or even a failure to generate the plasma. Large flow rates could lead to a turbulent flow or a jet-like flow into the etch chamber, also causing an uneven distribution of etching species. An excessive residence time of the feed gas could lead to a depletion layer of reactive species over the substrate, changing the relative concentrations of particles in the plasma, and leading to non-uniform etch rates for the duration of the residence time. An etched surface may become contaminated from the backscattering, or redeposition and implantation, of non-volatile etch products. The effects of non-volatile etch products has been previously described in terms of selectivity, in the case of bilayer resists forming a protective SiO<sub>2</sub> passivating layer. However, the formation of undesired non-volatile etch products—including those formed by interactions with the etch chamber itself<sup>9</sup>—have the potential to redeposit onto the substrate. Such redeposition forms localized masked areas, or micromasks, that create pitting during further etching.<sup>10</sup> Contamination from polymeric residues has also been observed to inhibit uniform etching. Polymeric residues have been known to form in etch compositions with a low F/C ratio, fast-etching resists, long plasma residence times, high gas pressures, the presence of tetrafluoroethylene fixtures inside the etch chamber, solvent outgassing, and low power density. Other damage resulting in surface roughness has been observed as a result from the high energy radiation present in a plasma. Silicon dioxide has been found to be especially vulnerable to radiation damage.<sup>11</sup> In fact, the extent of gate oxide damage is proportional to the dc bias voltage of the plasma etch.<sup>12</sup> Although low-voltage damage can

be repaired by thermal annealing, any damage from a bias voltage of 500V or greater is irreversible.

The optimization of anisotropy, selectivity, and surface roughness is not straightforward, as these parameters do not vary independently with the possible experimental parameters. An anisotropic etch is best obtained through the choice of an etching method dominated by physical effects. The selectivity of an etch process can be tailored through an understanding of the chemical and physical reactivity of the etchant with the resist and the material to be etched. Post-etch surface roughness can be minimized using a uniform, contamination-free etch. As described above, the experimental parameters associated with optimizing each of these qualities are interrelated and complex. As such, many researchers have attempted to develop empirical models to describe the plasma etching of organic materials.<sup>13-16</sup>

Efforts toward elucidating empirical structure-property relationships for etch resistance have resulted in mixed success. Many researchers cite the Ohnishi parameter as a basis for the design of their resists.<sup>13</sup> The Ohnishi parameter states that

$$V \propto N / (N_C - N_O), \quad [4]$$

where  $V$  is the ion-beam etch rate of the polymer,  $N$  is the total number of atoms in the monomer unit,  $N_C$  is the number of carbon atoms in the monomer, and  $N_O$  is the number of oxygen atoms in the monomer. This early model of etch resistance in organic materials describes a distinct relationship between ion-beam etch rate and atomic composition of the resist. However, this relationship was found to not apply to the etching of resists in RIE plasma processes. The limitations of this parameter has led to many erroneous references to it, as few other empirical models have been available.<sup>17</sup> Additionally, while the resists Ohnishi analyzed were germane to lithography trends in the early 1980's, much has changed

since then, including the introduction of non-aromatic alicyclic structures, and much more highly fluorinated resists.

While Ohnishi's work focused on atomic composition of the resist, as it related to dry etch rates, the structural components of the resist were neglected. In an effort to address the structural differences in photoresists, Kunz and Allen developed another model relating etch rate to the weight fraction of the resist in cyclic structures.<sup>14</sup> The authors defined a ring parameter,  $r$ , where:

$$r = M_{\text{CR}} / M_{\text{TOT}}. \quad [5]$$

The mass of the carbon atoms in the resist involved in ring structures is  $M_{\text{CR}}$ , and  $M_{\text{TOT}}$  is the total mass of the resist. A third-order polynomial function of  $r$  was used to model the etch resistance of acrylate copolymer resists containing cyclic side groups, in the presence of an aggressive  $\text{Cl}_2$  etch process. The model fit fairly well to the actual etch data, though significant scatter of the data was apparent. Notably, this model does not discriminate between the etch rates of two different acyclic resists. The authors also acknowledged the difficulty in addressing the effects of complex parameters, such as different etch processes and the redeposition of etch products, using an empirical approach. Although this model yielded only moderate success in elucidating a trend for etch resistance, it represented a great shift in thinking about the etch resistance of photoresists. Specifically, this model introduced a more chemical approach to etch resistance: focusing on the way bonds in the resist are broken.

In a collaboration between IBM and BF Goodrich, researchers compiled a detailed analysis of nineteen methacrylate copolymers, and fourteen norbornene addition polymers.<sup>16</sup> The etch rates were compared, along with a novolac (SPR-510L) and Apex-E under

Sematech standard polysilicon and oxide etch conditions. An examination of the data plotted against the Ohnishi parameter and the ring parameter revealed mixed agreement. Incorporating portions of these models, the incremental structural parameter (ISP) model was derived, with good agreement between predicted and actual etch rates. This model also was unique in treating acid-labile groups separately, as these groups have a tendency to etch faster than otherwise predicted. The model was defined in a somewhat complicated manner, where the monomer structural contribution is

$$MSC = N_H Q_1 + \frac{(N_{C-C})^2 Q_2}{N_C} + N_{C-O} Q_3 + N_{C-N} Q_4 - \left[ (N_H)_{al} Q_1 + \frac{(N_{C-C})_{al}^2 Q_2}{(N_C)_{al}} \right] Q_5, \quad [6]$$

where  $N_H$  and  $N_C$  are the number of hydrogen and carbon atoms in the monomer,  $N_{C-C}$ ,  $N_{C-O}$ , and  $N_{C-N}$  represent the number of carbon-carbon bonds, carbon-oxygen bonds, and carbon-nitrogen bonds in the monomer, respectively, and each  $Q_i$  is an experimentally-determined constant for the etch process examined. The incremental structural parameter, ISP, is a weighted mole fraction of the MSC for each monomer type in the resist polymer. The etch rate of a photoresist is proportional to ISP. This model was a clear improvement over its predecessors, as far as modeling capability. The major weakness of the ISP model is the presence of an offset between polymers with different backbones, making the model non-universal. Also, the presence of halogen and elements that form refractory oxides in the resist was apparently neglected, though the presence and bonding structure of these elements may have a profound effect on the etch rate. Additionally, the authors mention that the presence of a PAG in the resist film can drastically change the etch behavior of the resist, though they concede that the mechanism of acid generation is unclear. Finally, the authors

wisely caution that any published data on etch rates or selectivity is highly based on the particular etch process used. This perspective emphasizes that the etching process is not well-understood, and one process cannot easily be translated into the terms of another. Furthermore, much work remains before a complete understanding of the plasma etching of organic materials can be attained.

### 3.1.2. Bilayer photoresists

#### 3.1.2.1. Motivation and background

Although the physical and chemical effects of plasma etching are not entirely understood, it is well-known that materials containing elements known to form refractory oxides will do so in the presence of an oxidizing plasma, such as  $O_2$ .<sup>18-23</sup> Examples of such elements include Si, Cr,<sup>24</sup> and Al.<sup>25</sup> In lithographic imaging, Si is most often used, as it also provides transparency at DUV exposure wavelengths. As mentioned earlier, these refractory oxides can serve as masking materials for further etch processes. Other elements commonly present in photoresists, notably carbon and hydrogen, will form volatile oxidized byproducts in the presence of an  $O_2$  plasma.<sup>23</sup> The use of materials known for their excellent etch resistance, in conjunction with materials that satisfy other required properties has led to the concept of a multilayer resist system.

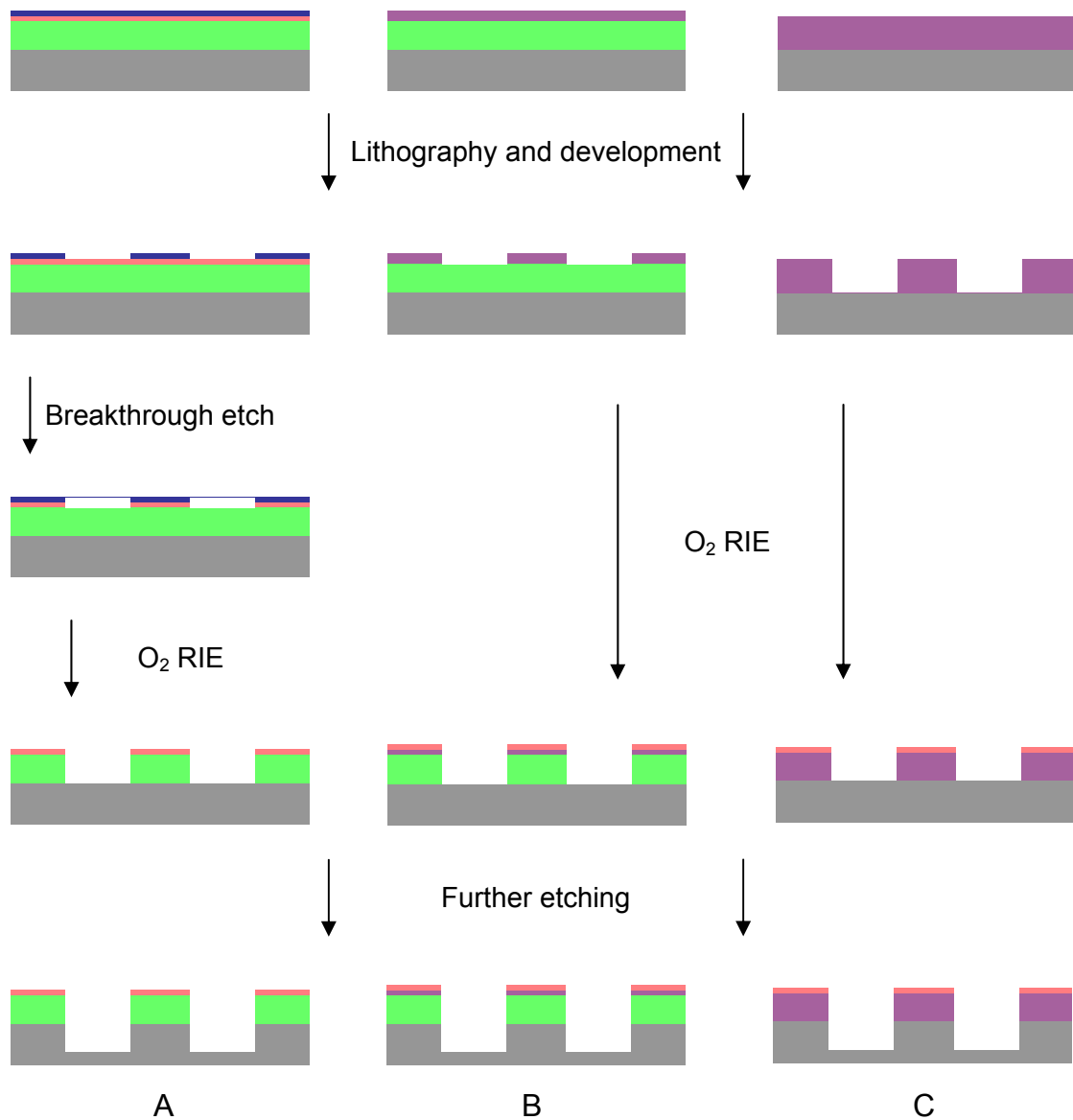


Figure 3.2. Multilayer resists for high aspect ratio etching: trilayer resist (A), bilayer resist (B), and single-coating bilayer resist (C).

The initial multilayer resist systems were implemented with three separately coated films.<sup>20</sup> The thin top layer was a photo-imagable polymer, which could be imaged and developed using traditional lithographic methods (Fig. 3.2). This layer consisted of a novolac resist or a cross-linkable styrenic polymer, for positive or negative-tone imaging. The thin middle layer served as the RIE barrier, typically made of a spin-on-glass material,



such as a tetraalkoxysilane, or a polysiloxane. In the presence of an O<sub>2</sub> plasma, this layer reacts to form a passivating SiO<sub>2</sub> barrier layer. Finally, the thick bottom layer was used to planarize the substrate, which may have been partially-patterned during an earlier step. The original motivation for multilayer resists was to address the formation of high aspect ratio images through dry plasma etching.<sup>26</sup> Also, the use of multilayer resists allayed concerns of imaging with DUV tools, which were expected to have a very limited DOF.<sup>20</sup> Imaging with a small DOF necessitated the use of thin imaging films, though often to the detriment of etching capabilities. Multilayer resist stacks, with a large planarizing layer, was the nexus between these lithographic constraints of narrow DOF and high etch resistance. Later work on multilayer resists condensed the imagable layer and the etch resistant layer into one material through the combination of silicon-containing groups, and acid-sensitive groups in one polymer. A protective SiO<sub>2</sub> layer could be formed from silylated portions of the resist in the presence of the O<sub>2</sub> plasma. While an intermediate layer could be eliminated in this manner, the narrow DOF requirements continued the necessity for a thick planarization layer. Using a bilayer approach effectively reduced the number of processing steps, as the initial breakthrough etch through the O<sub>2</sub> plasma-resistant layer was no longer necessary, and a third layer of the resist stack no longer needed to be coated. The use of a bilayer resist also has development advantages, since the patterning of a thin layer of film will not be as susceptible to image collapse as in the high aspect ratio structures developed in single-layer resists.<sup>27</sup> Of course, the process complexity is increased when multiple resist layers need to be coated. Therefore, further advances in lithographic processing have enabled “multilayer” resists to consist of a single-coated layer. The need for thinner resist films for smaller images, as well as the development of resists with greater selectivity have enabled the use of singly-coated

multilayer resist systems. The etch-resistant SiO<sub>2</sub> layer was formed as indicated for bilayer resists.

A successful bilayer resist will exhibit at least a 10:1 selectivity over polysilicon.<sup>26</sup> In order to achieve such results, it has been estimated that the photoresist must contain at least 9 wt% Si in order to form the SiO<sub>2</sub> passivating layer. There are multiple ways in which silicon can be incorporated into a photoresist to enhance the selectivity. These can be separated into three classes of materials: polysilanes, polysiloxanes, and silsesquioxanes. These materials and their uses as etch masks in bilayer resists will be discussed in the following sections.

### 3.1.2.2. Silicon in bilayer photoresists

#### 3.1.2.2.1. Polysilanes

Some initial, basic work to incorporate silicon into photoresists placed pendant silane groups onto existing polymer platforms, such as novolacs<sup>26,28</sup> and polyvinylsulfones<sup>29,30</sup> (Fig. 3.3). In novolac materials, p-trimethylsilylmethyl phenol has been used to replace a portion of the m- or p-cresol used for synthesizing the polymer resin.<sup>26</sup> In polymers containing up to 9.7 wt% Si, O<sub>2</sub> plasma etch rates have been observed to be as slow as 240 Å/min – in contrast to 2300 Å/min for a commercial Shipley novolac, HPR-204. Therefore, a thin layer of the patterned silylated novolac will etch approximately 9.5 times slower than the underlying thick layer of HPR-204, enabling high aspect ratio images. These etching results were obtained in an oxygen plasma, with a flow rate of 15 sccm, at a pressure of 20 mTorr, and with a bias voltage of -200V. The most significant disadvantage of this resist was its low T<sub>g</sub> at 26 °C. This only allowed very thin imaging layers, to minimize polymer flow during the PEB. Additionally, novolac-based resists are most useful at G-line and I-line technologies. Other lithographic technologies require

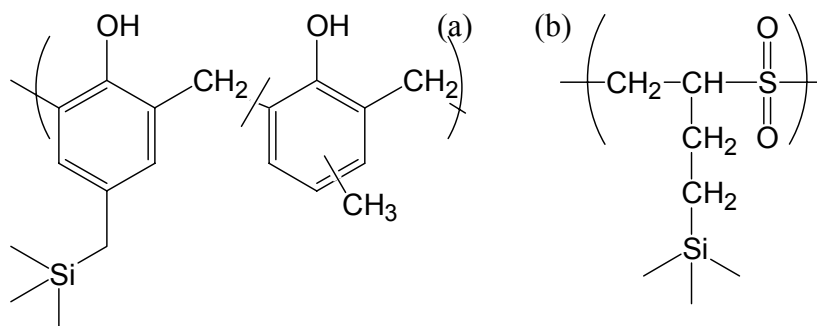


Figure 3.3. Polymer platforms containing silane side groups. (a) Novolac resin containing p-trimethylsilylmethyl phenol and (b) poly(3-butenyltrimethylsilane sulfone).

more transparent resists. For etch-resistant e-beam resists containing pendant silanes, Gozdz and coworkers have examined sulfur dioxide copolymers.<sup>29,30</sup> In the absence of silicon, these copolymers exhibit very poor etch resistance.<sup>30</sup> However, using monomers such as 3-butenyltrimethylsilane copolymers have been made as negative-tone e-beam resists that exhibit excellent O<sub>2</sub> plasma etch resistance.<sup>29</sup> For example, the copolymer shown in Fig. 3.3(b) contains 14.6 wt% Si, and etched at 5 – 10 Å/min, after an initial 1 – 2 minutes of fast etching during the formation of the SiO<sub>2</sub> barrier layer. “Standard” etch conditions were used.<sup>30</sup> Namely, the O<sub>2</sub> pressure was 15 mTorr, and the voltage bias was -400 V. Flow rates of O<sub>2</sub> were not disclosed. Further related research in this group has produced p-trimethylsilylstyrene and p-pentamethyldisilylstyrene copolymers with SO<sub>2</sub>. Under the latter etching conditions described, the disilylstyrene – SO<sub>2</sub> copolymer containing 18.8 wt% Si was found to etch at 25Å/min. While this rate is much faster than that of the silylated PBS analog, it is still remarkably slow. Either of these SO<sub>2</sub> copolymer platforms would exhibit excellent properties as etch-resistant, bilayer e-beam resists. Unlike the silylated novolac, these materials exhibited excellent thermal stability. The PBS analog was found to have a T<sub>g</sub> of 120 °C, while the styrenic copolymers each had T<sub>g</sub>’s greater than 150 °C. Unfortunately,

the etch rates for these silylated SO<sub>2</sub> copolymers cannot be directly compared with the etch performance of the silylated novolac described earlier. The lower pressure of the plasma used for etching the SO<sub>2</sub> copolymers versus that of the silylated novolac indicates a lower plasma density. This parameter alone suggests a slower etch for the SO<sub>2</sub> copolymers, as fewer plasma components are present at any given time. However, the greater bias voltage used for etching SO<sub>2</sub> copolymers suggests a faster etch rate, as ions in the plasma will bombard the polymer film surface with greater energy than in the etching of the novolac. Additionally, the undisclosed O<sub>2</sub> flow rate in the etching of SO<sub>2</sub> copolymers poses a quandry, as there is no way to compare the rate of fresh incoming etchant with that of the related novolac.

The use of silanes in bilayer photoresists has also been briefly examined from the perspective of using photosensitive polysilanes, with solubilizing side groups.<sup>31-33</sup> Akin to SO<sub>2</sub> copolymers, these materials undergo chain scission during exposure. A solubility contrast is achieved through the molecular weight difference between exposed and unexposed resist. Unlike typical novolac or chemical amplification resists, a high absorbance at the exposure wavelength is desirable. Typically, polysilanes exhibit an absorption maximum between 300 – 400 nm.<sup>32</sup> As Figure 3.4 illustrates, the absorbance at lower wavelengths is significant, as well, making these materials suitable for I-line, 248 nm, and possibly 193 nm exposures. While the photolability of polysilanes in solution is quite high, the photoscission reaction in the polymer film is significantly less efficient. This is suspected to be due to the greater ease of free radical recombination in the solid state. Furthermore, the contrast of these materials is hampered by potential cross-linking, which will counteract the

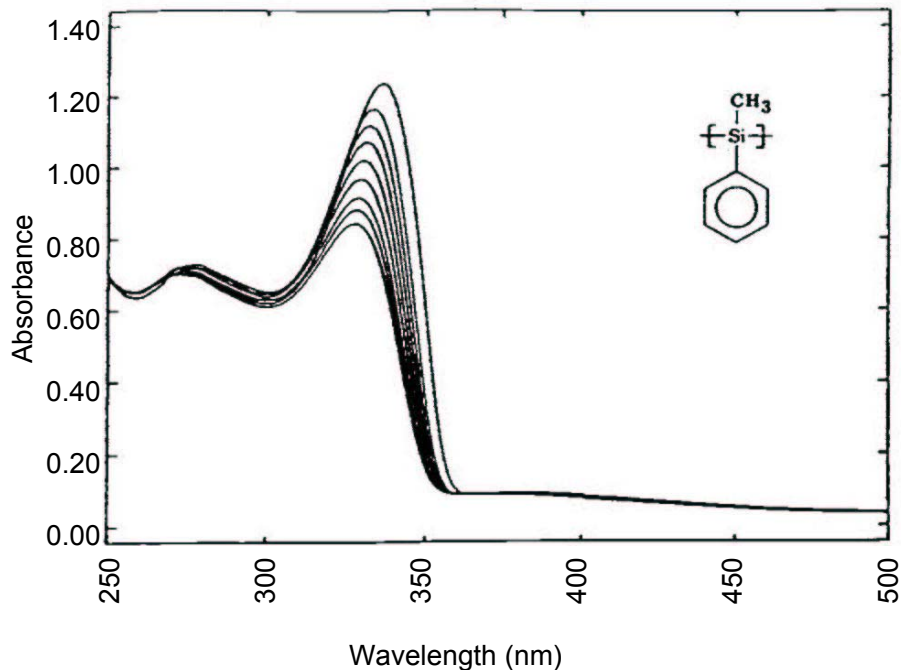


Figure 3.4. UV absorbance and photobleaching of an example polysilane.<sup>32</sup>

solubility contrast obtained through a molecular weight reduction from photoscission.<sup>32</sup> The sensitivity of these materials is related to their photobleaching rate at the exposure wavelength. Wallraff and coworkers have developed polysilanes exhibiting faster photobleaching rates, and thus greater sensitivities, through the manipulation of polymer side groups, and the addition of an aromatic sensitizer.<sup>32</sup> This work successfully decreased the required exposure dose from 150 mJ/cm<sup>2</sup> to 20 mJ/cm<sup>2</sup>. Dabbagh *et al.* described substantial issues in the use of a related material, plasma polymerized methylsilane (PPMS).<sup>33</sup> This material will oxidize in the presence of UV light, and can be developed in the positive tone using HF vapor. However, this resist system suffered from poor contrast, as the oxidation of the film was limited by O<sub>2</sub> diffusion into the film. Furthermore, a 100 – 300 Å residue layer remained post-development, which was resistant to oxide etching. An additional halogen

breakthrough etch was required to remove this residue, and subsequent O<sub>2</sub> etching resulted in poor image fidelity.

Silylated materials have been investigated as bilayer resists, both with silanes as side groups or comprising the main chain of the polymer. While these materials show some promise as etch resistant bilayer resists, limited success has been realized, and therefore they have not been extensively examined. A related class of materials, polysiloxanes, have been investigated in more detail as highly etch resistant top layer resists.

#### 3.1.2.2.2. Polysiloxanes

As with silylated resists, siloxanes have been examined both as a side-chain and the main chain of an etch resistant photoresist. As side chains in bilayer resists, methacryl-functionalized polydimethylsiloxanes (PDMS) have been copolymerized with acid cleavable *tert*-butylmethacrylate (TBMA).<sup>22,34</sup> Such copolymers were found to have the possibility of negative tone imaging in high-energy exposures, such as 157 nm optical and e-beam exposures, and positive tone imaging at DUV.<sup>34</sup> The negative tone behavior was due to crosslinking of the PDMS chains, and positive tone imaging could be realized with TMAH development. Unfortunately, the imaging of these copolymers could not be well-controlled. They were found to have poor film formation properties, and images swelled in the presence of aqueous base developer. Minimum resolution of TBMA copolymers was greater than 1 μm, but the resolution could be improved to 0.5 μm by replacing TBMA with tBOC-Sty.<sup>22</sup> Replacement of TBMA with tBOC-Sty also greatly improved the T<sub>g</sub>, from 14 °C to 106 °C. The tBOC-Sty copolymer was found to have an etch selectivity up to seven times slower than novolac. Low molecular weight PDMS macromers (<1K) were required to prevent microphase separation. Plasma etching of copolymers containing larger macromers has

resulted in non-uniform SiO<sub>2</sub> networks, which created pitting and poor image transfer.<sup>22,34</sup> However, related work, incorporating 10K vinyl-functionalized PDMS macromonomers into a PBS copolymer, demonstrated excellent image transfer with no observed pitting, though microphase separation was evidenced.<sup>21</sup>

Polysiloxanes have received limited attention as the top layer in bilayer resists, primarily because of their well-known low glass transition temperatures. Thin films of PDMS (100 nm) have been used, chiefly as a model negative-tone crosslinking polysiloxane, in the examination of surface roughness and LER as a function of various oxidizing plasma conditions.<sup>23,35</sup> Other polysiloxanes have incorporated acid cleavable groups, such as tBOC-Sty and norbornyl-2-*tert*-butoxycarbonate (NBtBOC).<sup>22</sup> As an advantage over graft copolymers, these materials easily incorporate a large weight percent Si, which enables high etch resistance. Unfortunately, the T<sub>g</sub>'s of these materials are quite low. The bulky substituents of the norbornyl polymer allow a T<sub>g</sub> of 60 °C, at best. The selectivity of these materials versus novolac in an O<sub>2</sub> plasma was sufficient for a bilayer resist. The tBOC-Sty polymer etched ten times slower, and the NBtBOC polymer etched six times slower than novolac. Unfortunately, the outgassing of volatile byproducts during O<sub>2</sub> plasma etching resulted in a porous film, which would prevent high-fidelity image transfer into the novolac layer (Figure 3.5). A brief report from Paraszczak and coworkers examined a variety of main-chain siloxane copolymers for their O<sub>2</sub> plasma etch performance.<sup>36</sup> It is interesting to note that, of the 11 polymers studied, the highly branched polysiloxanes etched the slowest, with only steam-grown SiO<sub>2</sub> etching slower. This suggests that a highly branched polysiloxane material will exhibit even greater O<sub>2</sub> plasma etch resistance than an ordinary linear polysiloxane.

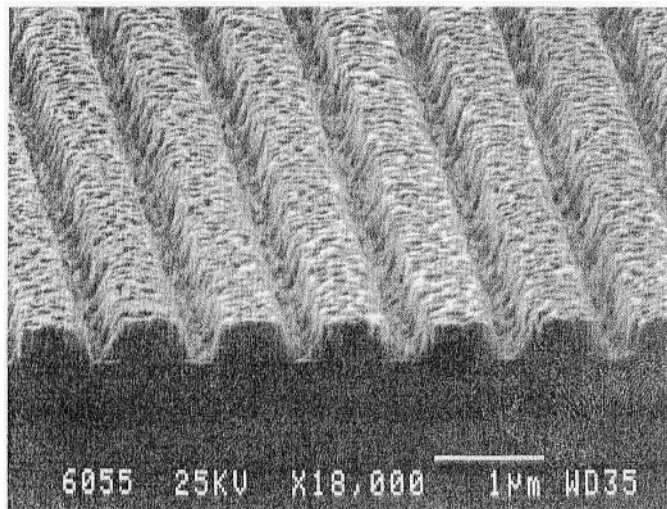


Figure 3.5. Porous images due to outgassing of tBOC-Sty functionalized polysiloxane after O<sub>2</sub> plasma etch.

The use of siloxanes in bilayer resists has been facilitated by relatively inexpensive starting materials and ease of synthesis. The high etch resistance capabilities of these materials make them attractive candidates for bilayer applications. Unfortunately, polysiloxane-based photoresists tend to exhibit low glass transition temperatures, which could erode imaged materials during the PEB. Further distortion of images has been observed from swelling in the presence of TMAH developer. However, the greatest barrier to commercial implementation of polysiloxane resists is their tendency to outgas during exposure. Siloxane-containing polymers have been found to outgas at a rate substantially greater than silane-containing polymers.<sup>37</sup> Deposition of silicon-based outgassing products on the final optical lens has been shown to cause irreversible damage to this expensive component of a lithography scanner. In an effort to minimize such outgassing, interconnected Si-O networks have received recent attention.

#### 3.1.2.2.3. Silsesquioxane-based polymers



Silsesquioxanes (SSQ) are siloxane-based materials in either a ladder or polyhedral architecture (Fig. 3.6). The interconnected Si-O network has been shown to outgas during 193 nm or 157 nm exposure at significantly lower level than either silanes or polysiloxanes.<sup>37</sup> Also, the lack of flexibility in these structures has enabled elevated glass

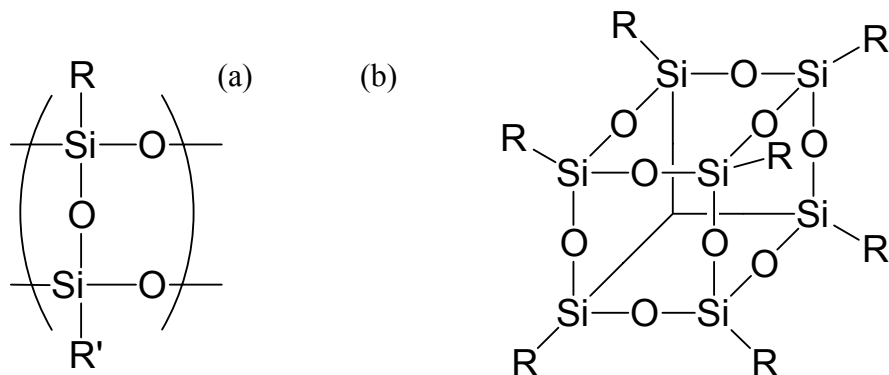


Figure 3.6. Different architectures of silsesquioxanes: (a) ladder-type silsesquioxane, and (b) polyhedral oligomeric silsesquioxane (POSS). The silicon and oxygen atoms in the background of (b) have been omitted for clarity.

transition temperatures, in stark contrast to the related polysiloxane materials. The earliest reports of SSQ materials used as photoresists have used the ladder-type SSQ. These resists were used in the negative tone, with cross-linking substituents, including methacryl<sup>38</sup> or allyl<sup>39</sup> groups. The methacryl-substituted SSQ was found to etch 11 – 18 times slower than an AZ novolac under and oxygen plasma, and the allyl-substituted SSQ etched 67 times slower than the MP-2400 novolac. It should be noted that the etch conditions were not clarified for each of these materials, and the comparative novolac materials were not the same. Therefore, the relative etch rates of the methacryl and allyl SSQ materials cannot be compared with this data. However, this data does indicate that ladder SSQ materials etch much slower than novolacs, making them suitable for bilayer applications. van de Grampel and coworkers have investigated a SSQ material that acts as a negative tone resist, based on

polycondensation reactions (Fig. 3.7).<sup>22</sup> Containing 21 wt% Si, this polymer etched 19 times slower than an AZ novolac. A prospective positive

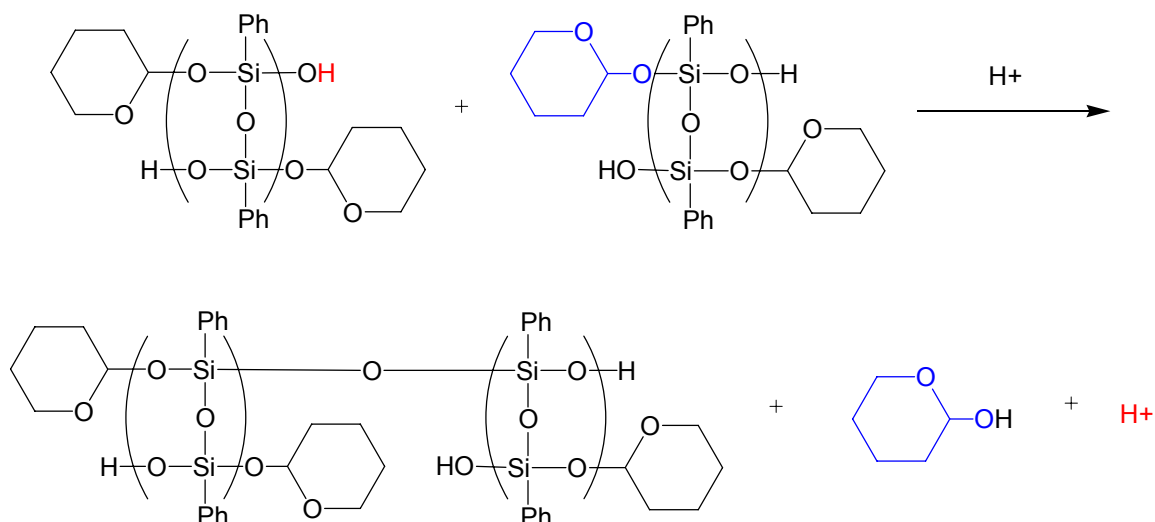


Figure 3.7. Polycondensation of a negative tone SSQ resist.

tone SSQ resist that has been examined is *p*-hydroxybenzyl-substituted SSQ, which uses a solubility difference attained through a photoactive compound, similar to how DNQ provides a solubility difference for novolac.<sup>40</sup> As desired, the etch ratio of this resist to that of novolac in an oxygen plasma was 1:28. While much of the research on ladder-type SSQ resists has been applied to I-line and 248 nm lithography, relatively little work has been done to apply these materials to 193 nm, 157 nm, and e-beam lithographies. Researchers at Selete described a silsesquioxane for use in bilayer resists at 157 nm.<sup>41</sup> This resist contained fluorinated side groups to minimize absorbance at 157 nm. While the nature of these side groups was not disclosed, a SSQ containing 16 wt% fluorine had an absorbance of 3.32  $\mu\text{m}^{-1}$ . Increasing the fluorine content to 29 wt% lowered the absorbance significantly to 1.85  $\mu\text{m}^{-1}$  at 157 nm. As with the previously described SSQ resists, this material performed well under

O<sub>2</sub> plasma etch conditions, etching 4 – 6 times slower than JSR's NFC-B200 novolac resist. While this resist etched slower than the reference novolac material, it is anticipated that the high fluorine content of the resist negatively impacted the etch resistance of this material.<sup>7,34</sup>

Concerns have arisen regarding ladder-type SSQ materials. Specifically, the lack of an exact molecular formula—even in materials bought from major vendors—has bothered researchers, as the material's identity is not well-understood or characterized.<sup>34</sup> Also, the presence of silanol groups, which may be present for condensation reactions in ladder SSQ resists, will be detrimental to the material's absorbance at DUV wavelengths. These issues could be eliminated through the use of a “small molecule” version of SSQ. Such materials are known as polyhedral oligomeric silsesquioxanes (POSS), and can be functionalized for ease of incorporation into a polymeric architecture (Fig. 3.6(b)). Each silicon in a POSS molecule contains an alkyl substituent. As already stated, one substituent can be functionalized with a polymerizable group; the remaining substituents are typically simple hydrocarbons. Gonsalves and coworkers described the use of POSS in photoresists as early as 2001.<sup>17</sup> This research incorporated a methacryl-functionalized POSS into a methacrylate copolymer for positive tone e-beam imaging. Unlike many of the materials described to this point, this resist was designed to be a single layer resist that could form an etch resistant top layer upon exposure to an O<sub>2</sub> plasma. The incorporation of POSS certainly aided in the elevation of glass transition temperatures for these materials, which ranged from 170 – 186 °C, depending on composition. In an oxidizing plasma, a copolymer containing 30 wt% POSS (6.7 wt% Si) was found to etch about 1/3 as fast as a similar formulation containing no POSS. This corresponded to an etch rate of 900 Å/min in plasma conditions of 60 mTorr pressure of CF<sub>4</sub> and O<sub>2</sub>, flowing at 12.6 and 30 sccm, respectively. The power density was

maintained at  $0.25 \text{ W/cm}^2$ . In fact, the authors found that the RIE rate dropped significantly in copolymers containing at least 20 wt% POSS (only 4.9 wt% Si!). The quantity of silicon incorporated into these polymers, leading to substantial etch resistance, is dramatically lower than the recommended 10 – 15 wt % silicon incorporation for a highly etch resistant material.<sup>19,20</sup> Detailed investigations of POSS-containing photoresists has been undertaken by Argitis and coworkers.<sup>34,42,43</sup> These resists have been primarily examined as positive tone resists for 157 nm and e-beam lithography. POSS groups were incorporated into polymers through a methacryl substituent. Other monomers included methacrylic acid, methyl methacrylate, itaconic anhydride, and *tert*-butyl methacrylate for a contrastable group. Two different alkyl POSS substituents were compared for lithographic performance: ethyl and cyclopentyl.<sup>34</sup> In otherwise identical polymers, the polymer containing ethyl-substituted POSS outperformed the cyclopentyl analog in absorbance at 157 nm, etch resistance, and post-etch roughness. The greater hydrocarbon content of cyclopentyl-POSS unsurprisingly results in a greater 157 nm absorbance, as the carbon-hydrogen bond is known to contribute to absorbance at this wavelength.<sup>44</sup> The authors of this study suggested that the diminished etch resistance and greater post-etch roughness observed in the cyclopentyl-POSS copolymer may be due to the bulky size of this substituent, and that it prevents the formation of a smooth silicon oxide film.<sup>34</sup> On the other hand, the copolymers containing 30 wt% ethyl-substituted POSS (9 wt% Si) were found to etch 20 times slower than hard baked novolac in an  $\text{O}_2$  plasma. Imaged lines and spaces could be resolved with this resist down to 100 nm using 157 nm exposure.<sup>42</sup> Although this resist fared better than the cyclopentyl analog, its absorbance at 157 nm ( $4.5 \mu\text{m}^{-1}$ ) limits it to bilayer applications.

Silsesquioxane materials provide the desired etch resistance for bilayer resist applications, with the added advantage of high glass transition temperatures, relative to other silicon-containing materials. These properties enable high aspect ratio imaging with ever smaller critical dimensions. Ladder-type silsesquioxanes were pivotal in the development of high T<sub>g</sub> silicon-containing resists, though their cross-linking mechanism for solubility switch, and inexact molecular formulas has limited their use. SSQ materials of known, oligomeric structure have only received recent attention as the etch-resistant portion of bilayer resists. The current synthesis of POSS architectures is low-yielding, which contributes to their high cost. However, with judicious incorporation of POSS groups into photoresists, these materials have great potential as bilayer resists.

### 3.1.3. Present approach

Despite the breadth of knowledge of materials for bilayer resists, no work has described the design of bilayer photoresists that could be developed in condensed carbon dioxide. In an effort to design materials that could be used for such a purpose, and also bear the desired properties of a resist, an addition polymer of norbornene-based monomers was pursued. As well-described in the previous chapter, norbornene addition polymers are expected to provide a high glass transition temperature. Also, POSS groups were targeted for the incorporation of silicon into the resist. With their well-defined architecture and low outgasing, POSS groups seemed the best choice among silicon-containing materials. Furthermore, norbornenyl-functionalized POSS materials were known to be commercially available. Based on previous research, we have estimated that POSS incorporation into norbornene-based photoresists at levels of 9 wt% Si were expected to decrease the O<sub>2</sub> plasma etch rate to 20 times slower than that of novolac.<sup>42</sup> The POSS moiety, in conjunction with highly

fluorinated monomers, was expected to provide the necessary CO<sub>2</sub> solubility for development of an imaged resist. Fluorinated monomers, described in Chapter 2, were used for this purpose. Chemical switching of these copolymers was to be carried out through the incorporation of NBHFA, which served well in SLR applications.

## 3.2. Experimental

### 3.2.1. Synthesis

#### 3.2.1.1. Materials

Methylene chloride (CH<sub>2</sub>Cl<sub>2</sub>, 99.5% Fisher) was dried over 4Å molecular sieves and degassed with argon. Allyl bromide (Aldrich), allylpalladium chloride dimer (allyl-Pd, 99% Strem), argon (Ar, Fisher), carbon black (Fisher), celite (Aldrich), di-*tert*-butylphenol (DBP, Aldrich), hexanes (Fisher), magnesium sulfate (MgSO<sub>4</sub>, Fisher), methanol (MeOH, Fisher), 1,1,1,3,3-pentafluorobutane (Solkane, Solvay Fluorides), 1H,1H-perfluorooctan-1-ol (Fluorosolutions), 50 w/w% potassium hydroxide (KOH) solution (Fisher), 1-[2-(5-norbornen-2-yl)ethyl]-3,5,7,9,11,13,15-heptacyclopentyl[9.5.1.1<sup>3,9</sup>.1<sup>5,15</sup>.1<sup>7,13</sup>]octasiloxane (NBPOSS, Sigma-Aldrich), silver hexafluoroantimonate (AgSbF<sub>6</sub>, 98% Strem), tetrabutyl ammonium hydrogen sulfate (TBAHS, Aldrich), tetrahydrofuran (THF), and  $\alpha,\alpha,\alpha$ -trifluorotoluene (TFT, Aldrich) were used as received. Allyl-Pd and AgSbF<sub>6</sub> were stored in a dry box prior to use. AgSbF<sub>6</sub> was stored away from light. Dicyclopentadiene (DCP, Aldrich) was cracked immediately prior to use.

#### 3.2.1.2. Equipment

Schlenk flasks and a custom-made fritted funnel, bearing a 14/20 male ground glass joint and a 14/20 female ground glass joint were made by Walt Boger of the University of North Carolina Chemistry Department glass shop. Reactions were heated in a mineral oil bath

(Fisher) on a heater/stir plate from Fisher Scientific. Air and moisture-sensitive reagents were prepared in an oxygen-free glove box from Vacuum Atmospheres Company.

### 3.2.1.3. Monomer synthesis

#### 3.2.1.3.1. (1H,1H-Perfluorooctyloxy)-propene (FAE)

A round bottom flask was charged with 1H,1H-perfluorooctan-1-ol (19.83 g, 62.75 mmol) and TBAHS (2.15 g, 6.34 mmol). Addition of 50 mL of a 50 w/w% aqueous KOH solution resulted in the formation of a fluffy white precipitate. The mixture was stirred at RT for 10 minutes, followed by the addition of allyl bromide (21.36 g, 176.53 mmol) in 50 mL CH<sub>2</sub>Cl<sub>2</sub>. The reaction mixture was gently heated at 40°C for 18h. The CH<sub>2</sub>Cl<sub>2</sub> layer was dried over MgSO<sub>4</sub>, filtered, and dried. Vacuum distillation afforded a colorless liquid product at 30°C (62%).

#### 3.2.1.3.2. 5-(1H,1H-Perfluorooctyloxymethyl)-norborn-2-ene (NBFAE)

A pressure tube was charged with cyclopentadiene (2.70 g, 40.90 mmol), FAE (12.16 g, 27.60 mmol), and DBP (27.4 mg, 0.13 mmol). The vessel was closed and heated to 170°C for 2 days. Vacuum distillation afforded a colorless liquid product at 55°C in 40% yield.

### 3.2.1.4. Polymer synthesis

#### 3.2.1.4.1. Addition polymerization

A typical polymerization using a palladium catalyst was carried out in an inert atmosphere, similar to literature procedures (Fig. 3.8).<sup>45</sup> A solution of allyl-Pd (4.4 mg, 12 μmol) and AgSbF<sub>6</sub> (13.5 mg, 39 μmol) in 5 mL CH<sub>2</sub>Cl<sub>2</sub> was stirred for 10 min. The catalyst solution was transferred *via* cannula onto a fitted ground glass frit and allowed to filter into a flask containing a mixture of NBFAE (364 mg, 719 μmol) and NBPOSS (653 mg, 596 μmol). The yellow reaction mixture was heated gently overnight at 30 – 35 °C. The

resultant gelatinous yellow solid was isolated *via* precipitation into hexanes. The polymer was redissolved in Solkane, treated with Celite and carbon black, then precipitated into methanol yielded a white powder in 57% yield.

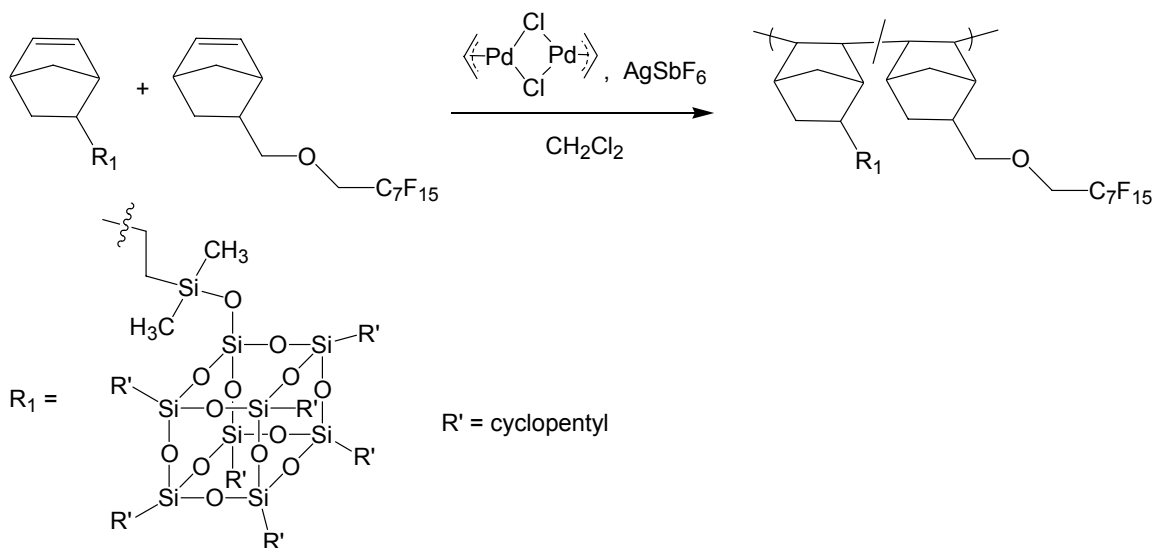


Figure 3.8. Synthesis of NBPOSS-NBFAE copolymer.

### 3.2.2. Characterization

#### 3.2.2.1. Nuclear Magnetic Resonance Spectroscopy (NMR)

$^1H$  and  $^{19}F$  NMR spectra were collected on a Bruker Avance 400 MHz spectrometer and analyzed using Mestre-C 2.3 software. Approximately 5 mg of each monomer sample was dissolved in 1 mL deuterated chloroform ( $CDCl_3$ , Cambridge Isotope Labs), with a TFT internal reference for  $^{19}F$  NMR. Polymer samples were dissolved in TFT, with a  $CDCl_3$  external lock solvent.  $^1H$  chemical shifts were referenced to  $CHCl_3$  at 7.24 ppm and  $^{19}F$  chemical shifts were referenced to TFT -63.72 ppm or fluorobenzene at -113.15 ppm. The labelling of carbon atom positions in norbornyl materials is in accordance with IUPAC definitions (Fig. 3.4).



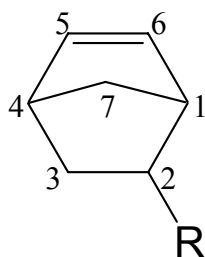


Figure 3.9. IUPAC numbering of a substituted norbornene molecule.

#### 3.2.2.2. Elemental Analysis

Elemental analysis of monomers and polymers for C, H, and F content was carried out by Atlantic Microlabs, Inc in Norcross, GA.

#### 3.2.2.3. Etching

Reactive ion etching (RIE) was performed at the NCSU Nanofabrication Facility, using a Semi Group RIE System 1000 TP tool. Samples with varying w/w% polymer in TFT were filtered through 0.45  $\mu\text{m}$  PTFE syringe filters. The filtered solutions were spin coated at 1100 rpm for 120 s on a Cookson Electronics Specialty Coating Systems G3P-8 spin coater onto 2-inch silicon wafers. The films were baked at 115  $^{\circ}\text{C}$  for 120 s. Films were etched for 1-8 minutes under an RIE plasma. The plasma used was a mixture of  $\text{CHF}_3$  (20 sccm) and  $\text{O}_2$  (5 sccm). The chamber pressure was 60 mTorr, the cathode configuration was  $\text{Al}_2\text{O}_3/\text{Al}$  and the power was 100W. Film thicknesses were measured before and after etching with interferometry.

#### 3.2.2.4. Interferometry

Interferometric measurements were obtained at the NCSU Nanofabrication Facility, using a Nanometrics NanoSpec AFT. The wavelength was scanned from 480 nm to 790 nm.

### 3.3. Results and discussion

#### 3.3.1. Monomer characterization

A discussion of the synthesis and characterization of FAE and NBFAE can be found in sections 2.3.1.2. and 2.3.1.3.

### 3.3.2. Polymer characterization

Copolymers of NBFAE and NBPOSS were identified by  $^1\text{H}$  NMR,  $^{19}\text{F}$  NMR, and elemental analysis.  $^{19}\text{F}$  NMR spectra displayed the expected resonances arising from the NBFAE monomer, with broadened peaks due to molecular tumbling.  $^1\text{H}$  NMR spectra (Fig. 3.6) showed resonances indicative of NBFAE, due to the O-CH<sub>2</sub>-R<sub>f</sub> signal at 3.8 ppm and the NB-CH<sub>2</sub>-O signal at 3.5 ppm. Key resonances were also found due to NBPOSS. These were present at 0.1 ppm, due to the dimethylsilyl group adjacent to the POSS structure and at 0.5 ppm, due to an overlapping resonance of the silyl methylene protons and the resonance of protons at the 3 position of the norbornene. Other key resonances identified were due to the cyclopentyl groups on the POSS: the silyl methine peak was at 1.0 ppm, and the large peaks at 1.7 and 1.5 ppm were due to the remaining cyclopentyl protons. Assignments for NBPOSS resonances were based on comparison with the monomer spectrum. The percent monomer incorporation was determined by a relative integration of the peaks at 4.0 – 3.0 ppm, due to four NBFAE protons, to the entire spectrum from 4.0 – -0.2 ppm. This method resulted in a calculated 48 mol% POSS incorporation, for 45 mol% NBPOSS loading. This is equivalent to 15.2 wt% Si incorporation into the polymer, and was expected to provide excellent O<sub>2</sub> plasma etch resistance. The silicon content was also independently calculated from elemental analysis data (Table 3.1). Based on an initial observation of the elemental analysis data for a NBPOSS copolymer with 45 mol% NBPOSS loading, it is evident that the incorporation ratio of the two monomers is nearly the same as the loading ratio. Using the found fluorine content to calculate the weight percent NBFAE, it was determined that the

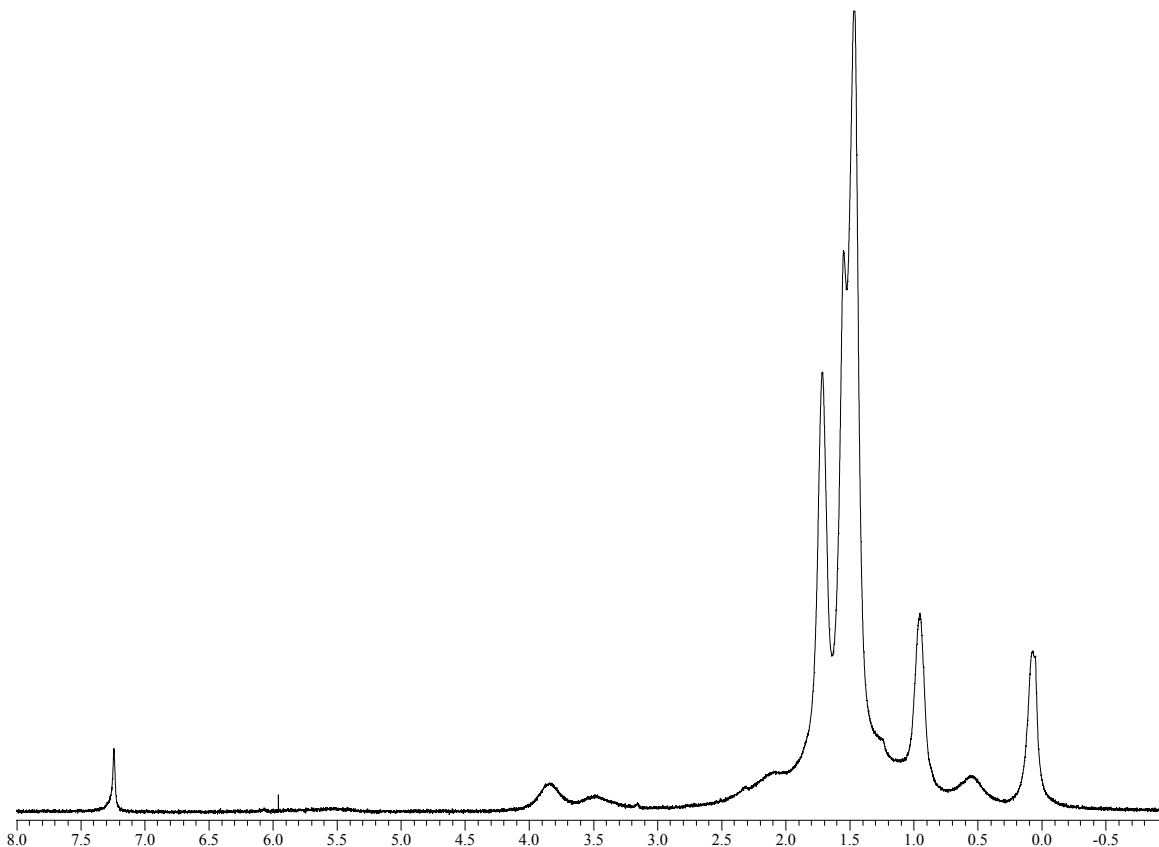


Figure 3.10.  $^1\text{H}$  NMR of poly(NBFAE/NBPOSS), containing 15 wt%Si. Percent POSS incorporation determined by relative integration of peaks at 4.0 – 3.0 ppm to entire spectrum.

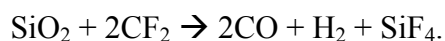
polymer contained 46 mol% NBPOSS, which corresponds to 14.8 wt% Si, in very good agreement with the NMR data. Another copolymer of NBFAE and NBPOSS was found to contain 9 wt% Si, using the same methods.

Element	Calculated	Found
C	45.05	45.69
H	5.38	5.69
F	24.11	19.97

Table 3.2. Elemental analysis of poly(NBFAE/POSS), containing 15%Si.

POSS-containing copolymers were evaluated for their resistance to RIE plasma etching. The oxidizing etch process used to evaluate these materials contained a mixture of  $\text{O}_2$  and  $\text{CHF}_3$ , rather than pure  $\text{O}_2$ , as this etch recipe had already been established for the etch tool,

and was known to have a slow etch rate for novolac.<sup>46</sup> Furthermore, the high fluorine content (20 – 56 wt%) gives these polymers the potential to etch at similar rates whether in a pure O<sub>2</sub> plasma or in a O<sub>2</sub>/fluorocarbon plasma. The highly fluorinated groups could serve as a F radical source in a pure O<sub>2</sub> etch, thereby changing the plasma composition to resemble an O<sub>2</sub>/fluorocarbon plasma.<sup>7,47</sup> The etch rates of the silicon-containing polymers were compared to the etch rate of Shipley 1813 Novolac resist (fig. 3.6). It was surprising to find that all the NBFAE/NBPOSS copolymers etched faster than the novolac. Even the copolymer containing 15 wt% silicon etched at 1.23 times as fast as the novolac. It is possible that this relatively poor etch performance may be due to the bulky cyclopentyl groups preventing the formation of a continuous SiO<sub>2</sub> layer.<sup>34</sup> Unfortunately, a norbornyl POSS monomer containing smaller alkyl side groups is not commercially available, and the synthesis of POSS materials are challenging. Another possible explanation for the etch rates found could be the concurrent formation and removal of silicon dioxide. The reactive O radicals and O<sub>2</sub> are expected to form the protective SiO<sub>2</sub> layer, while reactive F radicals are known to remove SiO<sub>2</sub> through the following reactions:<sup>47</sup>



As the materials studied here contained high fluorine contents, the removal of the SiO<sub>2</sub> protective layer would be unavoidable, even in the presence of a pure O<sub>2</sub> plasma etch. As these materials did not exhibit the desired etch resistance for a bilayer resist, further investigation into their properties was not pursued.

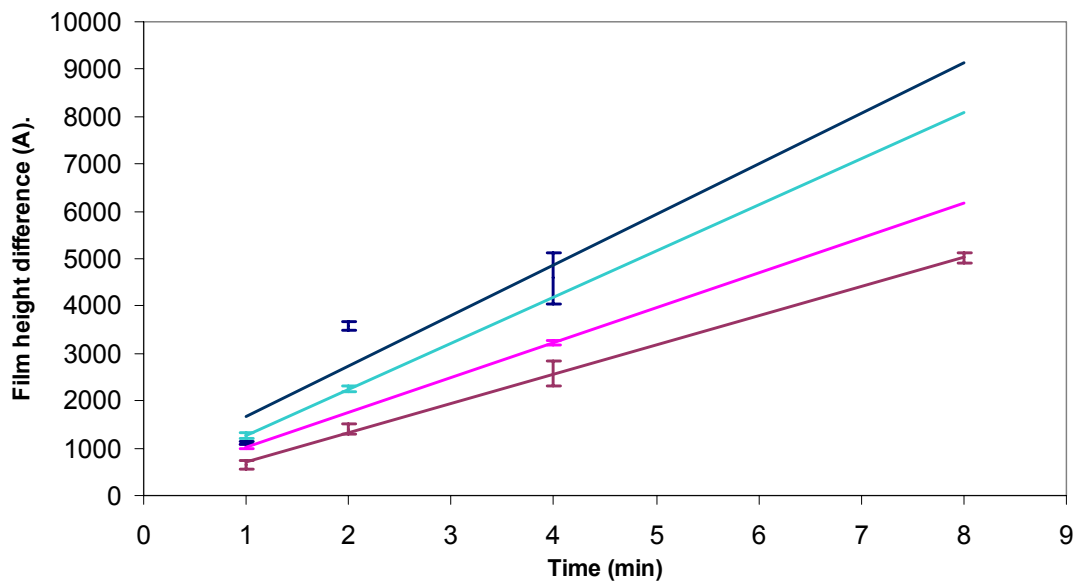


Figure 3.11. RIE data for copolymers of NBFAE and NBPOSS, containing 0 wt% Si (navy), 9 wt% Si (turquoise), and 15 wt% Si (pink). The etch data for Shipley 1813 Novolac is also shown (plum).

### 3.4. Conclusion

Bilayer photoresists have great potential to create high aspect ratio images. The most common implementation of bilayer resists incorporates moderate quantities of silicon, in order to form a refractory  $\text{SiO}_2$  passivating layer. The incorporation of Si through the use of POSS groups avoids the use of low  $T_g$  materials, which prevents image deformation during baking steps. Polymers described here for use as bilayer resists used POSS side groups, as well as highly fluorinated groups to enable  $\text{CO}_2$  solubility. Unfortunately, it appeared that such highly fluorinated groups were incompatible with the design of an etch resistant material. Future designs of  $\text{CO}_2$  soluble bilayer resists containing POSS will need to rely on siloxane content for  $\text{CO}_2$  solubility, rather than fluorine.

### 3.5. References

- 1) Lehmann, H. W., Plasma-assisted etching. In *Thin Film Processes II*, Vossen, J. L.; Kern, W., Eds. Academic Press, Inc.: New York, **1991**; 673-748.
- 2) Oehrlein, G., *J. Appl. Phys.* **1986**, *59*, 3053-3062.
- 3) Sze, S. M., *Semiconductor Devices: Physics and Technology*; John Wiley & Sons: New York, 1985; p 451-464.
- 4) Hartney, M. A.; Hess, D. W.; Soane, D. S., *J. Vac. Sci. Technol. B* **1989**, *7*, 1.
- 5) Furukawa, T.; Hagiwara, T.; Kawaguchi, E.; Matsunaga, K.; Suganaga, T.; Itani, T.; Fujii, K., *Proc SPIE (Adv. Resist Tech. Proc.)* **2004**, *5376*, 1064-1073.
- 6) Cook, J. M.; Benson, B. W., *J. Electrochem. Soc.* **1983**, *130*, 2459.
- 7) Collart, E. J. H.; Baggerman, J. A. G.; Visser, R. J., *J. Appl. Phys.* **1995**, *78*, 47-54.
- 8) Champman, B.; Minkievicz, V., *J. Vac. Sci. Technol.* **1978**, *15*, 329.
- 9) Stuart, R. V.; Wehner, G. K., *J. Appl. Phys.* **1962**, *33*, 2345.
- 10) Poll, H. U.; Meichsner, J.; Steinrucken, A., *Thin Solid Films* **1984**, *112*, 369.
- 11) (a) Pang, S. W.; Rathman, D. D.; Silverman, D. J.; Mountain, R. W.; DeGraff, P. D., *J. Appl. Phys.* **1983**, *54*, 3272; (b) Pang, S. W.; Horowitz, C. M.; Rathman, D. D.; Cabral, S. M.; Silverman, D. J.; Mountain, R. W., *Proc. Electrochem. Soc.* **1983**, *83-10*, 84.
- 12) Manchanda, L.; Schutz, R. J.; Van-Hise, C. W., *Proc. Electrochem. Soc.* **1987**, *87-11*, 263.
- 13) Gokan, H.; Esho, S.; Ohnishi, Y., *J. Electrochem. Soc.* **1983**, *130*, 143-146.
- 14) Kunz, R. R.; Palmateer, S. C.; Forte, A. R.; Allen, R. D.; Wallraff, G. M.; DiPietro, R. A.; Hofer, D. C., *Proc SPIE (Adv. Resist Tech. Proc.)* **1996**, *2724*, 365-376.
- 15) Dammel, R. R.; Ficner, S.; Oberlander, J.; Klauck-Jacobs, A.; Padmanaban, M.; Khanna, D. N.; Durham, D. L., *Proc SPIE (Adv. Resist Tech. Proc.)* **1998**, *3333*, 144-151.
- 16) Wallow, T.; Brock, P.; DiPietro, R.; Allen, R.; Opitz, J.; Sooriyakumaran, R.; Hofer, D.; Muete, J.; Byers, J.; Rich, G.; McCallum, M.; Schuetze, S.; Jayaraman, S.; Hullihen, K.; Vicari, R.; Rhodes, L.; Goodall, B.; Shick, R., *Proc SPIE (Adv. Resist Tech. Proc.)* **1998**, *3333*, 92-101.

- 17) Wu, H.; Hu, Y.; Gonsalves, K. E.; Yacaman, M. J., *J. Vac. Sci. Technol. B* **2001**, *19*, 851-855.
- 18) (a) Taylor, G. N.; Wolf, T. M., *Solid State Technology* **1980**, *20*, 1087; (b) Hashimoto, K.; Katsuyama, A.; Endo, M.; Sasago, M., *J. Vac. Sci. Technol. B* **1994**, *12*, 37-43.
- 19) Reichmanis, E.; Smolinsky, G.; Wilkings, C. W., Jr., *Solid State Technology* **1985**, 130-135.
- 20) Reichmanis, E.; Novembre, A. E.; Tarascon, R. G.; Shugard, A.; Thompson, L. F., Organosilicon polymers for microlithographic applications. In *Silicon-Based Polymer Science: A Comprehensive Resource*, Zeigler, J. M.; Fearon, F. W. G., Eds. American Chemical Society: Washington, DC, **1990**; *224*, 265-281.
- 21) DeSimone, J. M.; York, G. A.; McGrath, J. E.; Gozdz, A. S.; Bowden, M. J., *Macromolecules* **1991**, *24*, 5330-5339.
- 22) van de Grampel, J. C.; Puyenbroek, R.; Meetsma, A.; Rousseeuw, B. A. C.; van der Drift, E. W. J. M., New Polysiloxanes for chemically amplified resist applications. In *Microelectronics Technology*, Eds. American Chemical Society: New York, **1995**; *614*, 333-354.
- 23) Eon, D.; de Pouchques, L.; Peignon, M. C.; Candinaud, C.; Turban, G.; Tserepi, A.; Cordoyiannis, G.; Valamontes, E. S.; Raptis, I.; Gogolides, E., *Microelectron. Eng.* **2002**, *61-62*, 901-906.
- 24) Martin, L. J.; Wong, C. P., *IEEE Trans. Comp. Packag. Tech.* **2001**, *24*, 416-424.
- 25) Kitano, M.; Nagase, M.; Shirai, Y.; Ohmi, T., *Proc. Electrochem. Soc.* **2001**, *22* (*Corrosion and corrosion protection*), 115-121.
- 26) Tarascon, R. G.; Shugard, A.; Reichmanis, E., *Proc SPIE (Adv. Resist Tech. Proc.)* **1986**, *631*, 40-46.
- 27) Halle, S.; Thomas, A.; Armacost, M.; Dalton, T.; Chen, X. L.; Bukofsky, S.; Genz, O.; Lu, Z.; Butt, S.; Chen, Z.; Ferguson, R.; Coker, E.; Leidy, R.; Lin, Q.; Mahorowala, A.; Babich, K.; Petrillo, K.; Angelopoulos, M.; Ignatowicz, M.; Bui, B., *Proc SPIE (Opt. Microlith.)* **2001**, *4346*, 970-981.
- 28) Wilkins, C. W., Jr.; Reichmanis, E.; Wolf, T. M.; Smith, B. C., *J. Vac. Sci. Technol. B* **1985**, *3*, 306-309.
- 29) Gozdz, A. S.; Carnazza, C.; Bowden, M. J., *Proc SPIE (Adv. Resist Tech. Proc.)* **1986**, *631*, 2-7.

- 30) Gozdz, A. S.; Ono, H.; Ito, S.; Shellburne, J. A., III; Matsuda, M., *Proc SPIE (Adv. Resist Tech. Proc.)* **1991**, 1466, 200-205.
- 31) Hofer, D. C.; Miller, R. D.; Willson, C. G., *Proc SPIE (Adv. Resist Tech. Proc.)* **1984**, 469, 16.
- 32) Wallraff, G. M.; Miller, R. D.; Clecak, N.; Baier, M., *Proc SPIE (Adv. Resist Tech. Proc.)* **1991**, 1466, 211-217.
- 33) Dabbagh, G.; Hutton, R. S.; Cirelli, R. A.; Reichmanis, E.; Novembre, A. E.; Nalamasu, O., *Proc SPIE (Adv. Resist Tech. Proc.)* **1998**, 3333, 394-400.
- 34) Bellas, V.; Tegou, E.; Raptis, I.; Gogolides, E.; Argitis, P.; Iatrou, H.; Hadjichristidis, N.; Sarantopoulou, E.; Cefalas, A. C., *J. Vac. Sci. Technol. B* **2002**, 20, 2902-2908.
- 35) Tserepi, A.; Cordoyiannis, G.; Patsis, G. P.; Constantoudis, V.; Gogolides, E.; Valamontes, E. S.; Eon, D.; Peignon, M. C.; Cartry, G.; Cardinaud, C.; Turban, G., *J. Vac. Sci. Technol. B* **2003**, 21, 174-182.
- 36) Paraszczak, J.; Babich, E.; Hatzakis, M.; Shaw, J., *J. Vac. Sci. Technol. B* **1985**, 3, 358-359.
- 37) Barclay, G.; Kanagasabapathy, S.; Pohlers, G.; Mattia, J.; Xiong, K.; Ablaza, S.; Cameron, J.; Zampini, A.; Zhang, T.; Yamada, S.; Huby, F.; Wiley, K., *Proc SPIE (Adv. Resist Tech. Proc.)* **2003**, 5039, 433-441.
- 38) Morita, M.; Tanaka, A.; Onose, K., *J. Vac. Sci. Technol. B* **1986**, 4, 414-417.
- 39) Sakata, M.; Ito, T.; Yamashita, Y., *J. Photopolym. Sci. Technol.* **1989**, 2, 109-114.
- 40) Nate, K.; Mizushima, A.; Sugiyama, H., *Proc SPIE (Adv. Resist Tech. Proc.)* **1991**, 1466, 206-210.
- 41) Miyoshi, S.; Furukawa, T.; Kawaguchi, E.; Itani, T., *Proc SPIE (Adv. Resist Tech. Proc.)* **2003**, 5039, 462-471.
- 42) Tegou, E.; Bellas, V.; Gogolides, E.; Argitis, P.; Dean, K.; Eon, D.; Cartry, G.; Cardinaud, C., *Proc SPIE (Adv. Resist Tech. Proc.)* **2003**, 5039, 439-461.
- 43) (a) Tegou, E.; Bellas, V.; Gogolides, E.; Argitis, P.; Eon, D.; Cartry, G.; Cardinaud, C., *Chem. Mater.* **2004**, 16, 2567-2577; (b) Eon, D.; Cartry, G.; Fernandez, V.; Cardinaud, C.; Tegou, E.; Bellas, V.; Argitis, P.; Gogolides, E., *J. Vac. Sci. Technol. B* **2004**, 22, 2526-2532.



- 44) Kunz, R. R.; Bloomstein, T. M.; Hardy, D. E.; Goodman, R. B.; Downs, D. K.; Curtin, J. E., *J. Vac. Sci. Technol. B* **1999**, *17*, 3267-3272.
- 45) Okoroanyanwu, U.; Shimokawa, T.; Byers, J. D.; Willson, C. G., *J. Molec. Cat. A* **1998**, *133*, 93-114.
- 46) Yu, G., Personal communication, **2003**.
- 47) Williams, K. R.; Muller, R. S., *J. Microelectromech. Sys.* **1996**, *5*, 256-269.

## RECOMMENDATIONS FOR FUTURE WORK

## 4. Recommendations for future work

### 4.1. Optimization of lithographic resolution

As shown in chapter three, poly(NBFOA/NBHFA-BOC) could only be imaged to 1  $\mu\text{m}$  semidense lines. It is possible, through a systematic optimization of processing conditions, to obtain submicron resolution. For example, a change in the loading of the PAG can vary the sensitivity of the resist film. High PAG loading requires low doses to activate the PAG, but could lead to excessive acid diffusion during the subsequent PEB, leading to line thinning, in the case of negative tone development, and substantial line edge roughness. On the other hand, low PAG loading will require greater exposure doses—detrimental to the imaging tool lifetime—to ensure enough PAG is activated to clear the image. Excessive or insufficient acid diffusion will result in undesired CD variations. The photoresist film thickness can also affect the minimum resolution. Coating thinner films can maintain the exposure well within the DOF, thus enabling a more focused exposure, although thicker films provide a convenient route to high aspect ratio images. Additionally, the images obtained using poly(NBFOA/NBHFA-BOC) were subjected to a PAB temperature lower than the glass transition temperature of the polymer. It has been shown that a PAB above the  $T_g$  will increase the environmental stability of photoresists, as well as limit acid diffusion.<sup>1</sup> Therefore, it is expected that an increase of the PAB temperature above the  $T_g$  at 120 °C will anneal the film. This is particularly important for the long delay time introduced with  $\text{CO}_2$  processing. A further study of PAB time would be advantageous to determine the extent of thermal deprotection or thermal PAG activation at elevated temperatures. Another possible technique for the optimization of images includes the imaging of a focus-exposure matrix wafer at 193 nm. This would enable a precise determination of the DOF for the resist, thus

allowing further optimization of the resist thickness. This would also facilitate the location of optimal images, as the scanner's ideal parameters frequently shift.<sup>2</sup> To further improve development conditions, the design and manufacture of a low-volume high-pressure chamber that can accommodate a 6" wafer is needed. Such a chamber would permit the development of an entire wafer at once, thus eliminating variations associated with the current method of cleaving a wafer, and developing each wafer fragment individually. Developing a whole wafer at once also eliminates both the variations from and the duration of PED, inherent to the current method. Careful engineering considerations must be taken as far as the inlet and outlet locations, the control of CO<sub>2</sub> flow rates, and the mixing of CO<sub>2</sub> in the cell during development. Such steps will allow the imaged wafer to develop uniformly. The PED could be further minimized with the installation of this development chamber in the NCSU cleanroom, in close proximity to the ASML 193 nm scanner.

The balance of each of these steps requires careful consideration in order to optimize any photoresist system. Of course, as all these steps are intimately related, changes in one parameter will certainly affect the resist performance during subsequent steps. A statistical design of experiments could alleviate many of the trials needed to optimize processing, without the possibility of excessively narrowing the processing window.

#### 4.2. Molecular resists based on POSS

Non-polymeric photoresists have been a subject of recent interest. To date, these materials have comprised of calixarene molecular glasses.<sup>3</sup> E-beam imaging of these materials has produced sub-100 nm dense lines. The monodispersity, as well as the small size of the molecule, as compared to the size of a polymer, helps to minimize the effective pixel size of the resist. Unfortunately, such highly aromatic materials are too absorbant at

193 nm and 157 nm, precluding them from use as photoresists at these wavelengths. However, the concept of using molecular resists may be applied to other types of molecules. Specifically, polyhedral oligomeric silsesquioxanes (POSS) show promise for such an application, as polysiloxanes are known to exhibit low absorbance at these wavelengths, and the monodispersity should provide the small “pixel size” of a molecular resist. POSS materials are known to be ~1.5 nm in diameter, thus providing a pixel size well within the limits needed for current lithography research.<sup>4</sup> Various octa-substituted POSS materials are already commercially available, and have the potential to be employed in this application (Fig. 5.1). For example, an octylglycidyl-substituted POSS (g-octa-POSS)

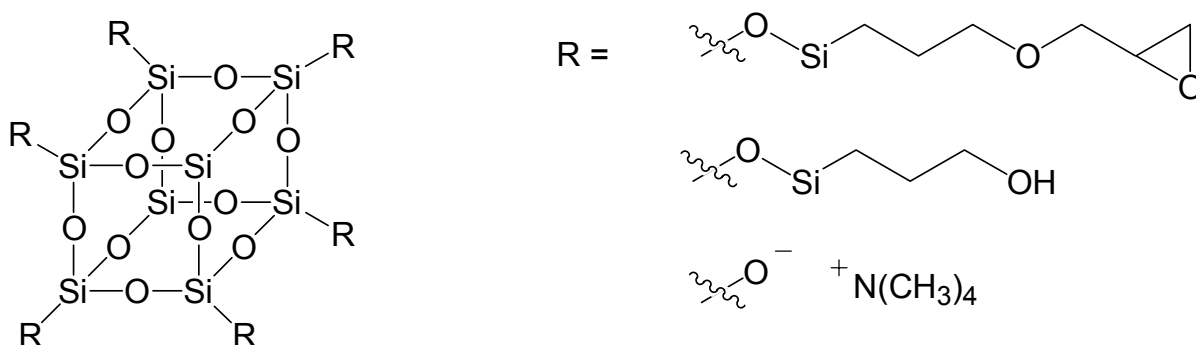


Figure 4.1. Some available starting materials for POSS-based molecular resists. Note that every Si has a pendant R-group, although two R groups have been omitted for visual clarity.

could be used as a cross-linking negative tone resist in the presence of a PAG, or under e-beam exposure. Unfortunately, g-octa-POSS and other octyl-substituted POSS materials are crystalline, thus limiting the research capability of this material class. However, Ober and coworkers have overcome this particular limitation in calixarene resists by alternating the substitution pattern of tBOC-protected phenyl rings between the para and meta positions. The different substitutions on the calixarene is enough to break up the crystallinity of the resist. A similar approach could be used to break up the crystallinity of POSS materials. For

example, the octyl(hydroxypropyl)-substituted POSS, shown in Figure 4.1, could be partially protected with an acid sensitive group, such as tBOC. Setting the stoichiometry of the protection reaction does not necessarily set the stereochemistry of the protection. For example, if two hydroxyl groups will be protected in the POSS molecule, then there are three ways the protecting groups can be placed relative to each other. The variation in stereochemistry of a partially-protected POSS may be sufficient to prevent crystallization. POSS-based resists could potentially be used as single-layer resists or bilayer resists in e-beam, 193, 193i, and 157 lithographies.

#### 4.3. References

- 1) Ito, H., *J. Polym. Sci. A* **2003**, *41*, 3863-3870.
- 2) Vallenga, D., Personal communication, **2005**.
- 3) Chang, S. W.; Felix, N.; Yang, D.; Ramakrishnan, A.; Ober, C. K., *PMSE Prepr.* **2005**, *92*, 131-132.
- 4) Tegou, E.; Bellas, V.; Gogolides, E.; Argitis, P.; Dean, K.; Eon, D.; Cartry, G.; Cardinaud, C., *Proc SPIE (Adv. Resist Tech. Proc.)* **2003**, *5039*, 439-461.